Université de Montréal

Étude de la fonction de luminosité des étoiles naines blanches de type DA dans le relevé Kiso

par

Marie-Michèle Limoges

Département de physique

Faculté des arts et des sciences

Mémoire présenté à la Faculté des études supérieures

en vue de l'obtention du grade de

Maître ès sciences (M.Sc.)

en physique

Avril, 2009

Université de Montréal

Faculté des études supérieures

Ce mémoire intitulé:

Étude de la fonction de luminosité des étoiles naines blanches de type DA dans le relevé Kiso

présenté par:

Marie-Michèle Limoges

a été évalué par un jury composé des personnes suivantes:

Gilles Fontaine,	président-rapporteur
Pierre Bergeron,	directeur de recherche
Nicole St-Louis,	membre du jury

Mémoire accepté le: _____

À Rita, Michel, Geneviève et Jean-Philippe, les étoiles les plus brillantes de mon Univers.

Sommaire

Une fonction de luminosité spectroscopique des naines blanches DA du relevé Kiso Ultraviolet Excess est déterminée. Les objectifs sont, en premier lieu, de comparer cette dernière avec la fonction de luminosité photométrique des naines blanches DA du relevé Kiso de Darling (1994) et, en second lieu, d'évaluer la complétude des relevés Kiso et Palomar Green (PG). L'étude débute par l'observation des naines blanches DA et DB de l'échantillon de Darling (1994). Les spectres obtenus permettent une reclassification spectrale majeure ainsi que la découverte de 3 systèmes de naines blanches binaires DA+DB. Les paramètres atmosphériques sont déterminés à l'aide de la méthode spectroscopique, par un ajustement des raies spectrales avec des modèles d'atmosphère. Cette méthode permet d'obtenir des valeurs de magnitude absolue (M_V) significativement plus précises que celles publiées dans Darling (1994), qui sont basées sur des calibrations photographiques. La différence entre les M_V spectroscopiques et photométriques atteint en moyenne 2-3 magnitudes, et parfois même 4 magnitudes. La comparaison de la fonction de luminosité calculée à l'aide de ces nouvelles magnitudes avec la fonction de luminosité des DA de Darling nous permet de constater que les nouvelles valeurs de M_V sont généralement plus brillantes que celles de Darling (1994), et que notre fonction de luminosité contient alors moins d'étoiles dans les intervalles les plus froids. Finalement, la superposition de notre fonction de luminosité avec celle de Liebert et al. (2005) (PG) nous apprend que la complétude des relevés Kiso et PG est similaire, et d'environ 60%, même si le relevé Kiso est plus profond.

Mots clés: étoiles : paramètres fondamentaux - naines blanches - fonction de luminosité - techniques: spectroscopique - binaires: spectroscopiques

Abstract

A spectroscopic luminosity function of DA white dwarfs from the Kiso Ultraviolet Excess Survey is determined. The major goals are to compare our results with the photometric luminosity function of DA white dwarfs from the Kiso survey of Darling (1994), and to evaluate the completeness of the Kiso and Palomar Green (PG) surveys. Our study begins with the observation of DA and DB white dwarfs from the sample of Darling (1994). These spectra allow a major spectral reclassification, and the discovery of 3 DA+DB double degenerate binary systems. The atmospheric parameters are determined using the spectroscopic method, by which the absorption lines of each spectrum are fitted with model atmospheres. This method allows us to obtain values of absolute magnitudes which are significantly more accurate than those published in Darling (1994), based on photographic calibrations. The differences between spectroscopic and photometric M_V values are as large as 2-3 magnitudes, and sometimes reach 4 magnitudes. The comparison of the luminosity function calculated using these improved M_V values shows that our function contains less stars in the cooler magnitude bins, which is the result of the fact that the new magnitudes are generally brighter than those of Darling (1994). Finally, from the comparison of our luminosity function with that of Liebert et al. (2005) (PG), we learn that the completeness of Kiso and PG surveys are similar, even if Kiso is deeper. The surveys are $\sim 60\%$ complete.

Subject headings: stars - fundamental parameters - white dwarfs - luminosity function - techniques: spectroscopic - binaries: spectroscopic

Table des matières

Table des figures

Liste des tableaux

Chapitre 1

Introduction

1.1 La fonction de luminosité

Les étoiles naines blanches ont atteint le stade final de leur évolution. Puisqu'elles ne produisent plus d'énergie, elles ne peuvent que se refroidir en dissipant le contenu de leur réservoir d'énergie thermique. De plus, cette fin est réservée aux étoiles de la séquence principale dont la masse se situe entre 0.07 et 8 $M_{\odot}$, ce qui représente plus de 97% des étoiles de la Galaxie. Grâce à ces caractéristiques, il est très utile de connaître le nombre de naines blanches en fonction de leur luminosité intrinsèque, ou fonction de luminosité. La fonction de luminosité est une mesure de la densité spatiale d'étoiles en fonction de la magnitude absolue. En supposant une masse moyenne pour l'échantillon, elle permet d'estimer la contribution des naines blanches à la densité de matière dans la galaxie.

La fonction de luminosité doit toujours être dérivée à partir d'un échantillon complet d'étoiles naines blanches. Elle contient alors des informations telle qu'une mesure directe du taux de mort stellaire dans le disque galactique local. Elle représente donc un excellent outil pour se renseigner sur l'historique de la formation stellaire dans le disque local. Si le taux de formation stellaire était constant, alors la pente de la fonction de luminosité serait lisse. Par contre, la présence de pics secondaires pourrait révéler, par exemple, un sursaut de formation stellaire vérifiable à l'aide de modèles théoriques.

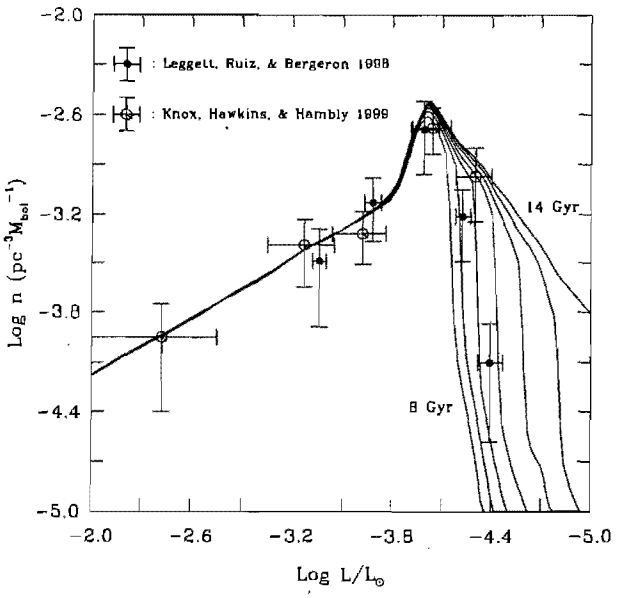

FIG. 1.1 – Comparaison d'une fonction de luminosité observée et d'une fonction de luminosité théorique des naines blanches. Les points observationnels proviennent de Leggett et al. (1998) et Knox et al. (1999). Les courbes représentent les fonctions de luminosité théoriques calculées avec des modèles de refroidissement et un coeur de C pur. Elles sont calculées en considérant des âges qui varient entre 8 et 14 Ga pour le disque local galactique, et elles sont normalisées près de $L/L_\odot \sim 10^{-3.5}$. La Figure est tirée de Fontaine et al. (2001).

Des modèles théoriques de fonctions de luminosité ont été développés, tels que dans Fontaine et al. (2001). La comparaison de ces modèles avec des fonctions de luminosité expérimentales permet de savoir si les modèles sont fidèles à la réalité, et donc de savoir si la théorie rattachée à l'évolution des naines blanches est bien comprise. Les résultats expérimentaux permettent de valider ou de contraindre le calcul théorique du taux de refroidissement des naines blanches, qui est essentiel à la fonction de luminosité théorique.

La fonction de luminosité théorique permet d'établir l'âge de la Galaxie. Elle se base sur le fait que les naines blanches les plus vieilles ont un âge total (temps de vie sur la séquence principale + temps de refroidissement) égal à l'âge du système stellaire auquel elles appartiennent. La partie ascendante de la fonction de luminosité, qui contient les étoiles chaudes, est peu sensible à l'âge du système stellaire, mais la partie descendante l'est beaucoup. Elle est aussi peuplée par les étoiles naines blanches les plus massives, les moins nombreuses et les plus vieilles d'une population donnée. La partie descendante de la fonction de luminosité est donc peuplée par les étoiles les plus froides.

La Figure 1.1, tirée de Fontaine et al. (2001), illustre la comparaison entre des fonctions de luminosité théoriques et observationnelles. Les courbes représentent des âges théoriques de 8 à 14 milliards d'années. Elles sont superposées à deux études. Celle de Leggett et al. (1998) provient d'un échantillon dont la détection est basée sur le mouvement propre et celle de Knox et al. (1999) provient d'un relevé colorimétrique. La comparaison montre que l'âge du disque local galactique serait de 11 milliards d'années et la densité de naines blanches calculée est de 0.0039 pc^{-3}. Les auteurs soulignent que cette valeur est cohérente avec celle de 0.003 étoiles pc^{-3} tirée de la fonction de luminosité des naines blanches froides de Liebert et al. (1988).

Il est utile de combiner la fonction de luminosité avec la fonction de masse, puisque cette dernière contient aussi des informations sur l'histoire de la formation stellaire dans la Galaxie. En plus d'être une propriété fondamentale d'une population d'étoiles, le nombre de naines blanches en fonction de la masse dans un échantillon complet nous renseigne sur la masse perdue durant l'évolution stellaire d'une distribution de masse initiale (Liebert et al. 2005).

1.2 Historique

Les relevés à grande échelle permettent d'avoir accès à de grands échantillons complets de naines blanches. Ainsi, il devient possible d'étudier statistiquement plusieurs caractéristiques des naines blanches, telles la fonction de luminosité et la fonction de masse. Les méthodes de détection sont basées sur différents critères, selon le relevé. Ceux qui se basent sur un excès dans l'ultraviolet sont souvent pauvres en étoiles froides. Elles représentent donc les fonctions de luminosité des étoiles chaudes. D'autres études ont rassemblé des naines blanches froides provenant de différents échantillons et de méthodes de détection différentes afin de pouvoir obtenir une fonction de luminosité des naines blanches froides.

1.2.1 Fonctions de luminosité des naines blanches froides

Les naines blanches les plus froides de la Galaxie sont également les plus difficiles à détecter, car leur luminosité intrinsèque est très faible. De plus, leur analyse est plus compliquée que pour leurs homologues chaudes, car elles se caractérisent souvent par une absence (ou quasi

absence) de signature spectrale. Dans le cas des naines blanches DA, le type spectral n'est souvent révélé que par la présence de Hα. Par contre, elles représentent un grand intérêt astrophysique. Tel que mentionné plus haut, elles forment la partie descendante de la fonction de luminosité. Ce sont elles qui, à l'aide d'une fonction de luminosité théorique, permettent de déterminer l'âge du disque galactique local.

On retrouve une fonction de luminosité des naines blanches froides dans Liebert et al. (1988). Leur échantillon contient 43 naines blanches froides tirées du Luyten Half-Second Catalog (Luyten 1979). Les objets ont été sélectionnés en fonction de leur mouvement propre. Les paramètres atmosphériques furent trouvés à partir de calibrations photométriques à cause de la rareté des raies spectrales. Les valeurs de magnitudes absolues dérivées à partir des paramètres atmosphériques ont été converties en magnitudes bolométriques afin de comparer la fonction de luminosité obtenue avec une fonction théorique. Ils ont observé une baisse dans le nombre d'étoiles due à l'âge fini du disque galactique. Les auteurs trouvent également une densité de 0.003 naines blanches par pc^3, ce qui représente environ 1% de la masse dynamique de la Galaxie. Par contre, les premiers à utiliser la baisse abrupte du nombre d'étoiles à une luminosité donnée ($\sim L/L_{\odot} = -4.5$) comme un indicateur de l'âge de la Galaxie sont Winget et al. (1987). La comparaison de leur fonction de luminosité avec des modèles d'évolution de naines blanches donne à la Galaxie 9.3 ± 2.0 milliards d'années.

Dix ans plus tard, Leggett et al. (1998) ont refait l'étude de Liebert et al. (1988) dans le but d'améliorer le calcul de la fonction de luminosité des naines blanches froides et de déterminer l'âge du disque local galactique. Ils ont repris l'échantillon de 43 naines blanches froides de Liebert et al. (1988). Les paramètres atmosphériques étaient toujours déterminés à l'aide d'ajustement des modèles d'atmosphère avec la photométrie, mais les auteurs ont utilisé les modèles améliorés de Bergeron et al. (1995). De plus, lorsque des raies spectrales étaient encore visibles, ils ont ajouté l'utilisation de la spectroscopie pour contraindre les abondances d'hydrogène et d'hélium. Finalement, ils avaient accès à de meilleures corrections bolométriques et aux nouveaux modèles d'évolution de Wood (1995). Les trois naines blanches les plus vieilles

du groupe sont des étoiles dont l'atmosphère est dominée par l'hélium qui auraient plus de 9 milliards d'années. Leur température effective se situe entre 4500 et 4800 K. Leur masse est un peu plus élevée que la moyenne de 0.6 $M_{\odot}$, ce qui explique leur évolution plus rapide. Les auteurs trouvent une densité légèrement supérieure à celle de Liebert et al. (1988), soit 3.39×10^{-3} naines blanches par pc^3. La superposition de leur fonction de luminosité aux modèles de Wood (1995) indique que le disque local galactique aurait 8±1.5 milliards d'années.

1.2.2 Fonctions de luminosité des naines blanches à haute température

1.2.2.1 Fonctions de luminosité photométriques

Le relevé Palomar Green (PG) utilisait une méthode de détection par excès dans l'ultraviolet. Un total de 1874 objets ont été identifiés dans une superficie de 10,714 degrés carrés. L'échantillon statistique complet compte 1715 objets, dont 348 sont des naines blanches de type DA. La complétude de l'échantillon est évaluée à 84% selon Green et al. (1986). La fonction de luminosité fut d'abord déterminée par Fleming et al. (1986) à partir de calibrations basées sur la photométrie. L'étude était limitée aux naines blanches de type DA. Puisque les étoiles furent détectées par excès dans l'ultraviolet, l'échantillon compte relativement peu d'étoiles à basse température.

Une autre fonction de luminosité dérivée à partir de calibrations photométriques fut publiée un peu plus tard, dans Darling (1994). Celle-ci comprenait 234 naines blanches de tous les types spectraux et l'échantillon provenait des objets détectés par le relevé Kiso. Ce dernier a permis de recenser 1186 objets à excès dans l'ultraviolet à l'aide du télescope Kiso Schmidt de 105 cm. Les résultats furent publiés sous la forme de deux catalogues, dans Noguchi et al. (1980) et Kondo et al. (1984). Les objets sont distribués dans 44 champs et ils se trouvent pour la plupart à une longitude galactique de 180°. Chacun des champs représente 36 degrés carrés sur la voute céleste, couvrant au total une superficie d'environ 1400 degrés carrés (après avoir soustrait le recoupement entre les champs). L'information sur les champs est disponible

dans le Kiso Information Bulletin[1] ou sur le web (Wide Field Plate Database[2]).

L'excès dans l'ultraviolet fut détecté visuellement à l'aide des indices photographiques UGR. Trois images, une dans chaque bande, furent prises successivement sur la même plaque, séparées par 20". Le critère de sélection était basé sur un excès dans la bande U, relativement aux bandes G et R (Noguchi et al. 1980). La magnitude limite de détection des plaques varie entre ~17 et 18.5. On doit cet écart à l'état de chaque plaque photographique (Maehara et al. 1986). La magnitude limite moyenne du relevé se situe à 17.7. Selon Darling (1994), lors du calcul de la fonction de luminosité, 94% des objets du relevé Kiso étaient spectroscopiquement identifiés. Ce relevé est également pauvre en naines blanches froides.

1.2.2.2 Fonctions de luminosité spectroscopiques

L'utilisation d'une méthode spectroscopique, c'est-à-dire un ajustement des raies spectrales avec des modèles d'atmosphères détaillés, permet de déterminer les paramètres atmosphériques ($T_{\rm eff}$, $\log g$) avec une grande précision. Il en est de même pour les valeurs de magnitude absolues dérivées à partir de ces paramètres atmosphériques. La fonction de luminosité dépend fortement des valeurs de M_V. Des magnitudes absolues plus précises impliquent donc une fonction luminosité qui représente mieux la population de naines blanches du disque galactique local.

Un tel calcul a été réalisé dans Liebert et al. (2005). Dans cet article, les auteurs déterminent la fonction de luminosité des naines blanches de type DA du relevé PG. Il s'agit donc d'une reprise du calcul fait par Fleming et al. (1986), où cette fois, les paramètres atmosphériques sont déterminés de manière spectroscopique. La méthode est basée sur celle décrite dans Bergeron et al. (1992). Encore une fois, ce relevé est beaucoup plus complet pour les étoiles les plus brillantes. La complétude de l'échantillon est évaluée à 75%.

À la Figure 10 de ce même article (reproduite ici à la Figure 1.2), les auteurs comparent

[1] Kiso Information Bulletin, 1979, Vol. 1, Tokyo Astronomical Observatory
[2] www.wfpa.bas.bg

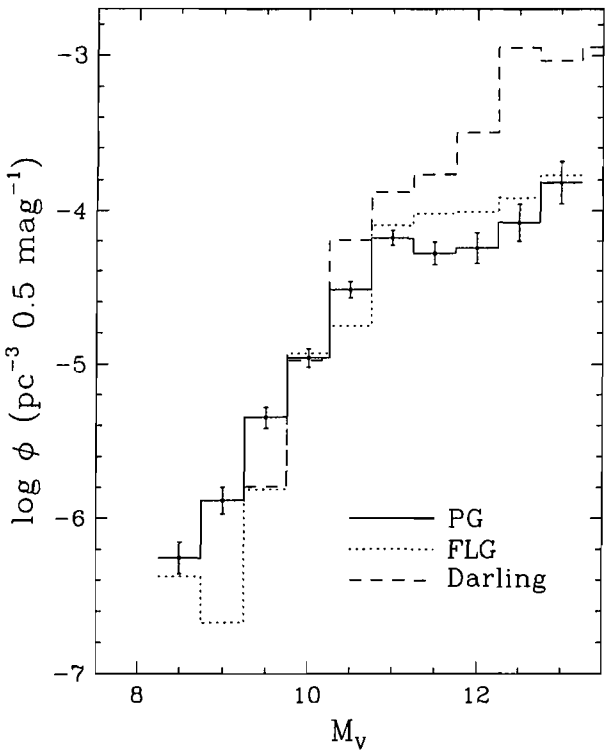

FIG. 1.2 – Fonction de luminosité des naines blanches de type DA de l'échantillon complet du relevé PG (Liebert et al. 2005) (trait plein), comparée à celle de Fleming et al. (1986) (pointillé) et à la fonction de luminosité des naines blanches du relevé Kiso, tous types spectraux confondus, de Darling (1994) (traits en tirets). La hauteur caractéristique de la Galaxie pour ces échantillons d'étoiles est de 250 pc. La Figure est tirée de Liebert et al. (2005).

leurs résulats à ceux de Fleming et al. (1986) et de Darling (1994). Ils en concluent que leur échantillon est moins complet que celui tiré du relevé Kiso. Par contre, une telle comparaison est difficilement réalisable. En effet, les résultats tirés de Darling (1994) proviennent d'un échantillon qui ne contient pas uniquement des naines blanches de type DA, mais aussi des DB, DC, DZ et DQ. De plus, Liebert et al. (2005) ont comparé leurs valeurs de magnitudes absolues dérivées de manière spectroscopique avec les magnitudes absolues d'un sous-échantillon des étoiles de Darling (1994). Ils ont observé une grande dispersion entre les valeurs de M_V spectroscopiques et photométriques. La fonction de luminosité de Darling (1994) reflète certainement cette dispersion.

Liebert et al. (2005) évaluent leur échantillon comme complet à 75%. Selon l'étude de Darling (1994), l'échantillon PG est complet à 75% jusqu'à une magnitude apparente de $B \sim 15.15 - 16.15$. Passée cette magnitude, l'échantillon deviendrait substantiellement incomplet. En effet, Darling (1994) évalue la complétude globale du relevé PG à 58%. Darling évalue son propre échantillon (KUV) comme étant complet à 75%, jusqu'à une magnitude d'envion 15 à

16, toujours dans la bande B. Les relevés Kiso et PG semblent donc similaires du point de vue de la complétude. En effet, dans Wegner & Darling (1994), on peut lire: « On the whole, the luminosity function derived compares relatively well with that from the PG survey (Fleming et al. 1986) ». Cette citation est démentie dans Liebert et al. (2005), puisque les auteurs affirment que la fonction de luminosité KUV contient significativement plus de naines blanches dans l'intervalle $M_V = 10.5 - 13.0$. Par contre, tel qu'il a déjà été mentionné, la fonction de luminosité KUV contient tous les types spectraux. Afin de comparer des valeurs semblables et ainsi pouvoir faire la lumière sur la complétude des relevés Kiso et PG, il faudrait connaître plus précisément la fonction de luminosité des naines blanches DA du relevé Kiso.

Avec l'avènement des relevés à grande échelle tels que le Sloan Digial Sky Survey (SDSS), le nombre de naines blanches connues ne cesse d'augmenter. La photométrie et l'astrométrie de ces étoiles sont déterminées avec toujours plus de précision. Il est donc possible d'avoir accès à des échantillons de naines blanches toujours plus grands. Il devient alors très tentant de les utiliser à des fins d'études statistiques.

Harris et al. (2006) et DeGennaro et al. (2008) ont déterminé la fonction de luminosité des naines blanches du relevé SDSS à l'aide, respectivement, des Data Release 3 et 4. Leurs échantillons contiennent respectivement 6000 et 7128 naines blanches. Par contre, les méthodes utilisées pour la sélection des objets font que les échantillons sont très peu complets. En effet, DeGennaro et al. (2008) ont évalué la complétude de leur échantillon de naines blanches à 51%. Ceci est attribuable, d'une part, au fait que les naines blanches avec $T_{\rm eff} \leq 8000$ K ne sont pas sélectionnées à cause des limites sur les couleurs qui permettent de séparer les étoiles de la séquence principale des naines blanches. De plus, les naines blanches magnétiques peuvent passer à travers les algorithmes de sélections sans être détectées. Aussi, tel que mentionné dans Gianninas et al. (2008), l'échantillon Sloan est limité aux objets de magnitude apparente très faible, due à la nature même du relevé. Ces études statistiques sont donc basées sur des échantillons qui sont incomplets. Pour tenter de contrer cet obstacle, les échantillons de Harris et al. (2006) et de DeGennaro et al. (2008) ont subi des corrections pour tenir compte de la

complétude. C'est également le cas de plusieurs autres échantillons, lorsque des études similaires sont menées. Par contre, il serait intéressant de réussir à obtenir un échantillon complet pour pouvoir baser ces corrections sur des critères concrets.

1.3 Justification de la nouvelle étude

La méthode spectroscopique telle que décrite dans Bergeron et al. (1992) permet de déterminer les paramètres atmosphériques ($T_{\rm eff}$, $\log g$) des étoiles naines blanches de manière très précise, par un ajustement des raies spectrales avec des modèles d'atmosphère. Nous avons donc entrepris de redériver la fonction de luminosité de Darling (1994) en utilisant des paramètres atmosphériques spectroscopiques. Nous serons alors en mesure de comparer les fonctions de luminosité spectroscopiques des naines blanches DA, et à la lumière de cette comparaison, d'évaluer de nouveau la complétude des échantillons PG et KUV. Après cette analyse, nous saurons si le relevé Kiso est vraiment plus complet que PG, et s'il représente un échantillon utile pour des études statistiques. Nous saurons si ce petit échantillon d'environ 200 naines blanches à excès dans l'ultraviolet peut être plus complet que celui tiré du relevé SDSS, à plus grande échelle.

Chapitre 2

Le calcul de la fonction de luminosité

La fonction de luminosité est une mesure de la densité spatiale de naines blanches. On peut donc la calculer en comptant le nombre de naines blanches contenues dans un certain volume. Cette méthode requiert de pouvoir détecter toutes les naines blanches dans un volume donné. Une méthode alternative serait d'additionner les contributions à la densité spatiale de chacune des naines blanches dans un échantillon limité par la magnitude. Ce sera la méthode adoptée ici.

La distance à laquelle se trouve chaque étoile définit un volume. Puisque les étoiles ne sont pas distribuées uniformément en hauteur, mais plutôt selon un disque exponentiel, on applique un facteur de correction de la forme e^{-z/z_0}, où $z = r \sin\theta$ est la distance de l'objet par rapport au plan de la Galaxie, et θ est la valeur absolue de la latitude galactique de l'objet, en radians. La constante z_0 vaut 250 pc et elle représente la hauteur caractéristique de la galaxie pour les naines blanches.

On obtient donc un « volume pondéré », v, qui se calcule ainsi, selon Boyle (1989) et l'équation (4.6) de Darling (1994):

$$v = \int_0^d e^{-z/z_0} \frac{dv'}{dr} dr = \int_0^d e^{-z/z_0}\ 4\pi r^2 dr \tag{2.1}$$

où $v' = \frac{4}{3}\pi r^3$ et d est la distance qui se calcule à l'aide des magnitudes apparentes et absolues:

$$d = 10^{(V - M_V + 5)/5} \tag{2.2}$$

Notre échantillon est limité par la magnitude, ce qui signifie qu'il doit être complet jusqu'à une certaine magnitude limite. Au-delà de cette limite, on ne peut pas avoir la certitude que tous les objets ont été détectés. Les étoiles qui ont une magnitude apparente plus faible que la magnitude limite seront retirées de l'échantillon complet. Ainsi, la magnitude limite du relevé est définie comme la magnitude apparente pour laquelle une étoile peut faire partie de l'échantillon complet. Pour une étoile donnée, $V_{\rm lim}$ définit une distance maximale à l'intérieur de laquelle laquelle l'objet peut être détecté, et qu'il fasse partie de l'échantillon complet. Cette distance définit un volume maximal, $v_{\rm max}$.

Pour trouver $v_{\rm max}$, il faut remplacer V par la magnitude limite du relevé dans la formule 2.2. On obtient alors la distance maximale de chaque étoile, $d_{\rm max}$, qu'on remplace dans l'équation 2.1:

$$d_{\rm max} = 10^{(V_{\rm lim} - M_V + 5)/5} \tag{2.3}$$

$$v_{\rm max} = \int_0^{d_{\rm max}} e^{-z/z_0}\ 4\pi r^2 dr \tag{2.4}$$

Par contre, tel que mentionné dans Green (1980), chacune des plaques photographiques a une magnitude limite différente. Il est alors proposé de définir un volume maximum par champ. Le volume maximum total pour une étoile donnée est la somme de tous ces petits volumes. L'auteur mentionne également que dans le cas où des champs se recoupent, l'aire de recouvrement est attribuée au champ qui possède la magnitude limite la plus faible. On obtient donc:

$$v_{\max} = \sum_{j=1}^{n_f} \frac{\omega_j}{4\pi} \int_0^{d_{max}} e^{-z/z_0} 4\pi r^2 dr \tag{2.5}$$

pour chaque étoile, et n_f est le nombre total de champs. On aura donc que $\sum_{j=1}^{n_f} \omega_j$ doit être égal à l'aire totale couverte par le relevé, puisque ω_j représente l'aire couverte par chaque champ.

Afin de calculer $v_{\max}$, il faut trouver la valeur de $V_{\lim}$ (voir les équations 2.3 et 2.4). La magnitude limite du relevé se trouve en utilisant la méthode $v/v_{\max}$. En effet, selon Schmidt (1968), la méthode pour s'assurer de la complétude d'un échantillon d'objets est d'obtenir $\langle v/v_{\max} \rangle = 0.5$. Il s'agit en fait d'un test d'uniformité. Tel que décrit plus haut, v est une mesure de la position de l'objet, et $v_{\max}$ correspond au volume maximum dans lequel la source peut être observée. Le rapport $v/v_{\max}$ est une mesure de la position de l'étoile dans le « volume observable ». Alors, si les étoiles sont distribuées uniformément à l'intérieur de $v_{\max}$, les valeurs de $\langle v/v_{\max} \rangle$ suivront une distribution uniforme entre 0 et 1, et $\langle v/v_{\max} \rangle = 0.5$.

Pour obtenir $V_{\lim}$, il s'agit donc de faire varier cette dernière valeur jusqu'à l'obtention de $\langle v/v_{\max} \rangle = 0.5$. Ainsi, l'échantillon est complet jusqu'à cette valeur de magnitude apparente. Il faut retirer de l'échantillon toutes les naines blanches dont $V < V_{\lim}$. Les étoiles qui restent définissent l'échantillon complet à partir duquel la fonction de luminosité peut maintenant être dérivée.

Puisque $v_{\max}$ représente le volume dans lequel il est possible de trouver une naine blanche, la contribution de chaque étoile à la densité spatiale locale est de $1/v_{\max}$. Cette méthode à été introduite pour la première fois par Schmidt (1968) pour le calcul de la fonction de luminosité des quasars. Elle a par la suite été grandement utilisée pour les étoiles. La fonction de luminosité différentielle (ϕ) est obtenue en effectuant la somme des contributions de chaque naine blanche à la densité spatiale. Pour chaque intervalle de magnitude absolue, la fonction

de luminosité se calcule donc de la manière suivante:

$$\phi(M_V) = \sum_{i=1}^{n_b} 1/v_{\max_i} \tag{2.6}$$

où

$$v_{\max_i} = \sum_{j=1}^{n_f} \frac{\omega_j}{4\pi} \int_0^{d_{\max}} 4\pi r^2 e^{-r\sin\theta/z_0} dr = \sum_j^{n_f} \omega_j \frac{x^2 z_0^3}{\sin^3\theta} \left(\frac{2}{x^2}(1-(1+x)e^{-x}) - e^{-x}\right) \tag{2.7}$$

où $x = r\sin\theta/z_0$ et n_b est le nombre d'étoiles dans chaque intervalle de magnitude absolue. L'incertitude est donnée par l'erreur statistique qui s'applique si on considère que les étoiles sont distribuées uniformément dans l'espace. Alors, l'incertitude pour chaque intervalle de magnitude correspond à $\sigma_\phi = [\sum_{i=1}^{n_b} (1/v_{\max_i})^2]^{1/2}$ (Boyle 1989). Il s'agit de la somme quadratique des erreurs sur les contributions de chaque étoile.

2.1 L'étude photométrique de Darling (1994)

L'échantillon de Darling (1994) contient 234 naines blanches, de plusieurs types spectraux (voir le Tableau 2.1), qui proviennent du catalogue KUV publié dans Noguchi et al. (1980) et Kondo et al. (1984). Ces naines blanches, qu'on retrouve au Tableau 4.3 de la thèse de Darling, furent spectrosopiquement identifiées dans une série de 10 articles (voir Darling & Wegner 1996 et les références incluses). Le Tableau 4.3 contient 194 naines blanches de type DA. L'auteur a par la suite assigné une valeur de M_V nécessaire au calcul de v et de $v_{\max}$ pour chacune des étoiles de l'échantillon. Dans Darling (1994), la photométrie UBV du relevé Kiso était disponible pour 125 étoiles. Il a dérivé la magnitude absolue à l'aide de la relation empirique entre l'indice $(B-V)$ d'un objet et sa magnitude absolue. L'équation suivante provient Dahn et al. (1982)

Si $(B-V) \geq 0.4$:

$$M_V = 11.43 + 7.25(B-V) - 3.42(B-V)^2 \tag{2.8}$$

Les prochaines relations sont tirées de Sion & Liebert (1977)

Si $(B-V) \leq 0.4$ et pour une DA:

$$M_V = 11.246(B-V+1)^{0.60} - 0.045 \tag{2.9}$$

Si $(B-V) \leq 0.4$ et pour une non-DA:

$$M_V = 11.916(B-V+1)^{0.44} - 0.011 \tag{2.10}$$

Dans le catalogue de McCook & Sion (1987), 9 valeurs de magnitudes absolues étaient disponibles. Pour les 100 étoiles restantes, aucun indice de couleur n'était disponible. Il les a donc estimés à partir d'une étude statistique des indices de couleurs qu'il possédait et de l'indice photographique *CI*, qui est en fait l'indice de couleurs $(U-G)$. Il s'agit d'un ajustement linéaire entre les indices $(B-V)$ et *CI* (voir Figure 4.1 de Darling 1994):

$$(B-V) = 0.22CI + 0.35 \tag{2.11}$$

En réalité, cette relation n'est pas linéaire, puisque la Figure 4.1 de Darling (1994) montre une grande dispersion de part et d'autre de la droite. Cette relation relève donc d'une approximation basée sur la photométrie. La magnitude absolue de chaque étoile fut ensuite calculée à partir de ces indices $(B-V)$. Les magnitudes absolues sont à la base de la fonction de luminosité. Il est donc crucial de les déterminer de la manière la plus précise possible. Une fonction de luminosité fut ensuite calculée à l'aide de ces magnitudes absolues, pour les 197 naines blanches faisant partie de l'échantillon complet, tous types spectraux inclus.

2.2 Contenu spectroscopique de l'échantillon

Afin d'obtenir une fonction de luminosité des naines blanches DA du relevé Kiso, nous devions d'abord observer toutes les naines blanches DA du relevé. Notre échantillon de départ fut le Tableau 4.3 de Darling (1994). Des spectres furent donc obtenus pour chaque naine blanche de type DA et DB, puisque nous ferons une analyse subséquente de ces étoiles DB. Ensuite,

nous avons identifié dans la littérature 7 naines blanches de types DA, DB et DO appartenant au relevé Kiso, mais qui ne faisaient pas partie de l'échantillon de Darling (1994). Nous avons donc obtenu des spectres pour ces objets. La Figure 2.1 montre que la majorité des spectres obtenus ont un rapport signal sur bruit égal ou plus élevé que 50, nous permettant une classification spectrale précise et réduisant l'incertitude sur les paramètres atmosphériques.

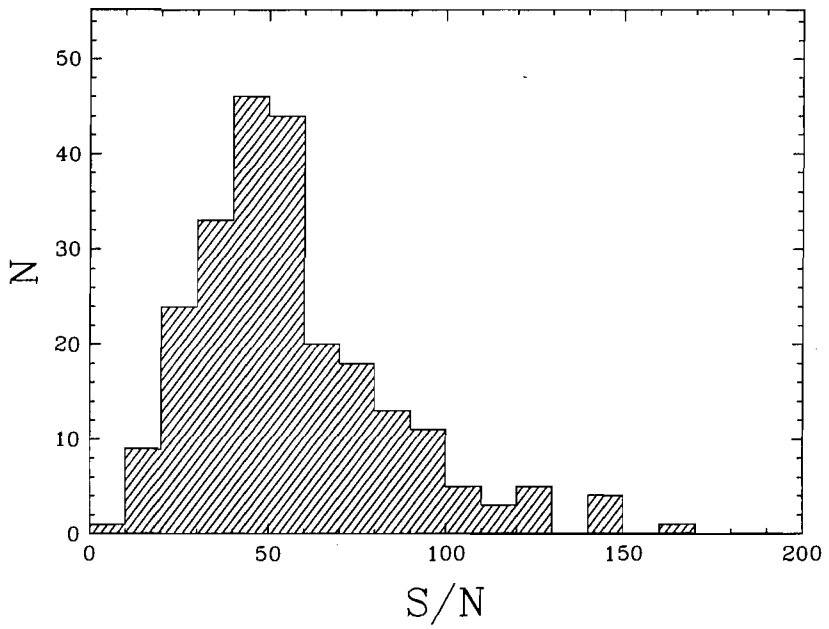

FIG. 2.1 – Distribution du rapport signal sur bruit pour tous les spectres de notre échantillon de naines blanches.

TAB. 2.1 – Contenu spectroscopique de l'échantillon

	DA	DB	DA+DB	DC,DQ,DZ	DO	Magnétique (DA)	Total
Cette étude	168	20	3	14	1	4	210
Darling (1994)	194	25	-	15	0	-	234

L'obtention de spectres à meilleur signal sur bruit et à meilleure résolution nous a permis de procéder à une nouvelle classification spectrale, qui est résumée au Tableau 2.1. Notre échantillon de naines blanches DA contient 175 objets, soit 168 DA (dont une DAO, une naine blanche dont l'atmosphère est dominée par l'hydrogène, dont le spectre contient à la

fois des raies d'hydrogène et des raies d'hélium ionisé), 4 DA magnétiques et 3 qui proviennent de systèmes binaires DA+DB. En effet, notre analyse a permis la découverte de 3 systèmes binaires non résolus, soit KUV 02196+2816, KUV 03399+0015 et KUV 14197+2514. Avec les 3 DB binaires, le nombre de naines blanches dont l'atmosphère est dominée par l'hélium est de 24, incluant une DO. De plus, notre échantillon compte quelques DC, DQ et DZ. Lors de notre classification spectrale, nous avons identifié 30 naines blanches qui auraient dû être classées comme des sous-naines ou des étoiles de la séquence principale. Le plus intéressant de ces objets est sans doute la sous-naine chaude de type O KUV 16032+1735, qui avait été classée comme une DA magnétique par Wegner & Swanson (1990). Tous les spectres de notre échantillon de naines blanches sont présentés à l'Annexe A.

2.3 Présentation des articles et des annexes

Toutes les étapes qui ont suivi l'observation de notre échantillon de naines blanches sont présentées au Chapitre 3. On y retrouve une description détaillée de la classification spectrale effectuée, ainsi qu'une discussion sur les objets qui représentent un intérêt astrophysique particulier, tels les 3 systèmes DA+DB et la sdO KUV 16032+1735. Les paramètres atmosphériques pour les 175 DA de notre échantillon, ainsi que les caractéristiques de chacune de ces étoiles sont fournies au Tableau 3.3. On retrouve également au Chapitre 3 une étude de la distribution de masse des DA, ainsi que la comparaison entre les valeurs de M_V déterminées à l'aide de la méthode spectroscopique et celles de Darling (1994). Finalement, notre étude de la fonction de luminosité des naines blanches DA est présentée. On y retrouve la comparaison de notre fonction de luminosité des naines blanches DA avec celle de Darling (DA seulement), et celle de Liebert et al. (2005). Le Chapitre 4 contient l'entièreté de l'analyse du système DA+DB KUV 02196+2816. Les deux autres systèmes doublement dégénérés seront traités dans un prochain article (Limoges & Bergeron 2009, en préparation).

Les spectres des naines blanches de notre échantillon sont présentés à l'Annexe A, regroupés par type spectral. La première de ces figures, la Figure A.1, contient les 175 DA, en ordre décroissant de température effective. Nous avons regroupé les spectres des 4 naines blanches

magnétiques à la Figure A.2, où la force du champ magnétique augmente de haut en bas. Les spectres et les valeurs de $T_{\rm eff}$ des 3 systèmes DA+DB sont montrés à la Figure A.3, tandis que les DB (et la DO) occupent la Figure A.4. Finalement, la Figure A.5 présente les DC, DZ et DQ. L'Annexe B, regroupe les informations sur les champs du relevé Kiso dont nous avons eu besoin pour le calcul de la fonction de luminosité. La dernière colonne contient l'aire que nous avons attribué à chacun des champs selon les critères de Green (1980).

Chapitre 3

A Spectroscopic Analysis of DA White Dwarfs in the Kiso Survey

M.-M. Limoges[1], P. Bergeron[1]

To be submitted to *The Astrophysical Journal*

April 2009

[1]Département de Physique, Université de Montréal, C.P. 6128, Succ. Centre-Ville, Montréal, Québec H3C 3J7, Canada; [information retirée / information withdrawn], [information retirée / information withdrawn].

3.1 Abstract

We present a spectroscopic analysis of the DA white dwarfs identified in the Kiso survey. Spectroscopic observations at high signal-to-noise ratio have been obtained for all DA and DB stars in the Kiso Schmidt ultraviolet excess survey (KUV stars). These observations led to the reclassification of several KUV objects, including the discovery of three unresolved DA+DB double degenerate binaries. The atmospheric parameters ($T_{\rm eff}$ and $\log g$) are obtained from detailed model atmosphere fits to optical spectroscopic data. The surface gravity distribution of our sample is characterized by a mean value of $\log g = 7.919$ and a dispersion of 0.282 dex, while the mean mass has a value of 0.605 $M_{\odot}$ and a dispersion of 0.135 $M_{\odot}$. Absolute visual magnitudes obtained from our spectroscopic fits allow us to derive an improved luminosity function for the DA stars in the Kiso survey. This luminosity function is found to be significantly different than earlier estimates based on empirical photometric calibrations of M_V for the same sample, particularly for the fainter magnitude bins. Our improved luminosity function now appears entirely consistent with that obtained for the PG survey using the same spectroscopic approach. We obtain a value for the total local space density of DA white dwarfs in the Kiso survey of 2.70×10^{-4} for $M_V \leq 12.75$. This value is about half the value found in the PG survey. The completeness of both the KUV and PG surveys is briefly discussed.

3.2 Introduction

White dwarf stars represent the final stage of stellar evolution for main sequence stars whose masses lie between 0.07 and 8 $M_{\odot}$, representing about 97% of the stars in the Galaxy. As the result of the cessation of nuclear reactions, they simply cool off while dissipating the content of their thermal reservoir. Because of these characteristics, the white dwarf luminosity function, the number of white dwarfs as a function of their intrinsic luminosity, is a powerful tool. The luminosity function is a measure of the space density of stars as a function of the absolute magnitude. It thus provides an estimate of the contribution of white dwarf stars to the density of matter in the Galaxy. When the luminosity function is derived from a com-

plete sample of white dwarfs, it contains information such as a direct measure of the stellar death rate in the local galactic disk. The comparison with theoretical evolutionary models (see, e.g., Fontaine et al. 2001) then allows us to measure the age of various components of the Galaxy. Likewise, the mass distribution contains information about the amount of mass lost during the evolution of an initial mass distribution (Liebert et al. 2005, hereafter LBH05).

Luminosity functions have been determined for cool white dwarfs discovered in high proper motion surveys, and for hot white dwarfs through UV color excess surveys. The cool end of the luminosity function was studied by Liebert et al. (1988) and Leggett et al. (1998), while the hot end was analyzed by Fleming et al. (1986) using white dwarfs identified in the Palomar-Green (PG) survey (Green et al. 1986) and by Darling (1994; see also Wegner & Darling 1994) using the Kiso Schmidt ultraviolet excess survey (KUV). LBH05 have recently improved upon the analysis of Fleming et al. (1986) by applying the spectroscopic method (Bergeron et al. 1992) to measure the effective temperatures and surface gravities of all the DA stars identified in the PG survey. The improved atmospheric parameters allowed a better determination of the absolute visual magnitude (M_V) of each star, and in turn the accuracy of the luminosity function calculation. More recently, a similar approach was applied by Harris et al. (2006) to a sample of 6000 white dwarfs (or white dwarf candidates) identified in the Sloan Digital Sky Survey (SDSS) Data Release 3. The luminosity function based on the SDSS extends to redder colors than the PG or Kiso surveys, but does not extend to low enough temperatures to cover the end of the white dwarf cooling sequence, although discoveries made through proper motion diagrams may soon change this picture (Kilic et al. 2006).

In order to measure the luminosity function of white dwarf stars, one needs to carefully define a statistically complete sample. This is a major endeavor, both for common proper motion or UV color excess surveys. Darling (1994) attempted to estimate the completeness of the PG and KUV surveys by counting the number of stars discovered in the overlapping fields of both surveys (see also Section 3.5.4 below). LBH05 discuss at length the completeness of the PG survey (their Section 4) by comparing their improved luminosity function based on

spectroscopic M_V values with the results of Darling (1994) for the KUV survey (see Figure 10 of LBH05). They evaluate the completeness of the PG survey to 75%, while Darling (1994) found a lower value of 58%. However, this comparison between the PG and the Kiso surveys is fundamentally flawed for at least two reasons. First, in the case of the PG survey, only DA stars are considered while for the Kiso survey, white dwarf stars of *all spectral types* are used in the calculation of the luminosity function. Second, and most importantly, the results of Darling (1994) are based on M_V values determined from empirical photometric calibrations; this is similar to the approach used by Fleming et al. (1986) for the PG survey.

In this paper, we present a study aimed at improving the luminosity function of white dwarf stars by applying the spectroscopic method to the DA stars identified in the Kiso survey. While our primary goal is to improve the comparison of the DA luminosity functions derived from the PG and Kiso surveys, we also provide an analysis of the global properties of the KUV sample and demonstrate how samples of relatively bright white dwarf stars still hide objects of significant astrophysical interest. Our sample drawn from the Kiso survey is presented in Section 3.3 and analyzed in Section 3.4 using the spectroscopic technique. The absolute visual magnitudes obtained from these accurate atmospheric parameter determinations are then used in Section 3.5 to calculate an improved luminosity function for these stars. A detailed comparison with the results of the PG survey is also presented. Our conclusions follow in Section 3.6.

3.3 Spectroscopic Content of the Kiso Survey

The Kiso Ultraviolet Excess Survey (KUV) was a photometric search for UV-excess objects, performed with the 105-cm Schmidt telescope at Kiso Observatory. A total of 1186 objects were found in 44 fields in a belt from the northern to the southern galactic pole at a galactic longitude of 180°. The fields of the survey have a mean limiting magnitude of $V = 17.7$ and cover a total area of 1400 square degrees (Noguchi et al. 1980; Kondo et al. 1984).

Our original goal was to secure optical spectroscopic observations for all white dwarfs in the

Kiso survey, regardless of their spectral type. Our starting point is the list of objects taken from Table 4.3 of Darling (1994). This list includes 234 white dwarfs identified in the Kiso survey, which at that point in time was only 94% completed (a total of about 250 white dwarfs was expected to be found after completion of the survey). Since cool white dwarfs are difficult to analyze without photometric data, we have decided to focus our attention towards the hot end of the sample and exclude from our spectroscopic survey all 15 cool white dwarfs of the DQ, DZ, and DC spectral types. We have thus retained a sample of 219 white dwarfs for follow-up spectroscopic observations. Optical spectra for the majority of the objects in this sample have been obtained with the Steward Observatory 2.3-m telescope equipped with the Boller & Chivens spectrograph and a Loral CCD detector. The 4.5" slit together with the 600 l mm^{-1} grating in first order provided a spectral coverage of $\lambda\lambda$3200–5300 at an intermediate resolution of $\sim$ 6 Å FWHM. The spectra for the remaining southern objects were obtained with the Carnegie Observatories' 2.5-m du Pont telescope at Las Campanas (Chile), equipped with the Boller & Chivens spectrograph and a Tektronic (Tek 5) CCD detector. The 1.5" slit and the 600 l mm^{-1} grating provided a spectral coverage of $\lambda\lambda$3500-6600 at a resolution of $\sim$ 3 Å FWHM. Exposure times were set to reach a signal-to-noise ratio (S/N) of at least 50.

The better resolution and higher S/N of our observations allowed us to revise the spectral classification of many objects in this first sample of 219 stars. At lower resolution, for instance, spectra of B subdwarfs can be easily confused with a DA star (see LBH05 for several examples). We found 30 objects in Darling's sample of DA and DB stars that turned out to be subdwarfs or main sequence stars, 23 of which have been reclassified as a result of our observations. These 30 objects are displayed in Figure 3.1 and reported in Table 3.1, together with references to the original reclassification. Worth mentioning in this figure is KUV 16032+1735, first identified as a magnetic DA white dwarf by Wegner & Swanson (1990). A closer examination of our spectrum reveals no sign of a magnetic field, however, and an attempt to fit this star with our DA model grid suggests an effective temperature above 100,000 K. An independent analysis of this object, which will be reported elsewhere, reveals that KUV 16032+1735 is actually a hot sdO star with $T_{\rm eff} = 84,000 \pm 7000$ K, $\log g = 6.7 \pm 0.2$,

and $\log N(\mathrm{He})/N(\mathrm{H}) = -1.9 \pm 0.2$. Additional white dwarfs identified in the KUV survey have also been observed as part our spectroscopic follow-up. These are listed in Table 3.2. None of these were part of the original data set used by Darling (1994), either because they had been discovered afterwards, or for reasons unknown to us. For instance, KUV 14161+2255 (DB) had been reported by Wegner & Swanson (1990) and should have been, in principle, part of Darling's analysis.

Representative DA and DB/DO spectra from our survey are displayed in Figures 3.2 and 3.3, respectively, in order of decreasing effective temperature, while magnetic DA white dwarfs are displayed in Figure 3.4. The He II λ4686 absorption feature is clearly visible in the spectrum of the DAO star KUV 03459+0037 shown in Figure 3.2. The spectrum for this star was obtained from the SDSS Data Release Web site.[2] Also shown in the same figure are representative DA stars with an unresolved M-dwarf companion (KUV 01162−2311, KUV 03036−0043, KUV 04295+1739); we have a total of six DA+dM systems in our survey. We also show in Figure 3.3 the spectrum of the DO star KUV 01018−1818 with a very strong He II λ4686 line. Also observed is the presence of Hβ in several DB stars in our sample (thus DBA stars). Discussed further below are three unresolved double-degenerate systems composed of DA+DB white dwarfs that exhibit both hydrogen and helium lines. One of these systems, KUV 02196+2816, has already been analyzed in detail by Limoges et al. (2009). The results for the other systems, KUV 03399+0015 and KUV 14197+2514, are presented in the next section.

Our final spectroscopic sample is thus the combination of the 219 hot white dwarf candidates from Darling (1994), minus the 30 misclassified objects listed in Table 3.1, to which we add the 7 additional white dwarfs listed in Table 3.2, for a total of 196 spectroscopically confirmed white dwarfs, three of which are unresolved double degenerates (thus a total of 199 white dwarfs). In summary, we thus have 175 DA stars (including one DAO and 4 magnetics), 23 DB stars, and one DO star. In this paper, we restrict our analysis to the DA stars; a similar analysis of the DO/DB stars in our sample will be reported elsewhere.

[2] http://www.sdss.org/dr7

3.4 Atmospheric Parameter Determination

Our model atmospheres and synthetic spectra for DA stars are described at length in LBH05 and references therein. These are pure hydrogen, plane-parallel model atmospheres. Non-local thermodynamic equilibrium (NLTE) effects are explicitly taken into account above $T_{\rm eff} = 20,000$ K and energy transport by convection is included in cooler models following the ML2/$\alpha = 0.6$ prescription of the mixing-length theory (see Bergeron et al. 1995). The theoretical spectra are calculated within the occupation formalism of Hummer & Mihalas (1988), which provides a detailed treatment of the level populations as well as a consistent description of bound-bound and bound-free opacities. Our fitting technique relies on the non-linear least-squares method of Levenberg-Marquardt (Press et al. 1986), which is based on a steepest descent method. The model spectra (convolved with a Gaussian instrumental profile) and the optical spectrum of each star are first normalized to a continuum set to unity. The calculation of χ^2 is then carried out in terms of these normalized line profiles only. Atmospheric parameters – $T_{\rm eff}$, $\log g$ – are considered free parameters in the fitting procedure. For DA+dM binaries, Hβ is simply removed from the χ^2 fit when the line is contaminated by the M-dwarf companion.

Atmospheric parameters for the 4 magnetic DA stars displayed in Figure 3.4 are taken from the literature: KUV 03292+0035 has a magnetic field of 12 MG (Jordan 1993) and an effective temperature of $T_{\rm eff} \sim 15,500$ K (Schmidt et al. 2003). The value of the magnetic field for KUV 08165+3741 is 9 MG (Angel et al. 1974) with $T_{\rm eff} \sim 11,000$ K according to Jordan (2001). Liebert et al. (1985) report 29 MG for KUV 23162+1220 and $T_{\rm eff} \sim 10,400$ K based on *IUE* data. Finally, KUV 23296+2642 has a magnetic field of 2.3 MG, with $T_{\rm eff} = 9400$ K and $\log g = 8.02$ (Bergeron et al. 2001). For the first three magnetic white dwarfs, we simply assume $\log g = 8$.

The DA white dwarfs concealed in DA+DB unresolved double degenerate systems require a special treatment. The first such system discovered in our survey, KUV 02196+2816, was spectroscopically identified as a DBA star by Darling & Wegner (1996) but should have been

classified as a DAB star since the hydrogen lines are actually stronger than the helium lines. Limoges et al. (2009) showed that the optical spectrum of this object cannot be reproduced by assuming model atmospheres with a homogeneous hydrogen and helium composition, or even stratified atmospheres, and that the hydrogen and helium lines observed in the spectrum of KUV 02196+2816 can be perfectly reproduced by assuming a double degenerate binary composed of a DA star and a DB star. In this case the predicted spectrum is obtained by combining pure hydrogen and pure helium model spectra, weighted by their respective radius. The detailed analysis yields $T_{\rm eff} = 27,170$ K and $\log g = 8.09$ for the DA star, and $T_{\rm eff} = 36,340$ K and $\log g = 8.09$ for the DB star. We have identified two additional systems in our spectroscopic survey, KUV 03399+0015 and KUV 14197+2514. KUV 03399+0015 was first identified as a DA? by Darling & Wegner (1994), and later as a DAB by Eisenstein et al. (2006), while KUV 14197+2514 has been classified as a DBA star by Wegner & Swanson (1990). An analysis similar to that of KUV 02196+2816 of these two objects reveals that both spectra cannot be reproduced with single-star models, and that the hydrogen and helium line profiles can only be explained by assuming a composite DA+DB double degenerate model. Figure 3.5 summarizes our results for the three systems. A more detailed analysis of these binaries will be presented elsewhere (Limoges & Bergeron 2009, in preparation).

The atmospheric parameters for the 175 DA white dwarfs in our sample — 172 single stars and the three DA components from Figure 3.5 — are reported in Table 3.3. The values in parentheses represent the uncertainties of each parameter, calculated by combining the internal error obtained from the covariance matrix and the external error estimated at 1.2% in $T_{\rm eff}$ and 0.038 dex in $\log g$ (see LBH05 for details). The stellar mass (M) and uncertainty are derived from the carbon-core evolutionary models of Wood (1995) with thick hydrogen layers of $q({\rm H}) \equiv \log M_{\rm H}/M_\star = 10^{-4}$. These models are also used to compute the white dwarf cooling time ($\log \tau$, where τ is measured in years). The absolute visual magnitude (M_V) and luminosity (L) of each star are calculated using the prescription of Holberg & Bergeron (2006)[3], while the apparent V magnitudes are taken from the catalog of McCook & Sion (2006). The

[3]See http://www.astro.umontreal.ca/~bergeron/CoolingModels.

$1/v_{\rm max}$ value corresponds to the maximum volume in which it is possible to find a particular white dwarf given an limiting apparent V magnitude of the survey; this will be discussed further in Section 3.5. Note that the $1/v_{\rm max}$ value is provided only for white dwarfs in our statistically complete sample defined below.

The global properties of the DA stars in the KUV sample are summarized in Figure 3.6 in a mass versus effective temperature diagram. This figure indicates that the majority of our DA stars have effective temperatures between $T_{\rm eff} \sim 10,000$ K and 25,000 K. Only 12 stars in our sample have temperatures below 10,000 K; the coolest star in our sample is KUV 23235+2536 with $T_{\rm eff} = 5700$ K. An examination of Figure 3.6 reveals the well-known problem where the spectroscopic masses for DA stars show a significant increase below $T_{\rm eff} \sim 13,000$ K (see also LBH05). Various explanations have been proposed to account for this phenomenon (Bergeron et al. 2007), although none of these appear completely satisfactory to this date. The $\log g$ and mass distributions are shown in Figure 3.7 for the 134 DA stars above 13,000 K. The $\log g$ distribution has a mean value of $\log g = 7.919$ with a dispersion of 0.282 dex, while the mass distribution shows a peak value centered at 0.55 $M_{\odot}$ and a mean mass of 0.605 $M_{\odot}$ with a dispersion of 0.135 $M_{\odot}$. These mass values are virtually identical to those obtained by LBH05 for the PG sample (0.603 and 0.134 $M_{\odot}$, respectively).

3.5 Luminosity Function

3.5.1 General Considerations

We can now proceed to calculate the luminosity function of DA stars in the Kiso survey. Since we will compare our results with those of Darling (1994) and with the PG survey (LBH05), it is relevant to provide here some details of how these calculations are performed. The luminosity function is obtained following the $1/v_{\rm max}$ method, originally developed by Schmidt (1968) in the context of quasars. This method requires that we determine for each star the maximum volume, $v_{\rm max}$, in which the object would have been detected given the limiting magnitude of the survey. The distance to each star can be directly obtained from the apparent and absolute

V magnitudes. Since the stars are not uniformly distributed in the direction perpendicular to the galactic disk, but instead follow an exponential disk, we define a weighted volume $dv' = \exp(-z/z_0)\, dv$, where $z = r \sin\theta$ is the distance of the object from the galactic plane, z_0 is the Galactic disk scale height, and θ is the absolute value of the galactic latitude of the object. Here we assume $z_0 = 250$ pc as in LBH05.

The Kiso survey is a magnitude-limited survey, which implies that it must be complete down to a given limiting magnitude $V_{\rm lim}$. For a given star with a magnitude V, $V_{\rm lim}$ defines a maximum distance $d_{\rm max}$ at which an object could have been observed and still have been found in the survey. This in turn defines the maximum volume, $v_{\rm max}$. As mentioned in Green (1980), however, each photographic plate has a different limiting magnitude. It is then proposed to define a maximum volume for each field. The total maximum volume for a given star is thus the sum of all the small individual volumes. Also, in the case where two fields or more overlap, the area of overlap is given to the field with the fainter limiting magnitude. We finally obtain for each star

$$v_{\rm max} = \sum_{j=1}^{n_f} \frac{\omega_j}{4\pi} \int_0^{d_{\rm max}} e^{-z/z_0}\, 4\pi r^2 dr \tag{3.1}$$

where n_f is the total number of fields. Since ω_j represents the area covered by each field, $\sum_{j=1}^{n_f} \omega_j$ must be equal to the total area covered by the survey (in steradians). The limiting magnitude can be calculated following the $v/v_{\rm max}$ test of uniformity of Schmidt (1968). The method states that a sample is complete when the average value of $v/v_{\rm max}$ is equal to 0.5. Once the value of $V_{\rm lim}$ that satisfies this constraint has been found, all white dwarfs with V fainter than $V_{\rm lim}$ must be removed from the sample. The remaining stars define the complete sample from which the luminosity function can be derived.

Since $v_{\rm max}$ represents the volume within which it is possible to find a particular white dwarf, the contribution of each star to the local space density is then simply given by $1/v_{\rm max}$ (Schmidt 1968). The differential luminosity function as a function of M_V can finally be obtained by summing all the individual contributions to the local space density:

$$\phi(M_V) = \sum_{i=1}^{n_b} 1/v_{\max_i} \tag{3.2}$$

where n_b is the number of stars in each magnitude bin of the complete sample. The uncertainties are evaluated as if the stars were distributed randomly in space. The statistical uncertainty in each bin is then given by $\sigma_\phi = [\sum_{i=1}^{n_b} (1/v_{\max_i})^2]^{1/2}$ (Boyle 1989).

3.5.2 The Luminosity Function from Darling (1994)

In the next section, we will compare our luminosity function of DA stars based on spectroscopic estimates of M_V with the results of Darling (1994) based on empirical photometric calibrations of M_V. Prior to this, we must first demonstrate that we are able to reproduce the luminosity function displayed in his Figure 3.2 (also reproduced in Figure 10 of LBH05) using the V and M_V values provided in his Table 3.3. Note in this case that the luminosity function is calculated using all 234 white dwarf stars identified in the Kiso survey, all spectral types included. His method is identical to that described above with the only exception that there is no explicit sum over all fields in equation (1). Instead, the area of each field is assumed to be constant, in which case a single factor $\omega/4\pi$ appears in the equation, where ω for the Kiso survey is 1400 square degrees (or ~ 0.43 steradians). We know that in Wegner & Darling (1994), the luminosity function was scaled by a certain factor to account for the fact that the Kiso survey was not complete at that time. In Darling (1994), this factor had a value of 1186/1115 since the Kiso survey was only 94% complete. This correction factor is included in all our calculations below.

The comparison of the results between Darling's calculations and ours using the same stars, as well as V and M_V values, is displayed in Figure 3.8. Both functions have the same exact shape but ours is scaled downwards by a factor of ~ 2.5, which suggests a constant correction factor between both calculations. We also note that our calculation of the limiting magnitude of the survey using this sample agrees perfectly with the value obtained by Darling, $V_{\rm lim} = 17.35$. As it is not stated explicitly in Darling (1994) that his luminosity function contains a correction factor (to account for other types of incompleteness, for instance), we ignore the source of

the difference between our calculations and Darling's and use our method of calculation in the remainder of this paper[4]. We must finally mention that the code we are using here is the same as that used by LBH05 so the comparisons discussed below will be entirely consistent.

3.5.3 An Improved Luminosity Function for KUV White Dwarfs

The main goal of our spectroscopic survey is to improve upon the luminosity function of Darling (1994) by using spectroscopic values of M_V rather than empirical photometric calibrations. The absolute magnitudes are central to the calculation of the luminosity function and it is crucial to measure M_V values as accurately as possible. In Darling (1994), M_V values were assigned for 125 stars (out of 234) with measured $(B-V)$ using empirical $(B-V)-M_V$ relations derived by Sion & Liebert (1977) and Dahn et al. (1982) for hot and cool white dwarfs, respectively. Additional M_V values for 9 objects were directly taken from McCook & Sion (1987). Finally, a linear fit based on measured photometric $(B-V)$ and photographic $(m_U - m_G)$ color indices was then used to assign approximate $(B-V)$ values, and thus M_V values, to the remaining 100 stars without $(B-V)$ or M_V measurements. In reality, this relation is far from being linear and a substantial dispersion is present in the data (see Figure 4.1 of Darling 1994), potentially introducing a significant uncertainty in the M_V estimates.

Our spectroscopic M_V values taken from Table 3.3 are compared in Figure 3.9 with those derived by Darling (1994) for the 170 DA stars in common. In doing so, we explicitly exclude from Darling's sample all objects that have been spectroscopically misclassified in the Kiso survey (Table 3.1 and Figure 3.1). The differences observed are quite significant, with the empirical estimates being generally fainter than the spectroscopic values. In some cases, the differences can reach 2 to 3 magnitudes, and even 4 magnitudes in the most extreme case. It is therefore expected that the corresponding luminosity functions based on these absolute magnitudes will be affected as well.

With the spectroscopic M_V values for our sample of 175 DA stars defined in Table 3.3, we can

[4]We also contacted G.W. Darling directly and attempted to figure out the discrepancy but the original calculations are lost in the sands of time.

now proceed to the evaluation of the luminosity function. The first step is to find the limiting magnitude of the survey following the $v/v_{\rm max}$ method described above. We find $V_{\rm lim} = 17.39$, which defines a complete sample of 145 DA stars. This sample is indicated in Table 3.3 by a value of $1/v_{\rm max}$ in the appropriate column (otherwise the field is empty). The luminosity function is then simply computed by summing these values in appropriate bins (see equation 2), in this case half-magnitude bins.

To compare our results with those of Darling (1994), we use the same subset of 170 DA stars displayed in Figure 3.9 (where misclassified objects have been removed from Darling's sample). Even though the stars used in the comparison are the same, the absolute magnitudes in each sample are different, and so are the limiting magnitudes. We find using Darling's M_V values a limiting magnitude of $V_{\rm lim} = 17.35$, which defines a complete sample of 141 DA stars, while our spectroscopic M_V values yield $V_{\rm lim} = 17.40$ for a complete sample of 140 objects. The corresponding luminosity functions are compared in Figure 3.10. Despite the large differences in M_V values observed in Figure 3.9, the differences in the luminosity functions do not appear as significant. A similar conclusion was reached by LBH05 when comparing the luminosity function of PG stars with the earlier estimates of Fleming et al. (1986). We must note that the main effect here is to shift the number of stars from one bin to another. For instance, the largest difference observed is at the faint end of the luminosity function where our determination based on spectroscopic M_V values is lower than that of Darling. Indeed, a lot of the objects in these magnitude bins in Darling's analysis have been shifted to brighter bins as a result of his overestimates of M_V values (see Figure 3.9). As a consequence, we note the complete absence of stars in our $M_V = 14.5$ bin, while the 13.5 and 14.0 bins are populated by only 2 stars and 1 star, respectively.

With this improved luminosity function for the DA stars in the Kiso survey, it is now possible to make a detailed comparison with that obtained by LBH05 for the DA stars in the PG survey, which is based on the exact same analysis, including model atmospheres, observing setup, fitting technique, and luminosity function calculations. As mentioned explicitly in LBH05,

their luminosity function did not undergo any correction, as is the case with ours. It is then possible to compare the results from both functions directly. The comparison is presented in Figure 3.11. The first result is that both luminosity functions agree much better than estimated by LBH05, who concluded, based on the results shown in their Figure 10, that "the KUV luminosity function has significantly more stars than PG in the bins M_V 10.5 to 13.0, with the PG appearing to become incomplete by a factor of 4 in the 12.0 and the two fainter magnitude bins". The comparison shown here indicates on the contrary that both functions agree perfectly within the error bars. It is perhaps not surprising that the luminosity functions from the PG and Kiso surveys are so similar, since the detection method is the same (UV excess). So whatever incompleteness factors affect the PG survey seem to affect the Kiso survey as well.

Another way to compare both luminosity functions is to calculate the local space densities of white dwarfs, which can be simply obtained by integrating the luminosity function over a given range of M_V. We find a total local space density of white dwarfs of 5.40×10^{-4} pc^{-3}. For $M_V \leq 12.75$, we obtain 2.70×10^{-4} pc^{-3} while LBH05 report a value of $5.0 \pm 0.5 \times 10^{-4}$ in the same magnitude interval. The Kiso survey thus appears to be less complete than the PG survey in that range of absolute visual magnitude. The Kiso survey is certainly deeper than PG, and it should thus be more complete for fainter magnitude bins since the PG survey is known to be fairly incomplete at the faint end of the luminosity function (LBH05). We note, however, that the differences do not appear as large as previously estimated by LBH05, as discussed above.

3.5.4 Completeness of the PG and Kiso Surveys

By counting the number of KUV white dwarfs (all spectral types included) found by the PG survey in the overlapping fields (600 square degrees of overlap) and within the magnitude limit of the PG survey, Darling (1994) estimated the completeness of the PG survey to 57.5%, or 60.5% if white dwarfs not in the statistically complete PG sample are also included. However, as discussed in Section 2, many KUV white dwarfs turn out to be lower gravity objects. A similar estimate of the completeness of the PG survey based only on the spectroscopically

confirmed DA stars yields a value of 67.7%.

Darling (1994) also used the PG survey to estimate the completeness of the Kiso survey by turning the problem around, and by counting the number of PG stars in the overlapping fields, all spectral types included, that were actually missed in the Kiso survey. While the Kiso survey is much deeper ($V_{\rm lim} \sim 17.35$) than the PG survey ($V_{\rm lim} \sim 16.16$), only 74.2% of the white dwarfs in the overlapping fields of the PG survey were recovered in the Kiso survey! Since none of the new KUV stars (Table 3.2) are part of the PG sample, this estimate is still valid. Once again, using only our spectroscopically confirmed sample of DA stars, we find instead a value of 86.6% for the completeness of the Kiso survey. Given the results shown in Figure 3.11, it is likely that both the PG and Kiso surveys suffer from a comparable level of incompleteness. We refer the reader to the additional discussion of LBH05 (Section 4) regarding the completeness of the PG survey. Obviously, deeper and more complete surveys are still badly needed.

The Sloan Digital Sky Survey (SDSS) is certainly among the most important developments in the last few years in terms of observational data of white dwarf stars since the PG survey. The SDSS is looking at 10,000 deg^2 of high-latitude sky in five bandpasses ($ugriz$) and is producing images in these five bandpasses from which galaxies, quasars, and stars are selected for follow-up spectroscopy. The selection effects in this survey are important, as discussed in Kleinman et al. (2004) and Eisenstein et al. (2006), and therefore, it cannot be considered as a complete survey in any sense. For instance, DeGennaro et al. (2008) found a completeness of 51% for their uncorrected sample of white dwarfs from the SDSS, which is mainly composed of DA stars. Also, the S/N of the SDSS spectra is known to be proportional to the brightness of the object, since the integration time is fixed. This can lead to large uncertainties in the determination of the atmospheric parameters of fainter objects (Gianninas et al. 2005). Finally, as mentioned in Eisenstein et al. (2006), "completeness is not our goal", since they know that white dwarfs with $T_{\rm eff} \lesssim 8000$ K are lost because of the color-cut, and that magnetic white dwarfs can pass through the detection system without being noticed. DeGennaro et al.

(2008) are in possession of a much larger sample than ours, which allows them to divide their luminosity function into several mass components. However, when conducting a statistical analysis of a sample, the completeness of this sample should be a crucial parameter if the results are to be interpreted physically.

3.6 Conclusion

Our spectroscopic survey of white dwarfs in the Kiso survey has led to an important spectral reclassification of the sample published in Darling (1994). In particular, we have identified three unresolved double degenerate binaries. A two-component fit confirmed that KUV 02196+2816, KUV 03399+0015, and KUV 14197+2514 are unresolved double degenerate binaries composed of a DA and a DB star.

We then proceeded to the analysis of DA white dwarfs in the KUV sample, where the atmospheric parameters were determined from detailed model atmosphere fits to optical spectroscopic data. The DA stars found in the Kiso survey are characterized by a mean surface of gravity of $\log g = 7.919$ and a mean mass of 0.605 $M_{\odot}$. These values are consistent with the values found for the DA stars in the PG sample. The M_V values derived from the atmospheric parameters were compared with those of Darling (1994), which were obtained from photometric empirical calibrations. The differences were found to be significant, but had a somewhat smaller impact on the calculation of the luminosity function.

We then derived the luminosity function of DA stars from the Kiso survey. We find as a result of our improved M_V values a smaller number of stars in the fainter magnitude bins than estimated by Darling (1994). The comparison of our luminosity function with that of LBH05 reveals that both functions are similar. We obtained a total local space density of white dwarfs of 5.40×10^{-4} pc^{-3}, while this number drops to 2.70×10^{-4} pc^{-3} for $M_V \leq 12.75$. Our results are lower that those published in LBH05 for the PG survey. The completeness of the PG sample of DA stars determined from the KUV sample of DA stars is estimated at 67.7%. On the other hand, the comparison between the KUV and PG samples of DA white dwarfs

reveals a completeness of 86.6% for the brighter magnitude bins. For the fainter magnitude bins, the completeness of both surveys appears comparable.

This era of large scale surveys where the samples can contain up to thousands of stars will certainly help us in the characterization of our Galaxy. Accurate statistical analyses will then provide even more precise determinations of, for example, the white dwarf space densities in the different populations of the Galaxy, the stellar contribution to the mass of the Galaxy, the age of the local galactic disk, the stellar formation and death rates, etc. The issue of completeness is thus of great importance when statistical analyses of these samples are considered.

We would like to thank the director and staff of Steward Observatory for the use of their facilities. We would also like to thank M. Latour for the fit of KUV 16032+1735, and A. Gianninas for a careful reading of this manuscript. This work was supported in part by the NSERC Canada and by the Fund FQRNT (Québec). P.B. is a Cottrell Scholar of Research Corporation for Science Advancement.

3.7 References

Achilleos, N., & Wickramasinghe, D.T. 1989, ApJ, 346, 444

Angel, J.R.P., Carswell, R., Strittmatter, P.A., Beaver, E.A., & Harms, R. 1974, ApJ, 194, L47

Bergeron, P., Gianninas, A., & Boudreault, S. 2007, in Proc. 15th European Workshop on White Dwarfs, ed. R. Napiwotzki & M. Burleigh (San Francisco: ASP), 372, 29

Bergeron. P., Leggett, S.K., & Ruiz, M.T. 2001, ApJS, 133, 413

Bergeron, P., Saffer, R.A., & Liebert, J. 1992, ApJ, 394, 247

Bergeron, P., Wesemael, F., Lamontagne, R., Fontaine, G., Saffer, R.A., & Allard, N.F. 1995, ApJ, 449, 258

Boyle, B.J. 1989, MNRAS, 240, 533

Dahn, C.C., Harrington, R.S., Riepe, B.Y, Christy, J.W., Guetter, H.H., Kallarakal, V.V., Miranian, M., Walker, R.L., Vrba, F.J., Hewitt, A.V., Durham, W.S., & Ables, H.D. 2001, AJ, 87, 419

Darling, G.W. 1994, PhD thesis, Dartmouth College

Darling, G.W., & Wegner, G. 1994, ApJ, 108, 2025

Darling, G.W., & Wegner, G. 1996, ApJ, 111, 685

DeGennaro, S., von Hippel, T., Winget, D.E., Kepler, S.O., Nitta, A., Koester, D., & Althaus, L. 2008, AJ, 135, 1

Eisenstein, D.J., et al. 2006, ApJS, 167, 40

Fleming, T.A, Liebert, J., & Green, R.F. 1986, ApJ, 308, 176

Fontaine, G., Brassard, P., & Bergeron, P. 2001, PASP, 113, 409

Gianninas, A., Bergeron, P., & Fontaine, G. 2005, ApJ, 631, 1100

Green, R.F. 1980, ApJ, 238, 685

Green, R. F., Schmidt, M., & Liebert, J. 1986, ApJS, 61, 305

Harris, H.C., et al. 2006, AJ, 131, 571

Holberg, J.B., Barstow, M.A., & Burleigh, M.R. 2003, ApJS, 147, 145

Holberg, J.B., & Bergeron, P. 2006, ApJ, 132, 1221

Hummer, D.G., & Mihalas, D. 1988, ApJ, 331, 794

Jordan, S. 1993, in White Dwarfs: Advances in Observation and Theory, NATO ASI Series, ed. M. A. Barstow (Dordrecht: Kluwer Academic Publishers), 333

Jordan, S. 2001, in ASP Conf. Ser. Vol.226, 12th European Workshop on White Dwarfs, eds. J. L. Provencal, H. L. Shipman, J. MacDonald, & S. Goodchild, 269

Kawka, A., & Vennes, S. 2005, in ASP Conf. Ser. Vol.334, 14th European Workshop on White Dwarf Stars, eds. Koester, D., Moehler, S., 101

Kawka, A., Vennes, S., & Thorstensen, J.R. 2004, AJ, 3, 1702

Kidder, K.M. 1991, PhD thesis, University of Arizona

Kilic, M., Munn, J.A., Harris, H.C., Liebert, J., von Hippel, T., Williams, K.A., Metcalfe, T.S., Winget, D.E., & Levine, S.E. 2006, AJ, 131, 582

Kleinman, S.J., et al. 2004, ApJ, 607, 426

Kondo, M., Noguchi, T., & Maehara, H. 1984, Ann. Tokyo Astron. Obs., 20, 130

Lamontagne, R., Demers, S., Wesemael, F., Fontaine, G., & Irwin, M.J. 2000, AJ, 119, 241

Leggett, S.K., Ruiz, M.T., & Bergeron, P. 1998, ApJ, 497, 294

Liebert, J., Bergeron, P., & Holberg, J.B. 2005, ApJ, 156, 47 (LBH05)

Liebert, J., Dahn, C.C., & Monet, D.G. 1988, ApJ, 332, 891

Liebert, J., Schmidt, G.D., Sion, E.M., Starrfield, S.G., Green, R.F., & Boroson, T.A. 1985, PASP, 97, 158

Limoges, M.-M., Bergeron, P., & Dufour, P. 2009, ApJ, 696, 1461

Lisker, T., Heber, U., Napiwotzki, R., Christlieb, N., Han, Z., Homeier, D., & Reimers, D. 2005, A&A, 430, 223

McCook, G.P., & Sion, E.M. 1987, ApJS, 65, 603

McCook, G.P., & Sion, E.M. 2006, VizieR Online Data Catalog, 3235

Noguchi, T., Maehara, H., & Kondo, M. 1980, Ann. Tokyo Astron. Obs., 18, 55

Press, W. H., Flannery, B. P., Teukolsky, S. A., & Vetterling, W. T. 1986, Numerical Recipes (Cambridge: Cambridge University Press)

Schmidt, M. 1968, ApJ, 151, 393

Schmidt, G.D., et al. 2003, ApJ, 595, 1101

Sion, E.M., & Liebert, J. 1977, ApJ, 213, 468

Stroeer, A., Heber, U., Lisker, T., Napiwotzki, R., Dreizler, S., Christlieb, N., & Reimers, D. 2007, A&A, 462, 269

Wagner, M.R., Sion, E.M., Liebert, J., Starrfield, S.G., & Zotv, N. 1986, PASP, 98, 552

Wegner, G., & Darling, G. W. 1994, in Stellar and Circumstellar Astrophysics, eds. G. Wallerstein & A. Noriega-Crespo, ASP Conf. Series No. 57 (San Francisco CA: Astronomical Society of the Pacific), 178

Wegner, G., & Swanson, S.R. 1990, AJ, 99, 330

Wood, M. A. 1995, in 9th European Workshop on White Dwarfs, NATO ASI Series, eds. D. Koester & K. Werner (Berlin: Springer), 41

3.8 Tables

TAB. 3.1 – Misclassified Objects in the KUV Survey

KUV	WD	Old	New	Notes
00486−2016	0048−202	DA	sdB	1
01098−2629	0109−264	DA	sdB	1
01134−2423	0113−243	DA	sdB	2
01542−0710	0154−071	DA?	sdB	1
02222+3124	0222+314	DA	sdB	2
02409+3407	0240+341	DA	MS	2
04473+1737	0447+176	DB	sdOB	2
05097+1649	0509+168	DA	MS	3
05101+1619	0510+163	DA	MS	2
05260+2711	0526+271	DA	sdB	2
05296+2610	0529+261	DA	sdB	2
06274+2958	0627+299	DA	sdB	2
06289+3126	0628+314	DA	sdB	2
07528+4113	0752+412	DA?	sdB	2
09272+3854	0927+388	DA	sdB	2
09306+3740	0930+376	DA	sdB	2
09327+3937	0932+396	DA	sdB	2
09339+3821	0933+383	DA	sdB	4
09372+3933	0937+395	DA	sdB	2
09436+3709	0943+371	DA	sdB	2
09467+3809	0946+381	DA	sdB	2
12562+2839	1256+286	DA?	sdB	2
13024+2824	1302+284	DA	sdB	4, 5
13023+3145	1302+317	DB	sdOB	2
13046+3118	1304+313	DA	sdB	2
16032+1735	1603+175	DA	sdO	2
16118+3906	1611+390	DA	sdB	2
18169+6643	1816+667	DB	sdOB	2
22585+1533	2258+155	DB	sdO	6
23099+2548	2309+258	DA	sdB	2

Note. – (1) Lisker et al. 2005; (2) this work; (3) Kawka et al. 2004; (4) Not in McCook and Sion; (5) Holberg et al. 2003; (6) Stroeer et al. 2007.

TAB. 3.2 – Additional KUV White Dwarfs

KUV	WD	ST	Reference
01018−1818	0101−182	DO	Lamontagne et al. (2000)
03439−0048	0343−007	DA	Wagner et al. (1986)
03459+0037	0345+006	DAO	Eisenstein et al. (2006)
08422+3813	0842+382	DA	Kawka & Vennes (2005)
14161+2255	1416+229	DB	Wegner & Swanson (1990)
18004+6836	1800+685	DA	Kidder (1991)
18453+6819	1845+683	DA	Kidder (1991)

TAB. 3.3 – Atmospheric Parameters of DA Stars from the KUV Sample

KUV	WD	$T_{\rm eff}$	(K)	$\log g$	$M/M_\odot$	M_V	$\log L/L_\odot$	V	D(pc)	$1/v_{\rm max}$	$\log\tau$	Notes
00300−1810	0030−181	13,640	(362)	7.81 (0.06)	0.51 (0.03)	11.14	−2.17	16.36	135	1.74(−6)	8.39	
00328−1735	0032−175	9830	(142)	8.18 (0.05)	0.71 (0.03)	12.49	−2.96	14.88	30	9.68(−6)	8.96	
00329−1747	0032−177	16,600	(276)	7.86 (0.05)	0.54 (0.03)	10.85	−1.85	15.90	93	1.22(−6)	8.13	
00334−1738	0033−176	22,890	(476)	7.92 (0.06)	0.59 (0.03)	10.37	−1.32	17.60	279	—	7.62	
00337−1749	0033−178	24,150	(580)	7.20 (0.08)	0.37 (0.02)	9.01	−0.71	17.70	548	—	7.39	
00442−2156	0044−219	11,840	(205)	7.81 (0.07)	0.50 (0.04)	11.40	−2.42	17.26	148	2.40(−6)	8.55	
00582−1834	0058−185	17,790	(334)	7.95 (0.06)	0.59 (0.03)	10.86	−1.78	17.26	190	1.23(−6)	8.10	
01024−1836	0102−185	72,520	(1739)	7.15 (0.08)	0.48 (0.02)	7.07	+1.36	16.90	923	2.53(−8)	5.08	
01071−1917	0107−192	14,640	(255)	7.80 (0.05)	0.50 (0.03)	10.99	−2.04	16.30	115	1.44(−6)	8.28	
01138−2431	0113−245	58,430	(2102)	7.54 (0.13)	0.53 (0.04)	8.13	+0.65	17.67	810	—	6.11	
01157−2546	0115−257	14,900	(264)	7.91 (0.05)	0.57 (0.03)	11.12	−2.08	16.90	142	1.69(−6)	8.32	
01162−2311	0116−231	31,490	(490)	7.63 (0.06)	0.49 (0.02)	9.24	−0.56	16.46	189	1.90(−7)	6.92	1
01246−2546	0124−257	24,000	(391)	7.66 (0.05)	0.47 (0.02)	9.88	−1.07	16.37	143	3.86(−7)	7.35	
01308−2721	0130−273	22,550	(375)	7.85 (0.05)	0.56 (0.03)	10.30	−1.30	16.93	212	6.29(−7)	7.58	
01491−1127	0149−114	9070	(136)	7.95 (0.08)	0.57 (0.04)	12.45	−2.97	16.48	67	9.19(−6)	8.90	
01498−1227	0149−124	12,130	(198)	8.26 (0.05)	0.77 (0.04)	11.99	−2.64	16.51	110	5.07(−6)	8.78	
01518−0928	0151−094	26,080	(465)	7.66 (0.06)	0.48 (0.02)	9.71	−0.92	17.67	396	—	7.21	
01552−0703	0155−070	10,690	(165)	8.09 (0.06)	0.66 (0.04)	12.06	−2.76	16.35	67	5.55(−6)	8.81	
01595−1109	0159−111	11,100	(174)	8.19 (0.06)	0.72 (0.04)	12.11	−2.76	16.81	90	5.92(−6)	8.84	
02185+2923	0218+293	17,190	(294)	8.14 (0.05)	0.70 (0.03)	11.20	−1.96	17.50	181	—	8.30	
02196+2816	0219+282	27,170	(326)	8.09 (0.04)	0.69 (0.03)	10.28	+0.00	18.22	361	—	7.25	2
02245+3145	0224+317	14,550	(330)	7.77 (0.06)	0.49 (0.03)	10.96	−2.03	16.93	154	1.39(−6)	8.27	
02292+2704	0229+270	24,160	(368)	7.90 (0.05)	0.58 (0.02)	10.24	−1.21	15.58	117	5.86(−7)	7.48	
02295+3529	0229+354	12,860	(385)	7.78 (0.07)	0.49 (0.04)	11.21	−2.26	16.90	137	1.89(−6)	8.45	
02306+3420	0230+343	14,600	(242)	7.85 (0.05)	0.53 (0.03)	11.06	−2.07	16.00	97	1.57(−6)	8.31	
02386+3322	0238+333	13,390	(276)	8.23 (0.05)	0.75 (0.04)	11.78	−2.45	15.90	66	3.88(−6)	8.65	
02464+3239	0246+326	11,580	(170)	8.13 (0.05)	0.69 (0.03)	11.90	−2.65	15.57	60	4.52(−6)	8.75	
02503−0238	0250−026	14,740	(241)	7.87 (0.05)	0.54 (0.03)	11.08	−2.07	14.75	53	1.61(−6)	8.31	
03036−0043	0303−007	18,700	(387)	7.97 (0.06)	0.61 (0.04)	10.80	−1.71	16.21	120	1.14(−6)	8.05	1
03106−0719	0310−073	17,330	(315)	7.91 (0.05)	0.57 (0.03)	10.84	−1.80	16.67	148	1.20(−6)	8.10	

TAB. 3.3 – Continued

KUV	WD	$T_{\rm eff}$	(K)	$\log g$	$M/M_\odot$	M_V	$\log L/L_\odot$	V	D(pc)	$1/v_{\rm max}$	$\log\tau$	Notes
03123+0155	0312+019	41,350	(867)	7.88 (0.08)	0.62 (0.04)	9.18	−0.23	17.47	462	—	6.57	
03184−0211	0318−021	12,800	(217)	7.93 (0.05)	0.57 (0.03)	11.43	−2.36	16.01	82	2.49(−6)	8.52	
03205−0005	0320−000	13,180	(499)	7.73 (0.07)	0.47 (0.03)	11.09	−2.19	16.97	150	1.63(−6)	8.40	
03217−0240	0321−026	26,430	(521)	8.45 (0.08)	0.91 (0.05)	10.93	−1.41	17.67	222	—	7.92	
03290+0053	0328+008	34,610	(560)	7.92 (0.07)	0.62 (0.03)	9.51	−0.58	16.80	286	2.55(−7)	6.81	
03292+0035	0329+005	15,500	(296)	8.00 (0.06)	0.62 (0.04)	11.18	−2.06	16.70	127	1.82(−6)	8.33	3
03295−0108	0329−011	17,240	(313)	7.73 (0.06)	0.48 (0.03)	10.61	−1.71	17.17	205	9.09(−7)	7.99	
03301−0100	0330−009	33,410	(500)	7.91 (0.05)	0.61 (0.03)	9.56	−0.63	15.86	182	2.70(−7)	6.86	
03302−0143	0330−017	30,290	(460)	7.84 (0.05)	0.57 (0.03)	9.65	−0.76	17.12	311	2.98(−7)	7.00	
03351+0245	0335+027	15,900	(288)	7.96 (0.05)	0.59 (0.03)	11.07	−1.99	17.37	184	—	8.27	
03363+0400	0336+040	8840	(130)	8.17 (0.06)	0.70 (0.04)	12.87	−3.14	16.74	40	1.59(−5)	9.08	
03383−0146	0338−017	20,420	(369)	8.15 (0.05)	0.72 (0.03)	10.92	−1.66	17.53	209	—	8.07	
03399+0015	0339+002	13,680	(164)	7.97 (0.04)	0.59 (0.03)	11.35	+0.00	17.73	178	—	8.39	2
03416+0206	0341+021	22,190	(338)	7.44 (0.05)	0.41 (0.01)	9.62	−1.04	15.84	172	2.88(−7)	7.62	
03439−0048	0343−007	64,690	(1408)	7.56 (0.07)	0.56 (0.02)	8.03	+0.83	14.91	237	5.70(−8)	5.96	4
03442+0719	0344+073	10,930	(164)	7.84 (0.06)	0.51 (0.03)	11.62	−2.58	16.10	78	3.17(−6)	8.65	
03459+0037	0345+006	72,590	(3457)	7.02 (0.14)	0.40 (0.04)	6.71	+1.42	16.00	721	1.93(−8)	7.18	4, 5
03463−0108	0346−011	41,190	(766)	9.15 (0.07)	1.27 (0.03)	11.55	−1.19	14.28	31	2.90(−6)	8.00	
03521+0150	0352+018	21,950	(347)	7.93 (0.05)	0.59 (0.03)	10.45	−1.39	15.63	89	7.51(−7)	7.70	
03520+0500	0352+049	36,450	(594)	8.72 (0.06)	1.08 (0.03)	10.82	−1.05	16.29	118	1.17(−6)	7.73	
03520+0515	0352+052	10,280	(151)	8.10 (0.06)	0.66 (0.04)	12.20	−2.84	16.53	54	6.65(−6)	8.86	
03522+0737	0352+076	11,490	(183)	8.04 (0.06)	0.63 (0.04)	11.78	−2.61	16.75	99	3.88(−6)	8.70	
03526+0939	0352+096	14,030	(341)	8.19 (0.05)	0.73 (0.03)	11.64	−2.35	14.52	38	3.25(−6)	8.59	
03561+0807	0356+081	44,210	(851)	7.88 (0.07)	0.62 (0.03)	9.09	−0.11	15.93	332	1.62(−7)	6.49	
04100+1144	0410+117	20,440	(319)	7.96 (0.05)	0.61 (0.03)	10.63	−1.54	13.86	47	9.32(−7)	7.88	
04190+1522	0418+153	13,490	(346)	7.99 (0.05)	0.61 (0.03)	11.41	−2.30	16.62	110	2.43(−6)	8.50	
04211+1614	0421+162	19,110	(297)	8.07 (0.05)	0.67 (0.03)	10.92	−1.73	14.29	46	1.32(−6)	8.10	
04234+1222	0423+123	21,350	(497)	7.92 (0.07)	0.59 (0.04)	10.49	−1.44	16.90	191	7.88(−7)	7.77	
04239+1406	0423+141	12,820	(454)	8.89 (0.08)	1.15 (0.04)	13.01	−3.01	17.66	81	—	9.19	
04258+1652	0425+168	24,280	(370)	8.07 (0.05)	0.68 (0.03)	10.49	−1.31	14.02	48	7.88(−7)	7.68	

TAB. 3.3 – Continued

KUV	WD	$T_{\rm eff}$	(K)	$\log g$	$M/M_\odot$	M_V	$\log L/L_\odot$	V	D(pc)	$1/\upsilon_{\rm max}$	$\log\tau$	Notes
04262+1038	0426+106	10,380	(154)	8.66 (0.05)	1.02 (0.03)	13.12	−3.19	16.82	43	2.21(−5)	9.28	
04295+1739	0429+176	13,680	(651)	8.56 (0.09)	0.96 (0.05)	12.27	−2.63	13.93	21	7.28(−6)	8.86	1
04304+1339	0430+136	35,980	(817)	7.90 (0.11)	0.61 (0.05)	9.41	−0.50	16.50	262	2.29(−7)	6.76	1
04310+1236	0431+126	20,680	(323)	8.12 (0.05)	0.70 (0.03)	10.86	−1.62	14.18	47	1.23(−6)	8.03	
04370+1514	0437+152	18,350	(311)	7.43 (0.05)	0.40 (0.02)	9.96	−1.38	15.83	149	4.23(−7)	7.95	
04383+1054	0438+108	26,730	(391)	8.10 (0.05)	0.70 (0.03)	10.33	−1.15	13.83	50	6.51(−7)	7.49	
06548+3225	0654+324	21,580	(377)	8.11 (0.05)	0.69 (0.03)	10.76	−1.54	17.90	293	—	7.94	
07069+2929	0706+294	14,040	(253)	7.84 (0.05)	0.53 (0.03)	11.13	−2.14	15.44	73	1.72(−6)	8.36	
07170+3653	0717+368	24,270	(470)	7.85 (0.06)	0.56 (0.03)	10.15	−1.17	17.10	213	5.27(−7)	7.43	
07540+4015	0754+402	18,630	(457)	7.97 (0.08)	0.60 (0.04)	10.80	−1.71	16.70	151	1.14(−6)	8.05	
08016+4206	0801+421	13,730	(560)	8.14 (0.07)	0.69 (0.04)	11.59	−2.35	17.06	124	3.05(−6)	8.59	
08026+4118	0802+413	51,450	(967)	7.59 (0.06)	0.53 (0.02)	8.39	+0.37	15.16	166	7.99(−8)	6.31	
08039+4003	0803+400	12,450	(247)	8.07 (0.06)	0.65 (0.04)	11.66	−2.48	17.40	140	—	8.64	
08084+4221	0808+423	14,890	(446)	8.89 (0.05)	1.15 (0.03)	12.77	−2.75	16.76	62	1.40(−5)	9.02	
08100+3915	0810+392	22,160	(447)	7.96 (0.06)	0.61 (0.03)	10.49	−1.40	16.85	187	7.88(−7)	7.73	
08157+3739	0815+376	21,550	(360)	7.98 (0.05)	0.62 (0.03)	10.57	−1.46	16.44	168	8.67(−7)	7.80	
08157+3946	0815+397	37,820	(715)	7.78 (0.07)	0.56 (0.03)	9.14	−0.33	17.40	448	—	6.68	
08165+3741	0816+376	11,000	(627)	8.00 (0.06)	0.61 (0.04)	11.84	−2.66	15.63	56	4.19(−6)	8.77	6
08167+3844	0816+387	7700	(113)	8.07 (0.07)	0.64 (0.04)	13.26	−3.33	16.58	45	2.66(−5)	9.16	
08172+3838	0817+386	25,230	(384)	7.97 (0.05)	0.62 (0.03)	10.25	−1.17	15.73	122	5.93(−7)	7.45	
08628+4150	0826+418	10,270	(158)	8.12 (0.07)	0.68 (0.04)	12.23	−2.85	16.75	81	6.91(−6)	8.88	
08275+3252	0827+328	7510	(114)	8.56 (0.08)	0.96 (0.05)	14.13	−3.68	15.69	20	8.51(−5)	9.55	
08273+4101	0827+410	15,210	(254)	7.77 (0.05)	0.50 (0.03)	10.88	−1.96	15.92	101	1.26(−6)	8.21	
08308+3710	0830+371	9180	(133)	8.26 (0.06)	0.76 (0.04)	12.87	−3.13	16.01	42	1.59(−5)	9.08	
08317+4117	0831+412	31,030	(506)	8.47 (0.07)	0.93 (0.04)	10.63	−1.14	17.11	197	9.32(−7)	7.66	
08354+3639	0835+366	15,700	(284)	7.91 (0.05)	0.57 (0.03)	11.03	−1.98	17.87	233	—	8.25	
08368+4026	0836+404	11,870	(180)	8.10 (0.05)	0.67 (0.03)	11.80	−2.59	15.55	56	3.98(−6)	8.71	
08371+3754	0837+378	14,340	(439)	8.17 (0.06)	0.72 (0.04)	11.57	−2.30	17.50	153	—	8.56	
08378+3934	0837+395	20,870	(494)	7.87 (0.07)	0.56 (0.04)	10.46	−1.45	16.54	164	7.60(−7)	7.77	
08381+3737	0838+376	19,170	(330)	7.87 (0.05)	0.55 (0.03)	10.61	−1.60	16.99	189	9.09(−7)	7.91	

TAB. 3.3 – Continued

KUV	WD	$T_{\rm eff}$	(K)	$\log g$	$M/M_\odot$	M_V	$\log L/L_\odot$	V	D(pc)	$1/v_{\rm max}$	$\log\tau$	Notes
08397+3435	0839+345	17,540	(285)	8.07 (0.05)	0.66 (0.03)	11.06	−1.88	16.32	106	1.57(−6)	8.22	
08391+3800	0839+379	19,230	(365)	8.02 (0.06)	0.64 (0.03)	10.83	−1.69	16.32	125	1.19(−6)	8.05	
08411+3340	0841+336	24,300	(459)	8.03 (0.06)	0.65 (0.03)	10.42	−1.28	16.31	179	7.25(−7)	7.63	
08417+4112	0841+411	11,600	(207)	8.24 (0.07)	0.75 (0.04)	12.06	−2.71	17.40	117	—	8.82	
08422+3813	0842+382	8020	(116)	8.06 (0.06)	0.63 (0.04)	13.09	−3.25	16.03	29	2.13(−5)	9.11	4
08460+3441	0846+346	7640	(110)	8.11 (0.06)	0.66 (0.04)	13.35	−3.37	15.71	29	3.00(−5)	9.20	
08473+3838	0847+386	17,410	(288)	8.28 (0.05)	0.79 (0.03)	11.39	−2.02	17.67	180	—	8.37	
08504+4155	0850+419	18,200	(322)	7.90 (0.05)	0.56 (0.03)	10.74	−1.71	17.40	170	1.06(−6)	8.02	
08543+4028	0854+404	22,250	(340)	7.91 (0.05)	0.58 (0.02)	10.40	−1.36	14.90	79	7.08(−7)	7.66	
08587+3619	0858+363	11,970	(178)	8.17 (0.05)	0.71 (0.03)	11.89	−2.62	14.56	34	4.46(−6)	8.74	
09029+4153	0902+418	43,540	(1010)	8.07 (0.09)	0.71 (0.05)	9.42	−0.26	17.17	359	2.31(−7)	6.54	
09272+3930	0927+394	23,730	(479)	8.28 (0.06)	0.80 (0.04)	10.86	−1.48	17.67	233	—	7.94	
09288+3959	0928+399	25,510	(503)	7.97 (0.07)	0.63 (0.04)	10.24	−1.16	17.53	287	—	7.44	
09443+4229	0944+424	23,650	(368)	7.99 (0.05)	0.63 (0.03)	10.41	−1.30	16.43	160	7.16(−7)	7.62	
09479+3234	0947+325	22,060	(341)	8.31 (0.05)	0.82 (0.03)	11.04	−1.63	15.38	73	1.53(−6)	8.07	
09538+3405	0953+340	16,430	(385)	8.08 (0.07)	0.66 (0.04)	11.19	−2.00	16.76	130	1.85(−6)	8.32	
09583+3520	0958+353	40,210	(774)	7.91 (0.08)	0.63 (0.04)	9.27	−0.31	17.05	336	1.96(−7)	6.60	
10010+3318	1001+333	9760	(143)	8.21 (0.06)	0.73 (0.04)	12.56	−3.00	16.92	55	1.06(−5)	8.99	
10013+3614	1001+362	9450	(142)	7.33 (0.09)	0.33 (0.03)	11.32	−2.52	16.76	124	2.17(−6)	8.80	
10063+3522	1006+353	20,230	(501)	7.82 (0.08)	0.53 (0.04)	10.44	−1.48	17.83	300	—	7.79	
10090+3712	1008+372	15,190	(260)	7.89 (0.05)	0.56 (0.03)	11.06	−2.03	16.76	140	1.57(−6)	8.28	
10081+3817	1008+382	13,230	(330)	7.86 (0.05)	0.53 (0.03)	11.26	−2.25	16.29	101	2.02(−6)	8.45	
10115+3332	1011+335	20,070	(416)	8.07 (0.06)	0.67 (0.04)	10.83	−1.64	17.40	205	—	8.03	
11230+4240	1123+426	10,400	(156)	8.18 (0.06)	0.71 (0.04)	12.28	−2.86	16.40	87	7.37(−6)	8.90	
11265+3825	1126+384	25,150	(383)	7.90 (0.05)	0.59 (0.02)	10.16	−1.14	14.89	88	5.34(−7)	7.39	
11370+4222	1137+423	11,840	(178)	8.15 (0.05)	0.70 (0.03)	11.88	−2.62	16.56	86	4.41(−6)	8.74	
11390+4225	1139+424	27,160	(424)	7.90 (0.05)	0.59 (0.03)	9.99	−1.00	16.20	174	4.38(−7)	7.22	
11472+3858	1147+389	17,110	(318)	7.92 (0.06)	0.57 (0.03)	10.88	−1.83	17.46	206	—	8.13	
11491+4104	1149+410	14,070	(271)	7.84 (0.05)	0.53 (0.03)	11.12	−2.13	16.08	98	1.69(−6)	8.35	
12279+3044	1227+307	13,370	(542)	7.93 (0.07)	0.57 (0.04)	11.34	−2.27	17.70	187	—	8.49	

TAB. 3.3 – Continued

KUV	WD	$T_{\rm eff}$	(K)	$\log g$	$M/M_\odot$	M_V	$\log L/L_\odot$	V	D(pc)	$1/v_{\rm max}$	$\log\tau$	Notes
12353+2925	1235+294	18,910	(361)	7.88 (0.06)	0.56 (0.03)	10.65	−1.63	17.29	213	9.54(−7)	7.95	
12399+2744	1239+277	14,740	(256)	7.84 (0.05)	0.53 (0.03)	11.04	−2.05	15.67	85	1.53(−6)	8.29	
12420+2938	1241+296	17,710	(347)	7.84 (0.06)	0.54 (0.03)	10.71	−1.73	15.97	114	1.03(−6)	8.03	
12436+3011	1243+301	14,590	(370)	7.77 (0.07)	0.49 (0.04)	10.96	−2.03	17.60	212	—	8.28	
12474+3105	1247+310	11,940	(216)	8.34 (0.06)	0.82 (0.04)	12.15	−2.72	17.20	102	6.23(−6)	8.84	
12492+2937	1249+296	11,770	(211)	8.25 (0.06)	0.76 (0.04)	12.05	−2.69	16.83	89	5.48(−6)	8.81	
12574+2750	1257+278	8730	(127)	8.33 (0.06)	0.81 (0.04)	13.17	−3.26	15.40	27	2.36(−5)	9.19	
12587+2942	1258+297	14,730	(309)	7.88 (0.06)	0.55 (0.03)	11.10	−2.08	18.17	275	—	8.32	
13088+3139	1308+316	13,260	(444)	7.93 (0.06)	0.57 (0.04)	11.36	−2.29	16.79	121	2.28(−6)	8.50	
14083+3223	1408+323	18,150	(278)	7.95 (0.05)	0.59 (0.03)	10.82	−1.75	14.06	45	1.17(−6)	8.07	
14134+2311	1413+231	23,370	(414)	7.72 (0.05)	0.50 (0.02)	10.03	−1.16	16.71	236	4.59(−7)	7.43	
14138+2408	1413+241	16,340	(263)	8.08 (0.05)	0.66 (0.03)	11.20	−2.01	17.03	144	1.87(−6)	8.32	
14197+2514	1419+252	10,160	(332)	8.00 (0.06)	0.60 (0.03)	12.20	+0.00	16.90	151	—	8.76	
14205+2251	1420+228	17,200	(321)	7.86 (0.06)	0.55 (0.03)	10.79	−1.79	16.83	158	1.13(−6)	8.09	
14227+3340	1422+336	13,740	(426)	8.16 (0.06)	0.71 (0.04)	11.63	−2.37	17.06	124	3.21(−6)	8.60	
14287+3724	1428+373	14,010	(221)	7.36 (0.05)	0.36 (0.01)	10.35	−1.83	15.40	112	6.67(−7)	8.34	
14299+3720	1429+373	34,240	(507)	8.15 (0.05)	0.74 (0.03)	9.90	−0.75	15.26	118	3.95(−7)	6.95	
14310+2542	1431+257	22,940	(399)	7.21 (0.05)	0.37 (0.01)	9.12	−0.81	17.03	375	1.67(−7)	7.43	
15502+1819	1550+183	14,260	(271)	8.25 (0.05)	0.77 (0.03)	11.70	−2.36	14.60	43	3.50(−6)	8.59	
16055+1745	1605+177	13,830	(267)	7.68 (0.05)	0.45 (0.02)	10.91	−2.07	16.72	143	1.31(−6)	8.47	
16069+1810	1606+181	23,050	(397)	7.86 (0.05)	0.56 (0.03)	10.26	−1.27	16.91	233	6.00(−7)	7.54	
16075+2031	1607+205	11,150	(173)	7.82 (0.06)	0.50 (0.03)	11.54	−2.53	17.40	148	—	8.61	
16106+3820	1610+383	14,450	(278)	7.83 (0.05)	0.52 (0.03)	11.06	−2.08	16.60	117	1.57(−6)	8.31	
16195+4125	1619+414	14,710	(335)	7.92 (0.06)	0.57 (0.03)	11.15	−2.10	16.76	134	1.76(−6)	8.35	1
16268+4055	1626+409	21,370	(418)	8.02 (0.06)	0.64 (0.03)	10.64	−1.50	16.53	163	9.43(−7)	7.86	
16288+3904	1628+390	18,940	(340)	7.89 (0.05)	0.56 (0.03)	10.66	−1.63	16.70	169	9.66(−7)	7.95	
16319+3937	1631+396	17,320	(279)	7.65 (0.05)	0.45 (0.02)	10.45	−1.64	14.10	53	7.51(−7)	8.07	
16366+3506	1636+351	37,170	(564)	7.97 (0.05)	0.65 (0.03)	9.48	−0.49	14.91	121	2.47(−7)	6.72	
16376+3331	1637+335	10,260	(147)	8.20 (0.05)	0.73 (0.03)	12.36	−2.90	14.54	30	8.17(−6)	8.93	
16476+3733	1647+375	21,980	(340)	7.89 (0.05)	0.57 (0.02)	10.39	−1.37	14.97	82	6.99(−7)	7.66	

TAB. 3.3 – Continued

KUV	WD	$T_{\rm eff}$	(K)	$\log g$	$M/M_\odot$	M_V	$\log L/L_\odot$	V	D(pc)	$1/v_{\rm max}$	$\log \tau$	Notes
16484+3706	1648+371	43,110	(918)	7.56 (0.08)	0.49 (0.03)	8.56	+0.06	15.83	294	9.43(−8)	6.49	
18004+6836	1800+685	44,170	(763)	7.82 (0.06)	0.59 (0.03)	8.98	−0.07	14.72	133	1.44(−7)	6.49	4
18284+6650	1828+668	10,800	(163)	8.20 (0.06)	0.73 (0.04)	12.20	−2.81	16.65	77	6.65(−6)	8.87	
18332+6429	1833+644	47,260	(1532)	7.93 (0.13)	0.65 (0.06)	9.10	−0.03	16.90	363	1.64(−7)	6.42	1
18453+6819	1845+683	37,040	(576)	8.20 (0.05)	0.78 (0.03)	9.86	−0.64	15.00	106	3.78(−7)	6.81	4
21168+7338	2116+736	53,450	(1189)	7.60 (0.08)	0.54 (0.03)	8.36	+0.43	14.87	200	7.76(−8)	6.26	
21267+7326	2126+734	15,290	(223)	7.84 (0.04)	0.53 (0.02)	10.98	−1.99	12.78	23	1.43(−6)	8.24	
22543+1237	2254+126	11,640	(173)	8.05 (0.05)	0.64 (0.03)	11.77	−2.59	15.70	70	3.83(−6)	8.69	
22570+1349	2257+138	27,560	(403)	8.33 (0.05)	0.84 (0.03)	10.65	−1.25	16.67	158	9.54(−7)	7.72	
22573+1613	2257+162	24,580	(382)	7.49 (0.05)	0.43 (0.02)	9.50	−0.89	16.14	212	2.52(−7)	7.23	
23060+1303	2306+124	20,220	(318)	8.05 (0.05)	0.66 (0.03)	10.79	−1.62	15.23	77	1.13(−6)	7.99	
23061+1229	2306+130	13,250	(283)	7.92 (0.05)	0.56 (0.03)	11.34	−2.29	14.90	56	2.23(−6)	8.47	
23083+1642	2308+167	18,030	(320)	7.96 (0.05)	0.60 (0.03)	10.85	−1.76	17.02	186	1.22(−6)	8.09	
23098+1031	2309+105	54,410	(964)	7.90 (0.06)	0.65 (0.03)	8.88	+0.25	13.11	69	1.30(−7)	6.23	
23128+1157	2312+119	18,020	(308)	7.73 (0.05)	0.48 (0.02)	10.52	−1.63	17.83	289	—	7.91	
23149+1408	2314+141	17,740	(302)	7.78 (0.05)	0.50 (0.03)	10.61	−1.69	16.87	180	9.09(−7)	7.97	
23162+1220	2316+123	11,800	(377)	8.00 (0.06)	0.60 (0.04)	12.15	−2.83	15.35	44	6.23(−6)	8.85	7
23176+2650	2317+268	31,460	(487)	7.70 (0.06)	0.51 (0.02)	9.34	−0.60	16.17	246	2.12(−7)	6.93	
23189+0901	2318+090	29,060	(478)	7.99 (0.06)	0.64 (0.03)	9.98	−0.93	17.11	181	4.33(−7)	7.16	
23180+1242	2318+126	13,490	(334)	7.92 (0.05)	0.56 (0.03)	11.31	−2.25	16.25	98	2.15(−6)	8.46	
23220+0921	2322+093	14,060	(304)	7.81 (0.06)	0.51 (0.03)	11.08	−2.12	16.91	133	1.61(−6)	8.34	
23223+0953	2322+098	20,020	(340)	7.88 (0.05)	0.56 (0.03)	10.56	−1.53	16.72	213	8.56(−7)	7.85	
23235+2536	2323+256	5680	(218)	6.84 (0.67)	0.18 (0.27)	12.83	−3.17	17.06	6873	1.51(−5)	9.19	
23282+1046	2328+107	21,910	(356)	7.84 (0.05)	0.55 (0.02)	10.32	−1.34	15.53	110	6.44(−7)	7.62	
23296+2642	2329+267	9400	(240)	8.02 (0.28)	0.61 (0.04)	12.41	−2.95	15.15	39	8.72(−6)	8.92	8

Note. – (1) DA+dM; (2) Unresolved double degenerate; (3) Magnetic, $B = 12$ MG (Jordan 1993), $T_{\rm eff}$ from Schmidt et al. 2003; (4) Not in Darling 1994; (5) DAO star; (6) Magnetic, $B = 9$ MG (Angel et al. 1974)$T_{\rm eff}$ from Jordan 2001; (7) Magnetic, $B = 29$ MG (Achilleos & Wickramasinghe 1989), $T_{\rm eff}$ from Jordan (2001); (8) Magnetic, B (2.3 MG), $T_{\rm eff}$ and $\log g$ from Bergeron et al. 2001.

3.9 Figures

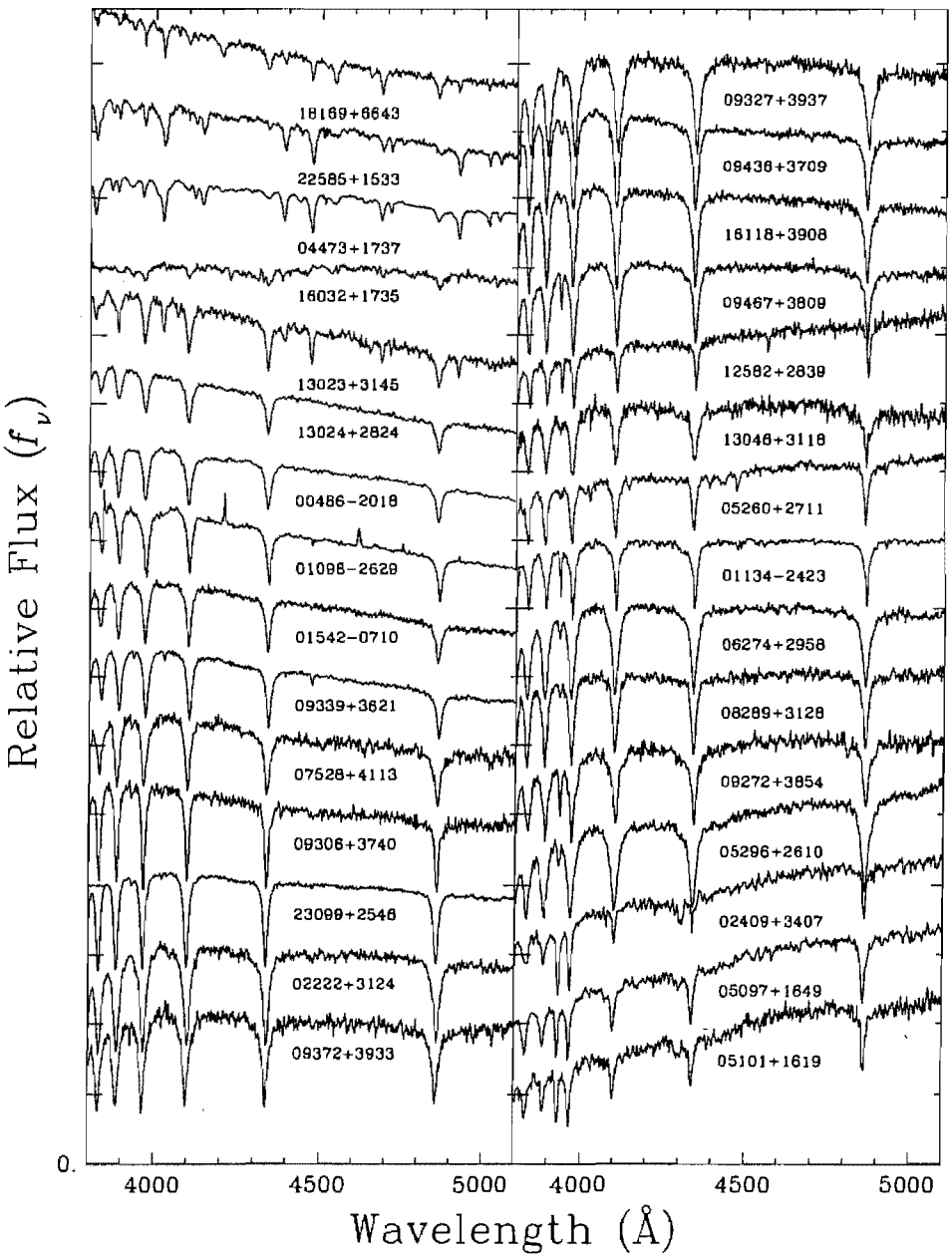

FIG. 3.1 – Optical spectra of hot subdwarfs or main sequence stars misclassified as DA stars in the Kiso survey (Darling 1994, and references therein). The objects are approximately ordered as a function of their slope. KUV 16032+1735 (left panel, fourth object from the top) is a hot ($T_{\rm eff} \sim 84,000$ K) sdO star.

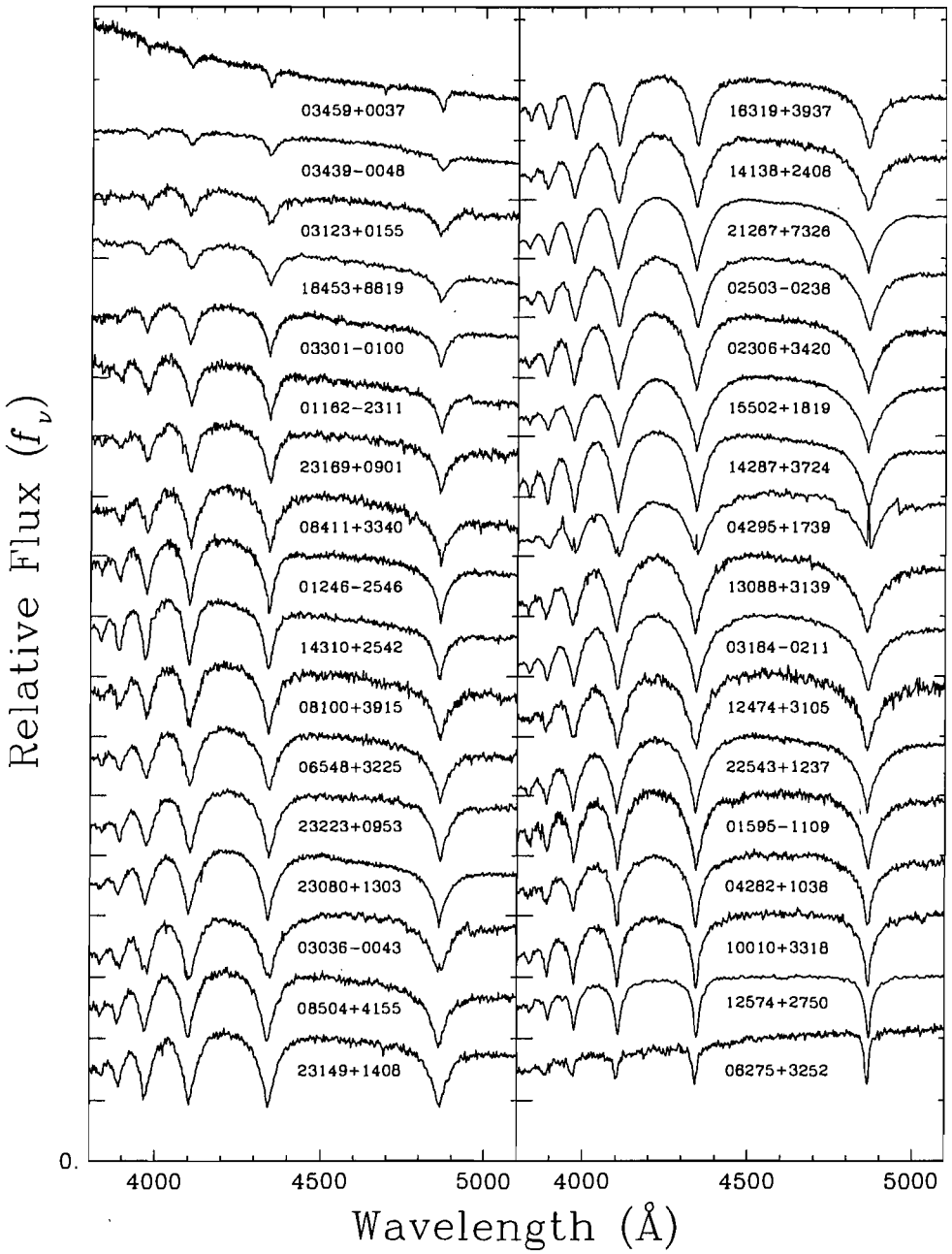

FIG. 3.2 – Optical spectra for a subsample of DA white dwarfs from the Kiso survey. The spectra are normalized at 4500 Å and are shifted vertically for clarity; the various zero points are indicated by long thick marks. The effective temperature decreases from upper left to bottom right. The hottest object in this sample is the DAO star KUV 03459+0037 displayed at the top of the left panel.

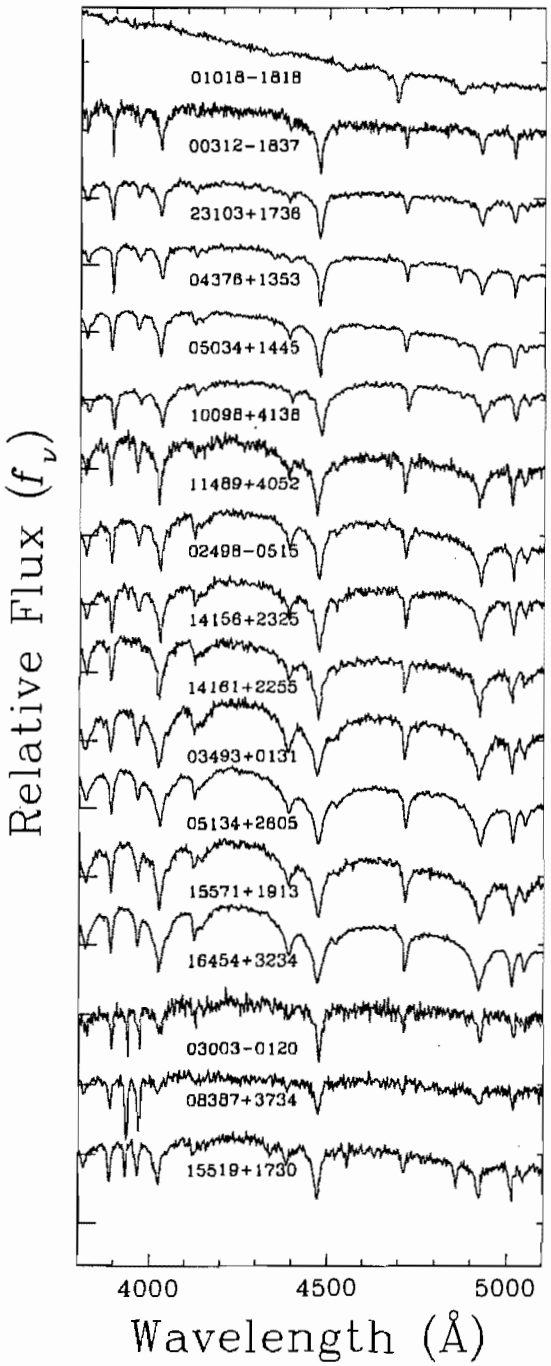

FIG. 3.3 – Same as Figure 3.2 but for a subsample of DO/DB/DBA white dwarfs from the Kiso survey. The hottest object in this sample is the DO star KUV 01018−1818 shown at the top.

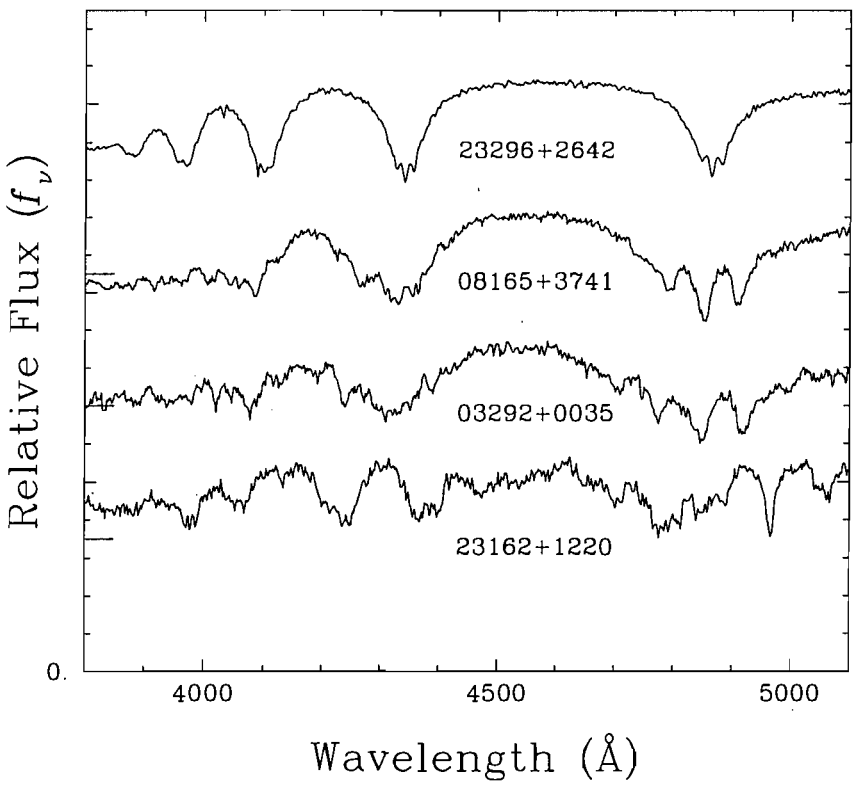

FIG. 3.4 – Same as Figure 3.2 but for the magnetic white dwarfs in the Kiso survey; these all have hydrogen-rich atmospheres. The strength of the magnetic field increases from top ($B \sim 2.3$ MG) to bottom ($B \sim 29$ MG, see references in Table 3.3).

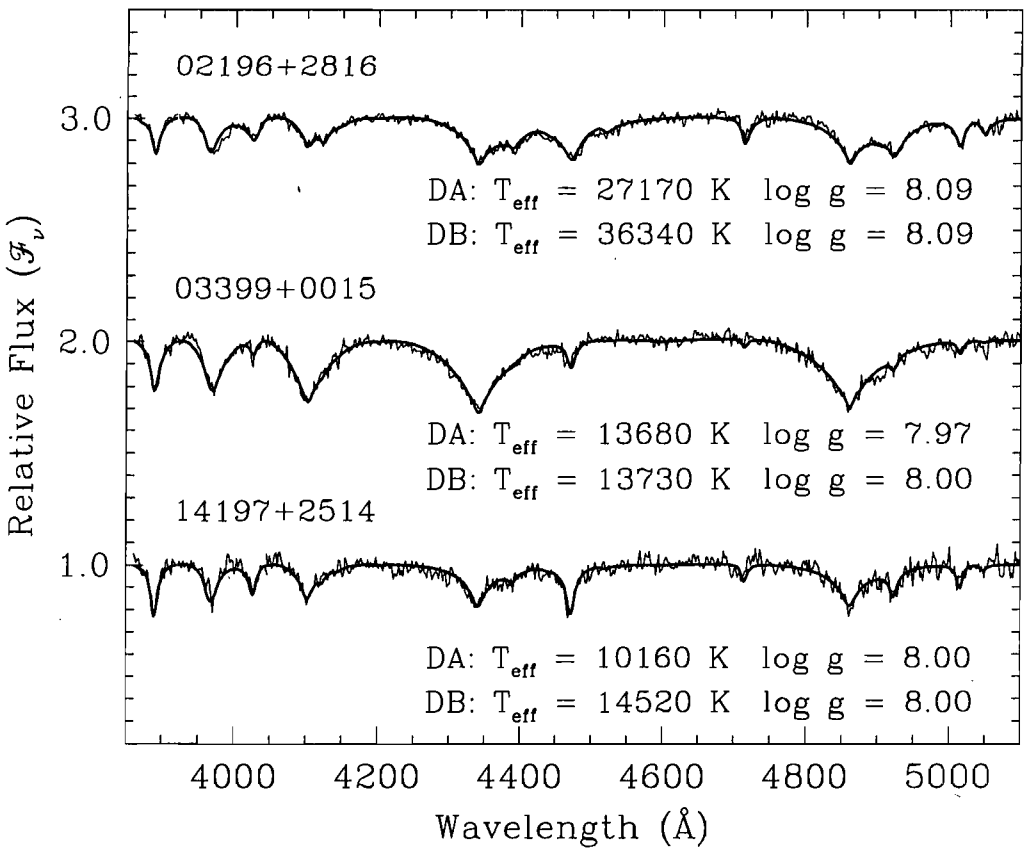

FIG. 3.5 – Our best fits to the optical spectra of the three DAB stars in our sample with composite DA+DB models. The atmospheric parameters for each solution are given in the figure. Both the observed and theoretical spectra are normalized to a continuum set to unity and the spectra are shifted from each other for clarity. The detailed analysis of KUV 02196+2816 has already been published in Limoges et al. (2009) while the details for KUV 03399+0015 and KUV 14197+2514 will be presented elsewhere.

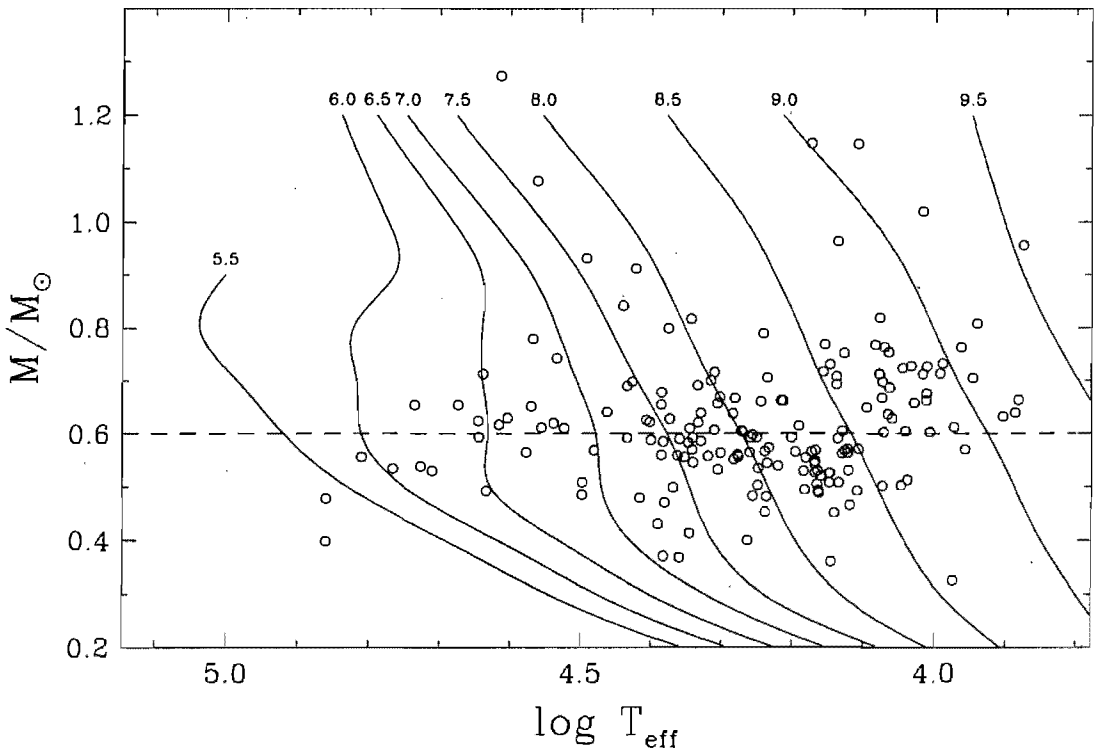

FIG. 3.6 – Masses of all DA stars in the Kiso survey as a function of $\log T_{\rm eff}$, together with the theoretical isochrones from Wood (1995). Isochrones are labeled in units of $\log \tau$, where τ is the white dwarf cooling age in years. The dashed line is meant to guide the eye towards the value of 0.6 $M_{\odot}$, which represents the mean mass of our distribution of white dwarfs.

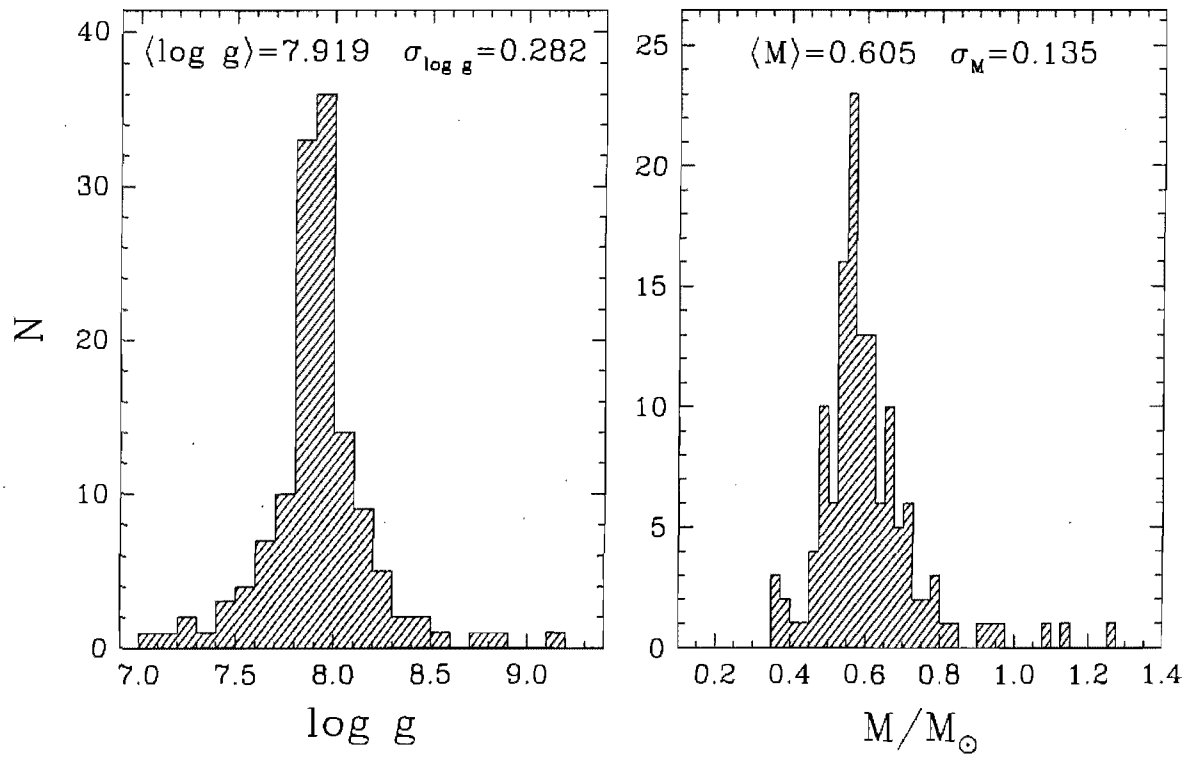

FIG. 3.7 – Surface gravity and mass distributions for the 134 DA stars in the KUV sample with $T_{\rm eff} > 13,000$ K. The masses of DA stars below this value may be biased, as explained in the text. Mean values and standard deviations of both distributions are indicated in each panel.

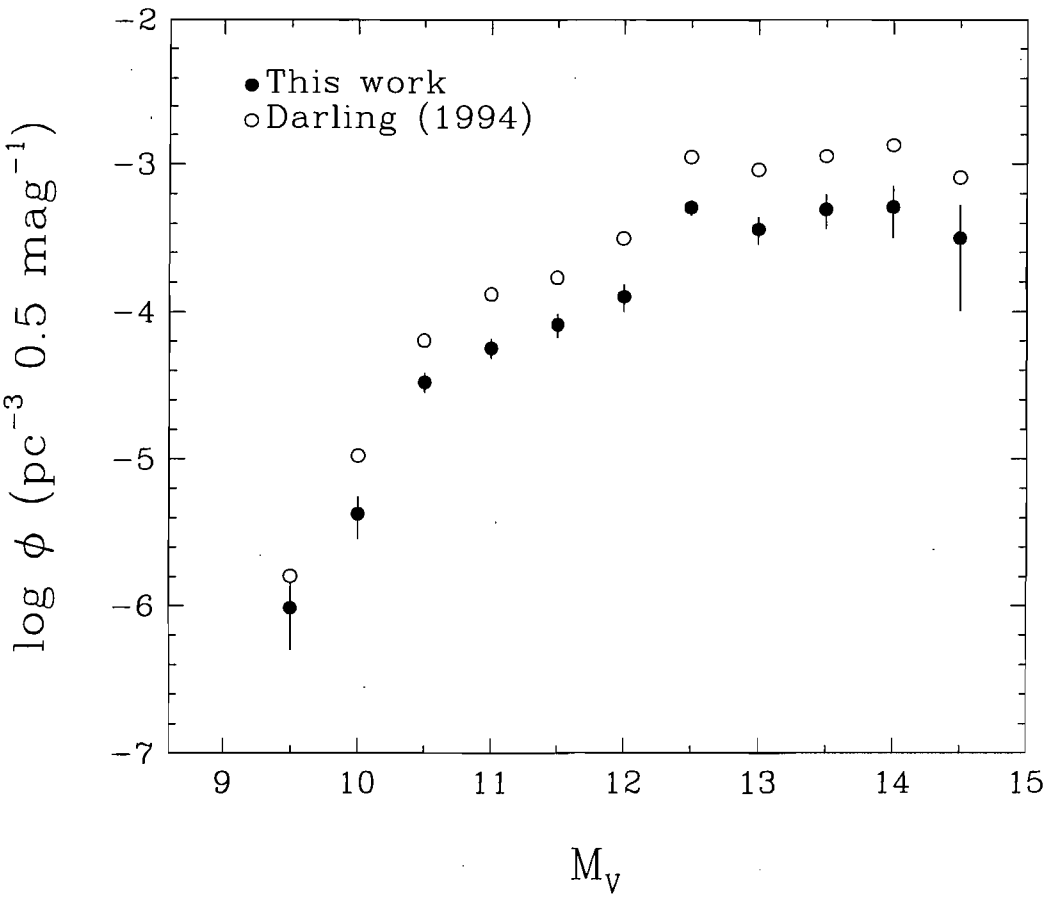

FIG. 3.8 – Luminosity function of white dwarf stars from the Kiso survey, all spectral types included. The open circles represent the results published in Table 4.5 of Darling (1994), while the filled circles correspond to our attempt at reproducing his results using the same input data and method of calculation.

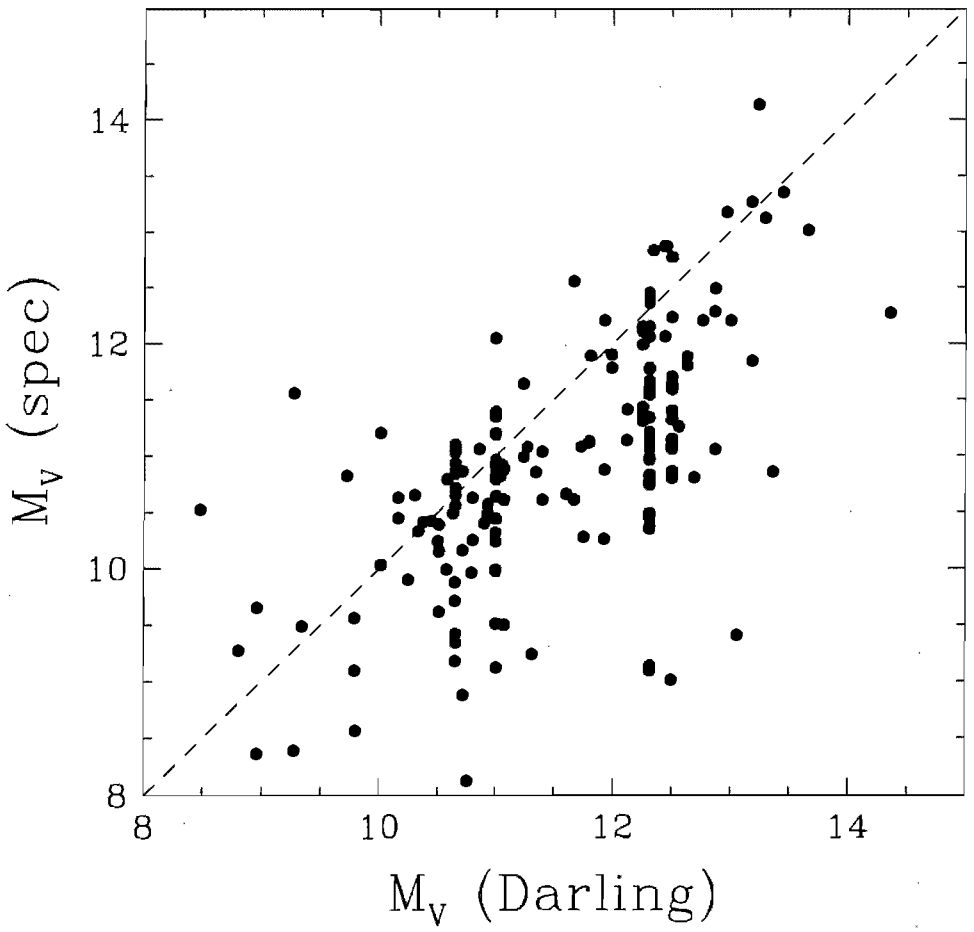

FIG. 3.9 – Comparison of the absolute visual magnitudes obtained from the empirical photometric calibration of Darling (1994) and from the spectroscopic method, for all DA stars in common.

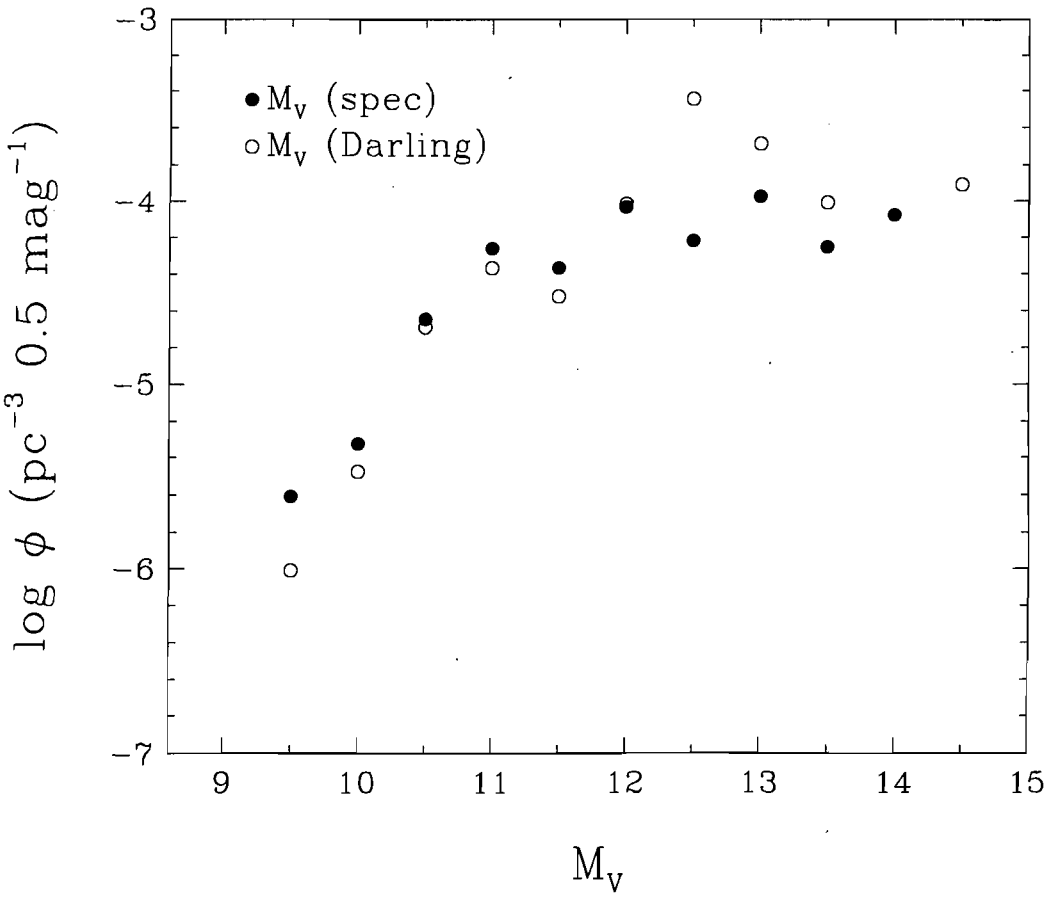

FIG. 3.10 – Luminosity functions for the DA stars in the Kiso survey that are in common between our sample and that of Darling (1994). The open circles correspond to the luminosity function calculated using the approximate M_V values provided in Table 4.3 of Darling (1994) while the filled circles make use of the spectroscopic M_V values given in our Table 3.3.

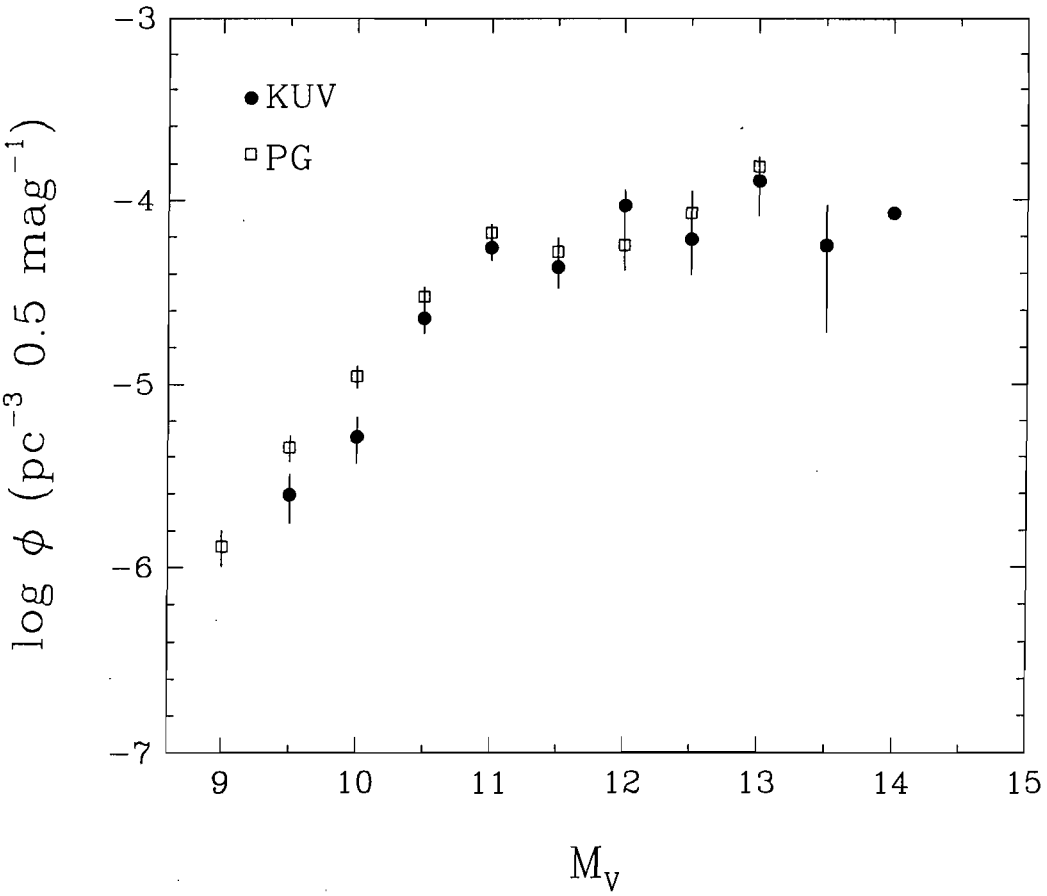

FIG. 3.11 – Comparison of the luminosity functions for DA white dwarfs in the Kiso survey (145 stars; this work) and in the PG survey (348 stars; LBH05).

Chapitre 4

Spectroscopic Analysis of the DBA White Dwarf KUV 0219+282: An Unresolved DA+DB Degenerate Binary

M.-M. Limoges[1], P. Bergeron[1], Pierre Dufour[1]

The Astrophysical Journal, 696, 1461-1465

May 2009

[1]Département de Physique, Université de Montréal, C.P. 6128, Succ. Centre-Ville, Montréal, Québec H3C 3J7, Canada; [information retirée / information withdrawn] [information retirée / information withdrawn]

4.1 Abstract

A spectroscopic analysis of the DBA (or DAB) white dwarf KUV 02196+2816 is presented. The observed hydrogen and helium line profiles are shown to be incompatible with model spectra calculated under the assumption of a homogeneous hydrogen and helium chemical composition. In contrast, an excellent fit to the optical spectrum of KUV 02196+2816 can be achieved if the object is interpreted as an unresolved double degenerate composed of a hydrogen-line DA star and a helium-line DB star. The atmospheric parameters obtained from the best fit are $T_{\rm eff} = 27,170$ K and $\log g = 8.09$ for the DA star, $T_{\rm eff} = 36,340$ K and $\log g = 8.09$ for the DB star, which implies that the total mass of the system ($M \sim 1.4\ M_{\odot}$) is very close to the Chandrasekhar limit. Moreover, the effective temperature of the DB stars lies well within the so-called DB gap where very few bright DB stars are found. The implications of this discovery with respect to the DAB and DBA spectral classes and to the evolution of double degenerate binaries are discussed.

4.2 Introduction

The discovery of double degenerate binary systems is crucial to our attempt at better constraining their origin and evolution. In particular, these binary systems are thought to be the progenitors of Type Ia supernovae if the total mass of the two components exceeds the Chandrasekhar limit and if their orbital period is small enough to allow them to merge within a Hubble time. However, only a small percentage of double degenerate binaries lead to supernova explosions according to Nelemans et al. (2001) and Napiwotzki et al. (2001). In 2006, only ten such binaries composed of two white dwarfs were known (van der Sluys et al. 2006). Since then, the SPY (ESO Supernovae Ia Progenitor surveY) radial velocity survey has observed more than 1000 white dwarfs and pre-white dwarfs (Napiwotzki et al. 2007). One of the conclusions of that survey is that double degenerate binaries cannot explain the existence of every low mass white dwarf (0.45 $M_{\odot}$ or less). Indeed, only 42% of low-mass He-core white dwarfs are found in close binary systems.

Double degenerate binaries are difficult to detect from single slit spectroscopy alone. This is particularly true for system composed of two DA stars since the composite spectrum can be reproduced almost perfectly with a single hydrogen-rich model atmosphere (Liebert et al. 1991). In order to detect such spectroscopically invisible DA+DA systems, Lajoie & Bergeron (2007) compared effective temperatures determined from optical and ultraviolet (IUE) spectra, and identified three candidate systems. Double degenerate systems composed of white dwarfs with different spectral types are easier to detect, however, since the modeling of these objects under the assumption of a single star leads to spurious results. This is precisely how Bergeron & Liebert (2002) showed that the DAB PG 1115+166 was in fact a double degenerate binary system composed of a DA and a DB star. Their analysis revealed that the optical spectrum could not be reproduced with a single model atmosphere with a mixed hydrogen and helium composition, or even a stratified chemical composition. Instead, the authors showed that a combination of a DA and a DB model spectrum could perfectly match the observed line profiles and photometry. Additional objects are also discussed in Pereira et al. (2005) and references therein. PG 1115+166 was first identified in the PG catalog (Green et al. 1986) as a DA5. Later, Maxted et al. (2002) confirmed the binary nature of PG 1115+166 and obtained an orbital period of 30.09 days, too long to allow the white dwarfs to merge within a Hubble time. The binary models of van der Sluys et al. (2006) explained that the older nature of the DB star in PG 1115+166 is the result of the loss of its hydrogen-rich outer layers after it has evolved into a giant phase.

We are currently conducting a spectroscopic survey of all the white dwarfs discovered in the Kiso Ultraviolet (KUV) survey with the aim of redetermining the luminosity function using the spectroscopic method of Bergeron et al. (1992, see also Liebert et al. 2005). One of these white dwarfs, KUV 02196+2816 (WD 0219+282, $V = 17.30$) was spectroscopically identified as a DBA star by Darling & Wegner (1996). However, this object should have been classified as a DAB star since the hydrogen lines are actually stronger than the helium lines (see § 2 below). DAB white dwarfs are particularly interesting since they may represent the key to our understanding of the evolution of DAO and hot DB stars, and of the existence of a strong

deficiency of DB stars between 30,000 and 45,000 K (see Vennes et al. 2004, for a review).

We report in this paper the discovery that KUV 02196+2816 is actually a double degenerate binary composed of a DA and a DB star. An analysis identical to that of PG 1115+166 by Bergeron & Liebert (2002) indeed reveals that the spectrum of KUV 02196+2816 cannot be reproduced by a single star model, and that a composite DA and DB model spectrum provides a much better fit to the observations. We first present our spectroscopic observations in § 2. The model atmosphere calculations described in § 3 are then used in § 4 to analyze in detail the optical spectrum of KUV 02196+2816 using homogeneous as well as composite model atmospheres. Our discussion follows in § 5.

4.3 Spectroscopic Observations

Optical spectroscopy for KUV 02196+2816 has been obtained on 2007 December 6 using the Steward Observatory 2.3-m telescope equipped with the Boller & Chivens spectrograph and a Loral CCD detector. The 4.″5 slit together with the 600 line mm^{-1} grating in first order provided a spectral coverage of 3200–5300 Å at an intermediate resolution of $\sim$ 6 Å FWHM.

Our optical spectrum for KUV 02196+2816 is displayed in Figure 4.1. The hydrogen Balmer lines are clearly stronger than the helium lines and the star should thus be classified as a DAB white dwarf. The spectrum of KUV 02196+2816 is also compared with GD 323, the prototype of the DAB class (Pereira et al. 2005), PG 1115+166 (Bergeron & Liebert 2002), and MCT 0453−2933 (Wesemael et al. 1994). PG 1115+166 has already been discussed above while MCT 0453−2933 has been analyzed by Wesemael et al. (1994) and was shown to be an unresolved composite system consisting of a DA white dwarf together with a DB or a DBA star. From repeated spectroscopic observations at Hα as part of the SPY survey, Napiwotzki et al. (2005) found variations of the line core shapes. In one of the spectra, they noticed a splitting at Hα (see also Fig. 7 of Voss et al. 2007), indicating that both stars in the binary system contain considerable amounts of hydrogen. It was concluded that MCT 0453−2933 is composed of a DA and a DBA, or even a DAB star.

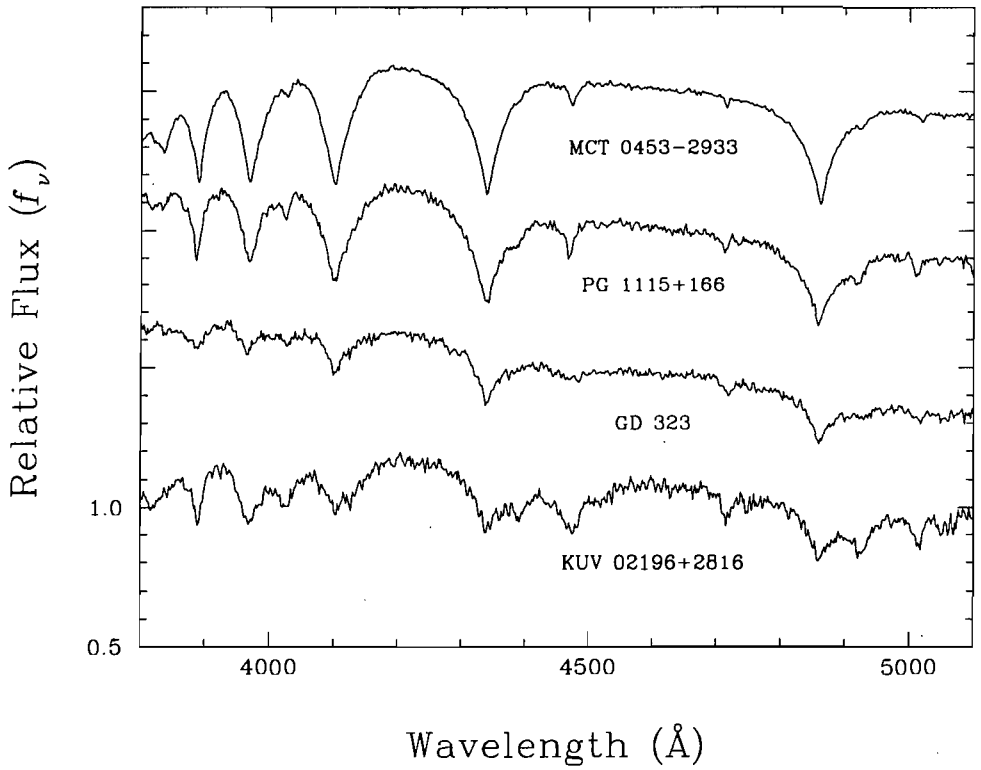

FIG. 4.1 – Comparison of our optical spectrum of the DAB star KUV 02196+2816 with those of the DAB stars GD 323, PG 1115+166, and MCT 0453−2933. The last two objects have been interpreted by Bergeron & Liebert (2002) and Wesemael et al. (1994), respectively, as unresolved composite systems consisting of a DA white dwarf and a DB or DBA companion. The spectra are normalized at 4400 Å and are shifted vertically by 0.5 for clarity.

The similarity between MCT 0453−2933 and PG 1115+166 has already been discussed in Bergeron & Liebert (2002), where the double degenerate binary nature of PG 1115+166 was unveiled. The spectrum of KUV 02196+2816 shows the same He I features as these two stars: the 4026 and 4471 Å absorption lines are about the same strength as those of PG 1115+166 while the features at 4713, 4921 and 5015 Å are only slightly stronger. The hydrogen Balmer lines are definitely weaker in the spectrum of KUV 02196+2816 than in PG 1115+166, however, and more typical of the strength observed in GD 323.

4.4 Model Atmospheres and Synthetic Spectra

The model atmospheres and synthetic spectra for DA stars are described at length in Liebert et al. (2005) and references therein. The models for DB and DBA stars used in this analysis rely

on a modified version of our model atmosphere code for DA stars in which we have included all the helium opacity sources from the DB model atmosphere code described in Beauchamp et al. (1996), and in particular the improved Stark profiles of neutral helium of Beauchamp et al. (1997). The mixed hydrogen and helium models assume a homogeneous chemical composition. We refrain here from using stratified models since Bergeron & Liebert (2002) demonstrated that such models could not improve the fit to the optical spectrum of PG 1115+166 with respect to homogeneous models. Also, because the hydrogen and helium lines in the spectrum of KUV 02196+2816 are almost of equal strength, DBA models with unusually high helium abundances had to be calculated for this analysis. Our DBA model grid covers a range of $T_{\rm eff}$ = 14,000 (2000) 50,000 K, $\log g$ = 7.0 (0.5) 8.5, and $\log N({\rm He})/N({\rm H}) = -1.0$ (0.5) 1.0, where the numbers in parentheses indicate the step value. Pure helium models were calculated as well.

4.5 Model Atmosphere Analysis

Our fitting technique relies on the nonlinear least-squares method of Levenberg-Marquardt (Press et al. 1986), which is based on a steepest descent method. The model spectra (convolved with a Gaussian instrumental profile) and the optical spectrum of KUV 02196+2816 are first normalized to a continuum set to unity. The calculation of χ^2 is then carried out in terms of these normalized line profiles only. All atmospheric parameters – $T_{\rm eff}$, $\log g$ and $N({\rm He})/N({\rm H})$ – are considered free parameters. When fitting DA+DB model spectra, the total flux of the system is obtained from the sum of the monochromatic Eddington fluxes of the individual components, weighted by their respective radius. The stellar radii are obtained from evolutionary models similar to those described in Fontaine et al. (2001) but with C/O cores, $q({\rm He}) \equiv \log M_{\rm He}/M_\star = 10^{-2}$ and $q({\rm H}) = 10^{-4}$, which are representative of hydrogen-atmosphere white dwarfs, and $q({\rm He}) = 10^{-2}$ and $q({\rm H}) = 10^{-10}$, which are representative of helium-atmosphere white dwarfs[2].

Our best fits to the optical spectrum of KUV 02196+2816 using homogeneous and composite

[2]see http://www.astro.umontreal.ca/~bergeron/CoolingModels/

DA+DB models are shown in Figure 4.2. The solution using homogeneous models depicts the same problem as that mentioned in Burleigh et al. (2001) with the fit to PG 1115+166: the He II λ4686 feature predicted by our models is not observed in the spectrum of KUV 02196+2816. We note, however, that Bergeron & Liebert (2002) did not encounter this problem while fitting the spectrum of PG 1115+166, even though this particular line was included in their model calculations. Our homogeneous solution for KUV 02196+2816 is $\sim$ 3000 K hotter and $\sim$ 0.2 dex lower in $\log g$ than that obtained for PG 1115+166, but more importantly, the helium abundance is about a factor of 40 larger, and our solution predicts a weak but detectable He II absorption feature that is simply not observed. We also see in Figure 4.2 that the low hydrogen Balmer lines (Hβ to Hδ) are predicted too strong while the higher members are too weak. The homogeneous model yields a satisfactory fit for the He I lines $\lambda\lambda$4026, 4713, and 5015, but a poor fit to the remaining helium lines.

Our grid of model atmospheres with mixed H/He compositions has already been applied successfully to fit DB and DBA stars (Beauchamp et al. 1996) or hotter DAO stars (Bergeron et al. 1994). Hence the bad fit displayed at the top of Figure 4.2 does not reflect the inability of our models to fit this star. We also note that Eisenstein et al. (2006) have obtained good fits to DB stars found in the Sloan Digital Sky Survey (SDSS) with temperatures similar to that of KUV 02196+2816 ($T_{\rm eff}$ = 35,200 K), although none of these hot DB stars had hydrogen abundances as high as that inferred here (N(H)/N(He) $\sim$ 0.7). Even if we ignore the bad quality of the fit depicted at the top of Figure 4.2, the atmospheric parameters we obtain for KUV 02196+2816 based on homogeneous models represent a problem from an astrophysical point of view. Indeed, the typical hydrogen abundances measured by Voss et al. (2007) in DBA stars from the SPY survey are of the order of N(H)/N(He) $\sim 10^{-5}$ to 10^{-4} (see their Table 2) — or even 10^{-3} in some extreme cases —, and most of them have effective temperatures well below 30,000 K. Similarly, the helium abundances measured in typical DAO and DAB stars range from N(He)/N(H) $\sim 10^{-4}$ to 0.1 (see Fig. 7 of Vennes et al. 2004). It is thus difficult to reconcile the atmospheric composition determined here for KUV 02196+2816 using homogeneous models with other single DAB/DAO or DBA white dwarfs.

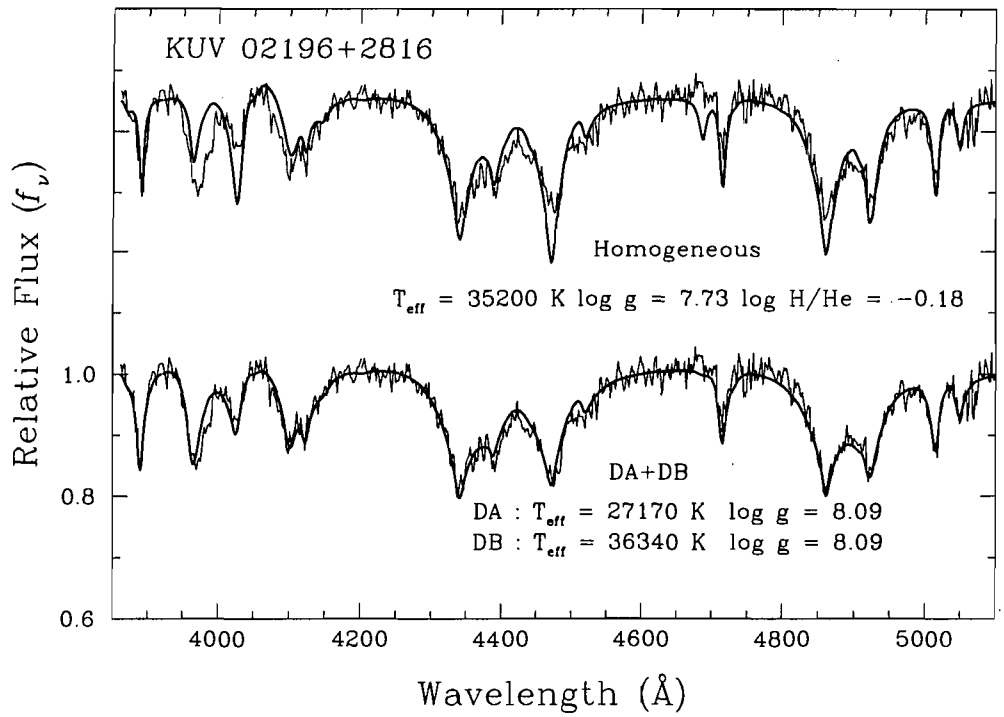

FIG. 4.2 – Our best fits to the optical spectrum of KUV 02196+2816 using homogeneous and composite DA+DB models. The atmospheric parameters for each solution are given in the figure. Both the observed and theoretical spectra are normalized to a continuum set to unity. The spectra are shifted by a factor of 0.4 from each other for clarity. Clearly, the DA+DB solution provides the best fit to the overall spectrum.

In contrast with the homogeneous solution, our DA+DB solution shown at the bottom of Figure 4.2 provides an excellent fit to the Balmer and neutral helium lines simultaneously. Our DA+DB fit yields a χ^2 value of 0.543, a value that is significantly lower than that obtained for the homogeneous solution, $\chi^2 = 1.416$. All observed features are reproduced in detail and this is clearly a much better solution for KUV 02196+2816. The effective temperature determined for the DA component is significantly lower than the value achieved under the assumption of a single object with a homogeneous composition. This is a direct consequence of the hydrogen lines being diluted by the continuum flux of the DB star (see below); the Balmer lines are weakened, and the effective temperature of the model needs to be increased to match the observed line profiles. The effective temperature of the DB component, $T_{\rm eff} = 36,340$ K, is

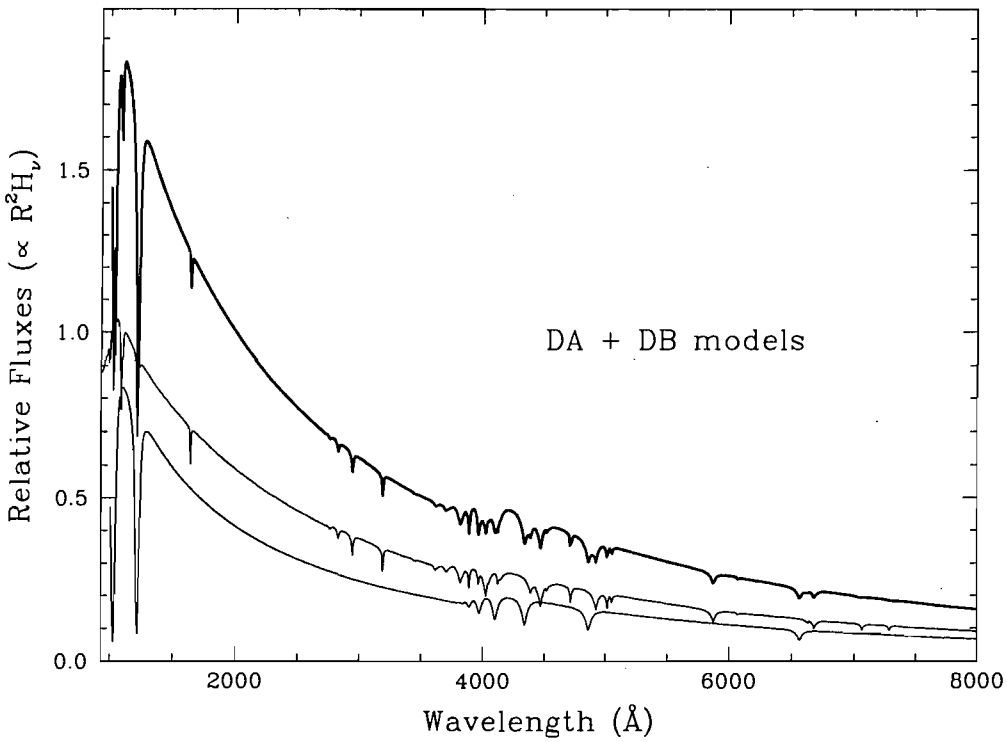

FIG. 4.3 – Relative energy distributions for our best composite DA+DB fit displayed in Figure 4.2. The thin lines show the individual contributions of the DA and DB components, properly weighted by their respective radius, while the thick line corresponds to the total monochromatic flux of the composite system.

higher than the value obtained with our homogeneous models, $T_{\rm eff} = 35,200$ K, yet the He II λ4686 feature only appears as a small depression in the blue wing of He I λ4713. Again in this case, the presence of the DA star dilutes all the helium lines present in the DB spectrum. But the main physical reason for this difference in strength is that the overall opacity of the mixed H/He model is lower than that of the pure helium model at the same effective temperature, resulting in lower atmospheric pressures, which in turn favors the ionization of helium in the mixed atmosphere. Hence the He II λ4686 feature appears stronger in the mixed model than in the pure helium model, even though the former is $\sim$ 1000 K cooler.

The surface gravities of both components of the system are almost identical, $\log g = 8.089$ for the DA and $\log g = 8.095$ for the DB. These values can be translated into masses and cooling ages using the evolutionary models described above. We obtain respectively for the DA and

the DB star 0.69 and 0.68 $M_{\odot}$, and cooling ages of 1.76×10^7 and 5.13×10^6 years. Since both stars have the same radius, the contribution of each component to the total luminosity is only a function of the effective temperature. Since the DB star is significantly hotter than the DA component, the former will contribute more to the combined luminosity of the system. This is illustrated quantitatively in Figure 4.6 where the contribution of each component to the total flux is depicted. There is a significant contribution of the flux of the DB star in the optical regions of the energy distribution. In particular, the cores of the lower Balmer lines are filled in by the continuum flux of the DB star, resulting in the poor fits of the homogeneous solution displayed in Figure 4.2 and discussed above.

4.6 Discussion

Our analysis has shown that the simultaneous presence of hydrogen and helium in the spectrum of KUV 02196+2816 is better explained in terms of an unresolved binary system composed of a DA white dwarf and a DB star. We note that in at least two instances, PG 1115+166 and MCT 0453−2933 (displayed in Fig. 4.1 and discussed above), this binary interpretation has been confirmed through spectral velocity variations, hence similar observations of KUV 02196+2816 should also confirm its binary nature. Despite the evidence of our spectroscopic analysis, we discuss in the following the difficulty with interpreting KUV 02196+2816 as a single star, even from an evolutionary point of view.

There are actually two scenarios that can produce mixed hydrogen and helium atmospheres in the temperature range considered here. The first scenario, discussed in the context of DBA stars, is the accretion of hydrogen from the interstellar medium onto a helium-dominated atmosphere. However, the stellar wind model proposed by Fontaine et al. (2005) might prevent the accretion of hydrogen for stars hotter than $T_{\rm eff} \sim 20,000$ K. Hence, the presence of hydrogen in KUV 02196+2816 cannot be explained by this scenario, and another explanation must be sought for the existence of KUV 02196+2816 if it is to be interpreted as a single star.

Another scenario has been proposed by Fontaine & Wesemael (1987), where residual amounts

of hydrogen left in the envelope of hot DO stars would gradually diffuse to the surface as the white dwarf evolves along the cooling sequence. This build up of hydrogen at the photosphere would gradually turn DO white dwarfs into DA stars. Prior to the SDSS, the absence of any helium-rich atmosphere white dwarfs below $T_{\rm eff} \sim 45,000$ K (and above 30,000 K) would impose a limit of $M_{\rm H} \gtrsim 10^{-16}\ M_{\odot}$ to the total mass of hydrogen left after the post-AGB phase. Such minute amounts of hydrogen are actually sufficient to turn *all* hot, helium-rich atmosphere white dwarfs into DA stars by the time they reach $T_{\rm eff} \sim 45,000$ K, which defines the blue edge of the so-called "DB gap", a range in effective temperature between $T_{\rm eff} \sim 30,000$ and 45,000 K where no helium atmosphere white dwarf (DO or DB stars) had ever been identified (Liebert et al. 1986).

More recently, however, the SDSS has revealed the existence of several hot DB stars in this gap (Eisenstein et al. 2006), although the fraction of helium-dominated atmospheres in this temperature range remains significantly lower than that found at higher or lower temperatures. We note that SDSS white dwarfs are much fainter than those investigated by Liebert et al. (1986) in the Palomar-Green sample. The implication of this result is that a few white dwarfs must necessarily survive the DO to DA transition at high temperatures. This in turn implies that the amount of hydrogen left in the envelope of pre-white dwarfs during the post-AGB phase is even smaller than previously anticipated. We must conclude that the born-again post-AGB scenario proposed by Werner & Herwig (2006) in which a violent mixing event is induced by a late helium flash in the post-AGB phase is efficient enough to leave virtually no hydrogen behind. The recent discovery by Dufour et al. (2007); Dufour et al. (2008) of a new class of white dwarf stars with carbon-rich atmospheres between $\sim 18,000$ and 24,000 K even suggests that these flash events might be efficient enough to leave no helium behind! In this context, it is perhaps no longer surprising to find hot DB stars in the gap. These hot DB stars are most likely the immediate progenitors of the carbon-rich atmosphere white dwarfs discovered by Dufour et al.

The significant increase in the number of helium-atmosphere DB white dwarfs below $T_{\rm eff} \sim$

30,000 K — whether in the PG or SDSS samples — can only be explained in terms of the convective dilution of the superficial hydrogen atmosphere by the underlying helium convective envelope, provided that the hydrogen layer is sufficiently thin ($M_{\rm H}/M_{\rm tot} \sim 10^{-15}$, MacDonald & Vennes 1991). As discussed by Bergeron & Liebert (2002), if the DO-to-DA and DA-to-DB transition scenarios discussed above are correct, white dwarfs with mixed hydrogen and helium compositions must be sought either at the hot end of the DB gap (or deficit) near 45,000 K where an extremely thin hydrogen atmosphere in diffusive equilibrium on top of the helium envelope would make the star appear as a DAO star, or near the cool end of the gap, where convective dilution of the thin hydrogen atmosphere occurs. Excellent candidates of such stars caught in the act of changing from one spectral type to another are PG 1305−017, a DAO star at $T_{\rm eff} = 44,000$ K whose spectrum is better reproduced with stratified atmospheres (Bergeron et al. 1994), and GD 323 (shown in Fig. 1), a DAB star at $T_{\rm eff} = 28,750$ K (Koester et al. 1994) whose spectrum exhibits spectroscopic variations that have been interpreted as surface abundance inhomogeneities resulting from the convective dilution of hydrogen into helium (Pereira et al. 2005).

Going back to KUV 02196+2816, its effective temperature near 35,000 K obtained under the assumption of homogeneous single-star models does not fit well into this picture. First, the convective efficiency of the helium envelope at that temperature (the He II convection zone in this case) is much too low to produce any dilution of the hydrogen superficial atmosphere. And second, since KUV 02196+2816 is a full 10,000 K cooler than the blue edge of the DB gap near 45,000 K, it has necessarily survived the DO-to-DA transition. This in turn implies that the *total* amount of hydrogen left in the envelope during the post-AGB phase must be extremely small, and certainly too small to account for the hydrogen abundance inferred from our homogeneous model atmosphere analysis.

Thus, the DA+DB solution proposed here for KUV 02196+2816 not only provides a much better fit to the optical spectrum than the single star model, but it also represents the only viable solution from an evolutionary point of view. Interestingly enough, the effective tem-

perature we infer for the DB component of the system, $T_{\rm eff} = 36,340$ K, puts it right in the middle of the DB gap. This makes the DB component of the KUV 02196+2816 system the brightest DB white dwarf ever identified in the gap. From the atmospheric parameters of the DA and DB stars, we estimate the absolute visual magnitude of the system at $M_V = 9.51$, which combined with the visual magnitude of $V = 17.30$ yields a distance of 360 pc.

Wachter et al. (2003) also found from the 2MASS photometry that KUV 02196+2816 was a good binary candidate composed of a white dwarf and a low-mass main-sequence star. This binary nature was confirmed by Farihi et al. (2006) in their study of white dwarf-red dwarf systems resolved with HST. Farihi et al. indeed found that KUV 02196+2816 has a red dwarf companion and both stars are believed to be gravitationally bound. Since KUV 02196+2816 itself is a double degenerate binary, the system is thus composed of three stars, two of which are unresolved. As mentioned above, high-resolution spectroscopic observations similar to that obtained by Napiwotzki et al. (2005) for the double degenerate system MCT 0453−2933 could help confirm our binary interpretation. Finally, we note that since the total mass of the KUV 02196+2816 system ($M \sim 1.4\ M_{\odot}$) is close to the Chandrasekhar limit, a precise measurement of its orbital period would establish whether KUV 02196+2816 represents a likely supernova candidate.

We thank the director and staff of Steward Observatory for the use of their facilities. We would also like to thank A. Gianninas for a careful reading of this manuscript. This work was supported in part by the NSERC Canada and by the Fund FQRNT (Québec). P.B. is a Cottrell Scholar of Research Corporation for Science Advancement.

Beauchamp, A., Wesemael, F., & Bergeron, P. 1997, ApJS, 108, 559

Beauchamp, A., Wesemael, F., Bergeron, P., Liebert, J., & Saffer, R. A. 1996, in ASP Conf. Ser. Vol. 96, Hydrogen-Deficient Stars, ed. S. Jeffery & U. Heber (San Francisco: ASP), 295

Bergeron, P., & Liebert, J. 2002, ApJ, 566, 1091

Bergeron, P., Saffer, R. A., & Liebert, J. 1992, ApJ, 394, 247

Bergeron, P., Wesemael, F., Beauchamp, A., Wood, M. A., Lamontagne, R., Fontaine, G., & Liebert, J. 1994, ApJ, 432, 305

Burleigh, M., Bannister, N., & Barstow, M., 2001, in ASP Conf. Ser. Vol. 226, 12th European Workshop on White Dwarf Stars, eds. J. L. Provencal, H. L. Shipman, J. MacDonald, & S. Goodchild, 135

Darling, G.W., & Wegner, G. 1996, ApJ, 111, 685

Dufour, P., Fontaine, G, Liebert, J., Schmidt, G.D., & Behara, N. 2008, ApJ, 683, 978

Dufour, P., Liebert, J., Fontaine, G, & Behara, N. 2007, Nature, 450, 522

Eisenstein, D.J., et al. 2006, AJ, 132, 676

Farihi, J., Hoard, D.W., & Wachter, S. 2006, ApJ, 646, 840

Fontaine, G., & Brassard, P., 2005, in ASP Conf. Ser. Vol.334, 14th European Workshop on White Dwarf Stars, eds. Koester, D., Moehler, S., 49

Fontaine, G., Brassard, P., & Bergeron, P. 2001, PASP, 113, 409

Fontaine, G., & Wesemael, F. 1987, in IAU Colloquium 95, The Second Conference on Faint Blue Stars, eds. A.G.D. Philip, D.S. Hayes and J. Liebert (Schenectady: L. Davis Press), 319

Green, R. F., Schmidt, M., & Liebert, J. 1986, ApJS, 61, 305

Koester, D., Liebert, J., & Saffer, R. A. 1994, ApJ, 422, 783

Lajoie, C.-P., & Bergeron, P. 2007, ApJ, 667, 1126

Liebert, J., Bergeron, P., & Holberg, J.B. 2005, ApJ, 156, 47

Liebert, J., Bergeron, P., & Saffer, R.A. 1991, in 7th European Workshop on White Dwarfs, NATO ASI Series, ed. G. Vauclair & E. M. Sion (Dordrecht: Kluwer Academic Publishers), 409

Liebert, J., Wesemael, F., Hansen, C. J., Fontaine, G., Shipman, H. L., Sion, E. M., Winget, D. E., & Green, R. F. 1986, ApJ, 309, 241

MacDonald, J., & Vennes, S. 1991, ApJ, 371, 719

Maxted, P.F.L., Burleigh, M.R., Marsh, T.R., Bannister, N.P., 2002, MNRAS, 334, 833

Napiwotzki, R., Christlieb, N., Drechsel, H., Hagen, H.-J., Heber, U., Homeier, D., Karl, C., Koester, D., Leibundgut, B., Marsh, T.R., Moehler, S., Nelemans, G., Pauli, E.-M., Reimers, D., Renzini, A., Yungelson, L., 2001, Astron. Nachr., 322, 411

Napiwotzki, R., Karl, C.A., Nelemans, G., Yungelson, L., Christlieb, N., Drechsel, H., Heber, U., Homeier, D., Koester, D., Leibundgut, B., Marsh, T.R., Moehler, S., Renzini, A., Reimers, D., 2007, in ASP Conf. Ser. Vol. 372, 15th European Workshop on White Dwarf Stars, eds. R. Napiwotzki & M.R. Burleigh, 387

Napiwotzki, R., Karl, C.A., Nelemans, G., Yungelson, L., Christlieb, N., Drechsel, H., Heber, U., Homeier, D., Koester, D., Kruk, J., Leibundgut, B., Marsh, T.R., Moehler, S., Renzini, A., Reimers, D., 2007, in ASP Conf. Ser. Vol. 334, 14th European Workshop on White Dwarf Stars, eds. D. Koester & S. Moehler, 375

Nelemans, G., Yugelson, L.R., Portegies Zwart, S.F., & Verbunt, F. 2001, ApJ, 365, 491

Pereira, C., Bergeron, P., & Wesemael, F. 2005, ApJ, 623, 1076

Press, W. H., Flannery, B. P., Teukolsky, S. A., & Vetterling, W. T. 1986, Numerical Recipes (Cambridge: Cambridge University Press)

van der Sluys, M.V., Verbunt, F., & Pols, O.R. 2006, A&A, 460, 209

Vennes, S., Dupuis, J., & Chayer, P. 2004, ApJ, 611, 1091

Voss, B., Koester, D., Napiwotzki, R., Christlieb, N., & Reimers, D. 2007, A&A, 470, 1079

Wachter, S., Hoard, W., Hansen, K.H., Wilcox, R., Taylor, H.M., & Finkelstein, S.L. 2003, ApJ, 586, 1356

Werner, K., & Herwig, F. 2006, PASP, 118, 183

Wesemael, F., Bergeron, P., Lamontagne, R., Fontaine, G., Beauchamp, A., Demers, S., Irwin, M. J., Holberg, J. B., Kepler, S. O., & Vennes, S. 1994, ApJ, 429, 369

Chapitre 5

Conclusion

L'analyse spectroscopique des naines blanches du relevé Kiso a débuté avec une reclassification spectrale majeure de l'échantillon de Darling (1994), et l'ajout de nouveaux objets. Une fois notre échantillon bien défini, nous avons calculé les paramètres atmosphériques de chacune des naines blanches DA afin d'en dériver les valeurs de magnitude absolue correspondantes. L'effet seul de l'obtention de M_V spectroscopiques est plutôt significatif, tel que démontré par la Figure 3.9. Les différences atteignent parfois jusqu'à 4 magnitudes. L'effet combiné des nouvelles valeurs de M_V sur la fonction de luminosité, quant à lui, a été montré à la Figure 3.10. On y a remarqué que le principal effet est de déplacer des étoiles dans les intervalles de magnitudes plus brillantes, accentuant ainsi le manque de naines blanches dans les intervalles les plus froids. De plus, le fait d'obtenir une fonction de luminosité spectroscopique des naines blanches DA nous a permis de constater que le relevé Kiso n'est pas aussi complet que ce que laissait penser la Figure 10 de Liebert et al. (2005). En effet, les fonctions de luminosité des DA tirées des relevés Kiso et PG sont très similaires, avec les points de la fonction KUV qui se retrouvent souvent en dessous de ceux du relevé PG. La comparaison des étoiles qui se trouvent à la fois dans les champs des deux relevés permet de constater que non seulement la complétude de KUV et PG est similaire, mais que même le relevé Kiso, qui est plus profond que PG, n'a détecté que 75% des objets que le relevé PG avait trouvés. Pourtant, l'échantillon KUV, par sa magnitude limite plus faible, est plus profond et devrait donc être plus complet que PG.

Bien que notre but premier était de déterminer une fonction de luminosité des naines blanches DA, notre analyse spectroscopique du relevé Kiso nous a permis de découvrir trois systèmes de naines blanches binaires. Tous les trois sont des systèmes DA+DB. Il serait donc intéressant de comprendre pourquoi, dans un aussi petit échantillon de 200 étoiles, trois DA+DB ont été découvertes, alors qu'il y en a si peu parmi l'ensemble des naines blanches connues. L'abondance relative de ces systèmes binaires doublement dégénérés soulève encore plus de questions. En effet, les systèmes DA+DB ont été découverts lorsque les abondances anormales, ainsi que la mauvaise qualité des résultats obtenus en supposant une seule étoile, ont attiré notre attention. De plus, le flux prédit en supposant une DBA ne correspond pas au flux dû à une DA et une DB. Ceci est reflété dans la pente du spectre. Par contre, un système DA+DA non-résolu sera spectroscopiquement non-détectable (Lajoie & Bergeron 2007), et la pente du flux prédit s'ajustera aux observations. Combien y a-t-il alors de systèmes binaires DA+DA parmi toutes les naines blanches à atmosphère dominée par l'hydrogène déjà découvertes?

L'objectif ultime reste l'obtention d'un échantillon d'étoiles dont la complétude approche les 100%, d'où il ressortirait des statistiques robustes quant aux propriétés de la Galaxie. Un tel espoir est fourni par le catalogue LSPM (Lépine & Shara 2005), qui a détecté toutes les étoiles avec un mouvement propre $> 15''$/année. Cette limite de détection est nettement meilleure que pour les relevés de mouvements propres précédents (NLTT, par exemple). De plus, le catalogue couvre le ciel de l'hémisphère nord en entier. Cet échantillon permettra, dans un premier cas, de faire un relevé des naines blanches à moins de 40 pc, et ainsi augmenter significativement le nombre de naines blanches proches. Une telle quantité de nouvelles naines blanches contient nécessairement son lot d'objets exotiques. De plus, ce relevé permet la détection d'étoiles froides, par opposition aux relevés à excès dans l'ultraviolet. Il est donc permis d'espérer que l'échantillon obtenu soit uniforme et statistiquement représentatif de la population stellaire, et qu'il pourra mener à une fonction de luminosité dont la partie froide serait caractérisée précisément. Cet échantillon pourrait alors ouvrir la voie à de robustes études statistiques et cosmochronologiques.

Bibliographie

Bergeron, P., Saffer, R., & Liebert, J. 1992, ApJ, 394, 228

Bergeron, P., Saumon, D., & Wesemael, F. 1995, ApJ, 443, 764

Boyle, B. 1989, MNRAS, 240, 533

Dahn, C. C., Harrington, R. S., Riepe, B. Y., Christy, J. W., Guetter, H. H., Kallarakal, V. V., Miranian, M., Walker, R. L., Vrba, F. J., Hewitt, A. V., Durham, W. S., & Ables, H. D. 1982, AJ, 87, 419

Darling, G. 1994, PhD thesis, Dartmouth College

Darling, G. W. & Wegner, G. 1996, AJ, 111, 865

DeGennaro, S., von Hippel, T., Winget, D. E., Kepler, S. O., Nitta, A., Koester, D., & Althaus, L. 2008, AJ, 135, 1

Dufour, P., Bergeron, P., Liebert, J., Harris, H. C., Knapp, G. R., Anderson, S. F., Hall, P. B., Strauss, M. A., Collinge, M. J., & Edwards, M. C. 2007, ApJ, 663, 1291

Eisenstein, D. J. et al. 2006, ApJS, 167, 40

Fleming, T., Liebert, J., & Green, R. 1986, ApJ, 308, 176

Fontaine, G., Brassard, P., & Bergeron, P. 2001, PASP, 113, 409

Gianninas, A., Bergeron, P., & Ruiz, M. T. 2008, in JPCS, 16th European Workshop on White Dwarf Stars, in press

Green, R. 1980, ApJ, 238, 685

Green, R., Schmidt, M., & Liebert, J. 1986, ApJS, 61, 305

Harris, H. C. et al. 2006, AJ, 131, 571

Holberg, J. B. & Bergeron, P. 2006, AJ, 132, 1221

Knox, R. A., Hawkins, M. R. S., & Hambly, N. C. 1999, MNRAS, 306, 736

Kondo, M., Noguchi, T., & Maehara, H. 1984, Annals of the Tokyo Astronomical Observatory, 20, 130

Lajoie, C.-P. & Bergeron, P. 2007, ApJ, 667, 1126

Leggett, S. K., Ruiz, M. T., & Bergeron, P. 1998, ApJ, 497, 294

Lépine, S. & Shara, M. M. 2005, AJ, 129, 1483

Liebert, J., Bergeron, P., & Holberg, J. 2005, ApJS, 156, 47

Liebert, J., Dahn, C. C., & Monet, D. G. 1988, ApJ, 332, 891

Limoges, M. ., Bergeron, P., & Dufour, P. 2009, ArXiv e-prints

Luyten, W. J. 1979, LHS catalogue. A catalogue of stars with proper motions exceeding 0"5 annually (Minneapolis: University of Minnesota, 1979, 2nd ed.)

Maehara, H., Noguchi, T., Kondo, M., Miyauchi-Isobe, N., & Takase, B. 1986, in Structure and Evolution of Active Galactic Nuclei, ed. G. Giuricin, M. Mezzetti, M. Ramella, & F. Mardirossian, Astrophysics and Space Science Library, Vol 121, 619–622

McCook, G. P. & Sion, E. M. 1987, ApJS, 65, 603

Noguchi, T., Maehara, H., & Kondo, M. 1980, Annals of the Tokyo Astronomical Observatory, 18, 55

Schmidt, M. 1968, ApJ, 151, 393

Sion, E. M. & Liebert, J. 1977, ApJ, 213, 468

Wegner, G. & Darling, G. 1994, in Stellar and Circumstellar Astrophysics, ed. G. Wallerstein & A. Noriega-Crespo, ASP Conf. Series No. 57, 178

Wegner, G. & Swanson, S. R. 1990, AJ, 99, 330

Winget, D. E., Hansen, C. J., Liebert, J., van Horn, H. M., Fontaine, G., Nather, R. E., Kepler, S. O., & Lamb, D. Q. 1987, ApJ, 315, L77

Wood, M. A. 1995, in 9th European Workshop on White Dwarfs, NATO ASI Series, ed. D. Koester & K. Werner, 41

Remerciements

Je tiens à remercier ma mère, Rita, et mon père, Michel, pour leur constant support et leurs nombreux encouragements. Vous êtes tous les deux des modèles de persévérance. Mon amour, Jean-Philippe, qu'est-ce que je ferais sans toi? Tu me soutiens et m'encourages au quotidien. Je veux également remercier « les filles d'astro », parce que c'est toujours un plaisir de vous retrouver tous les jours. Un merci spécial à Julie, avec qui ce fut un honneur d'étudier pendant 5 ans, et Marie-Ève, pour avoir pris soin de mon équilibre. Les hommes de mon groupe de recherche, merci de répondre toujours à mes nombreuses questions. Finalement, je remercie mon directeur de recherche, Pierre Bergeron, grâce à qui tout ceci est possible.

Annexe A

Spectres des naines blanches du relevé Kiso

Nous présentons ici les spectres en lumière visible de chacune des naines blanches du relevé Kiso. Les spectres des étoiles de type DA sont ordonnés en ordre décroissant de température, et les valeurs de $T_{\rm eff}$ sont indiquées à droite des spectres. Les DA magnétiques et les systèmes DA+DB sont tracés dans des figures séparées. La figure suivante contient les spectres des naines blanches DB et DO. Suivent ensuite les DQ, DC et DZ. Les spectres sont tracés sur plage spectrale de 3600 à 5200 Å.

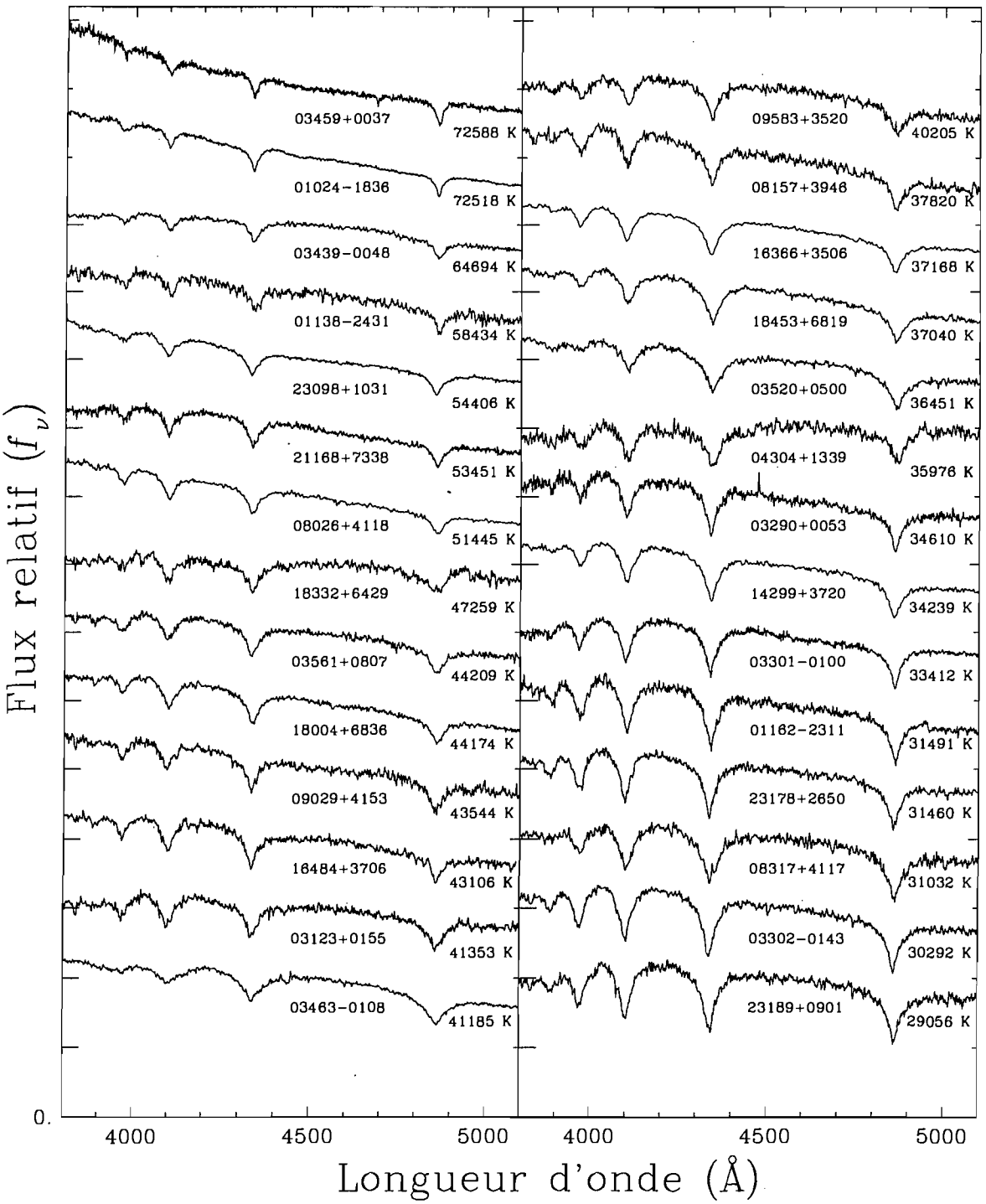

FIG. A.1 – (a) Spectres des naines blanches de type DA, en ordre décroissant de température effective. La première étoile en haut à gauche est une DAO. On remarque la raie d'He II λ4686. Les KUV 01162−2311, 04304+1339 et 18332+6429 sont des systèmes binaires non résolus, où le compagnon de la naine blanche est une naine M.

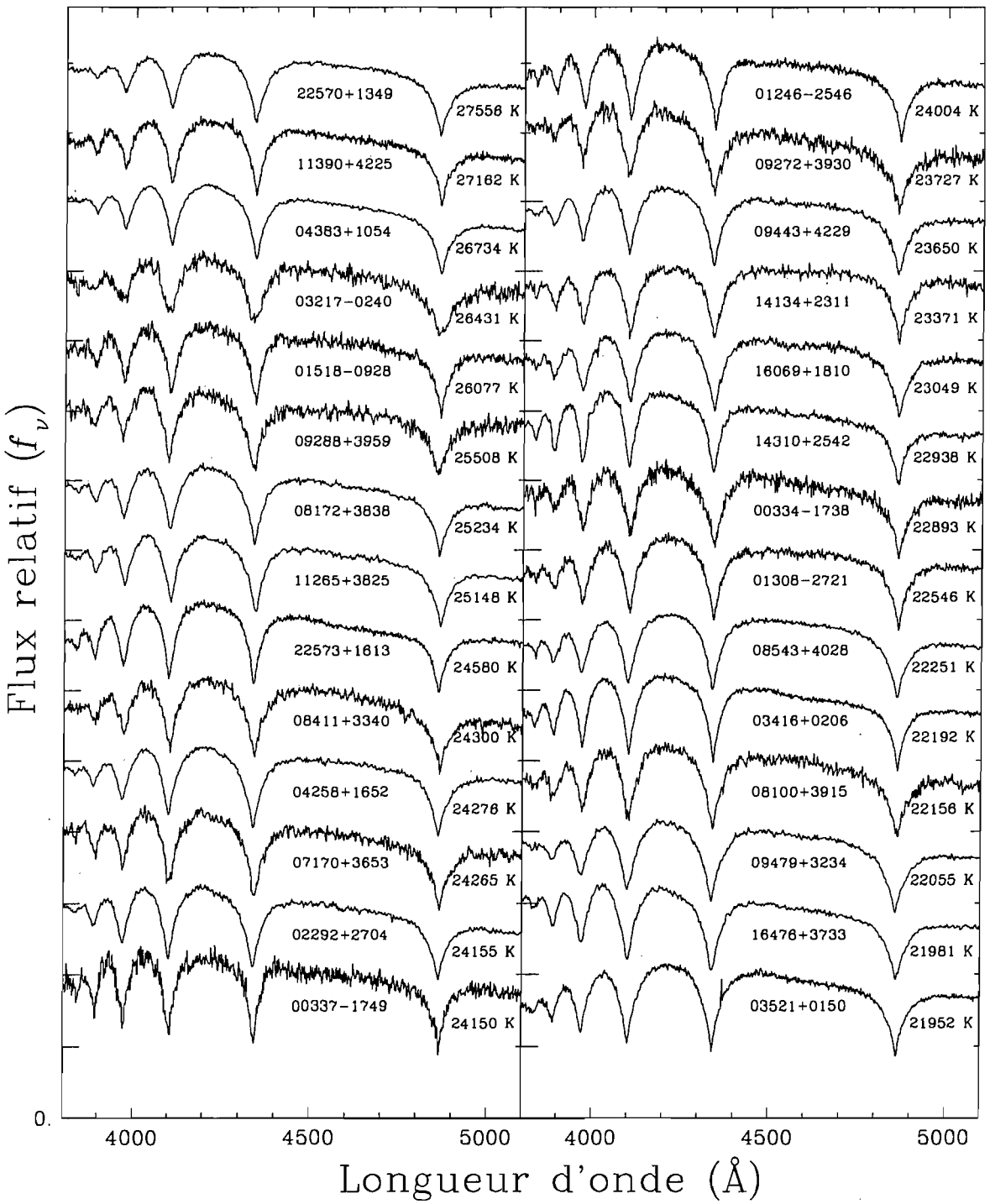

FIG. A.1 – (b) Spectres des naines blanches de type DA - suite.

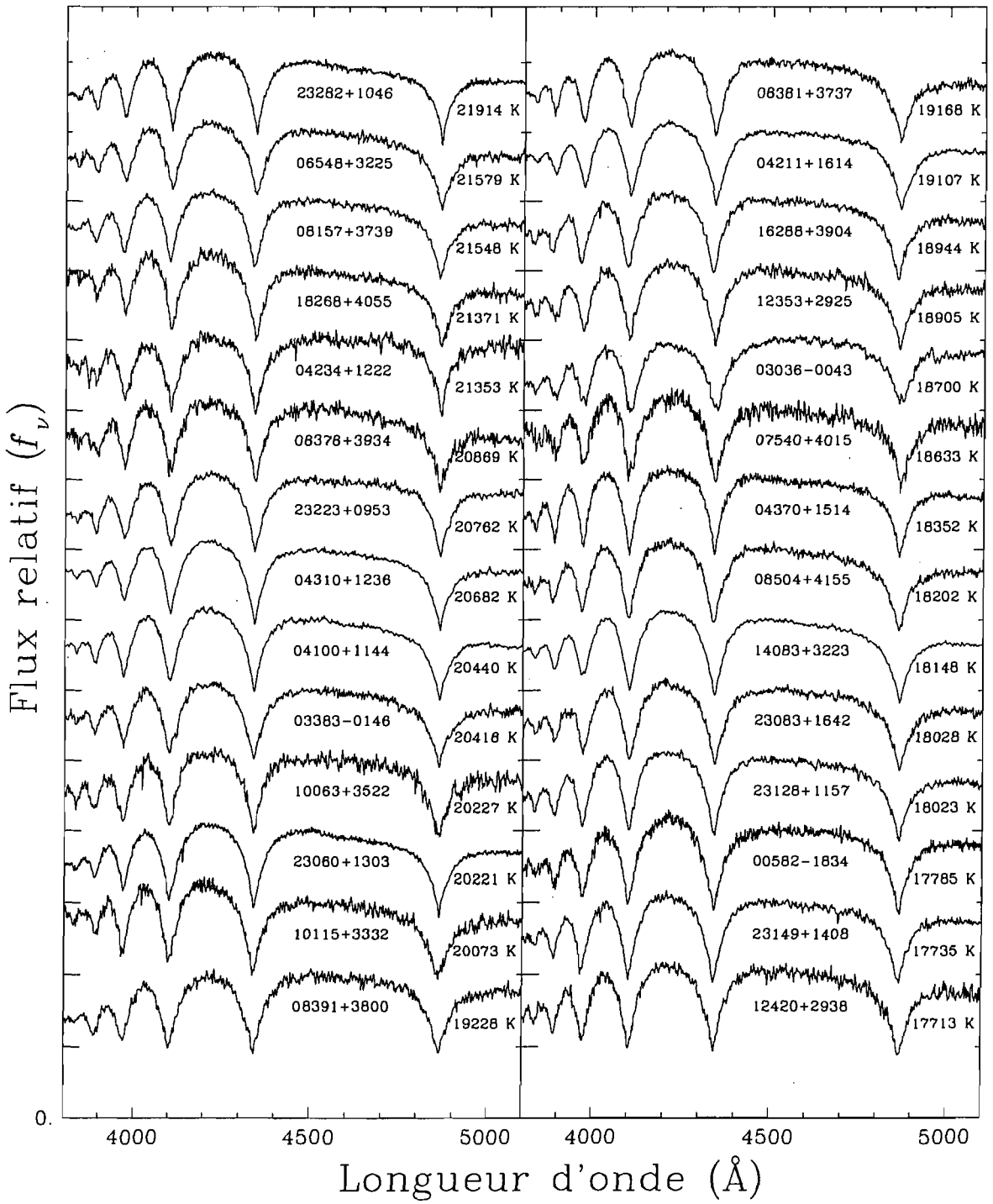

FIG. A.1 – (c) Spectres des naines blanches de type DA - suite. KUV 03036−0043 est un système binaire DA+dM non résolu.

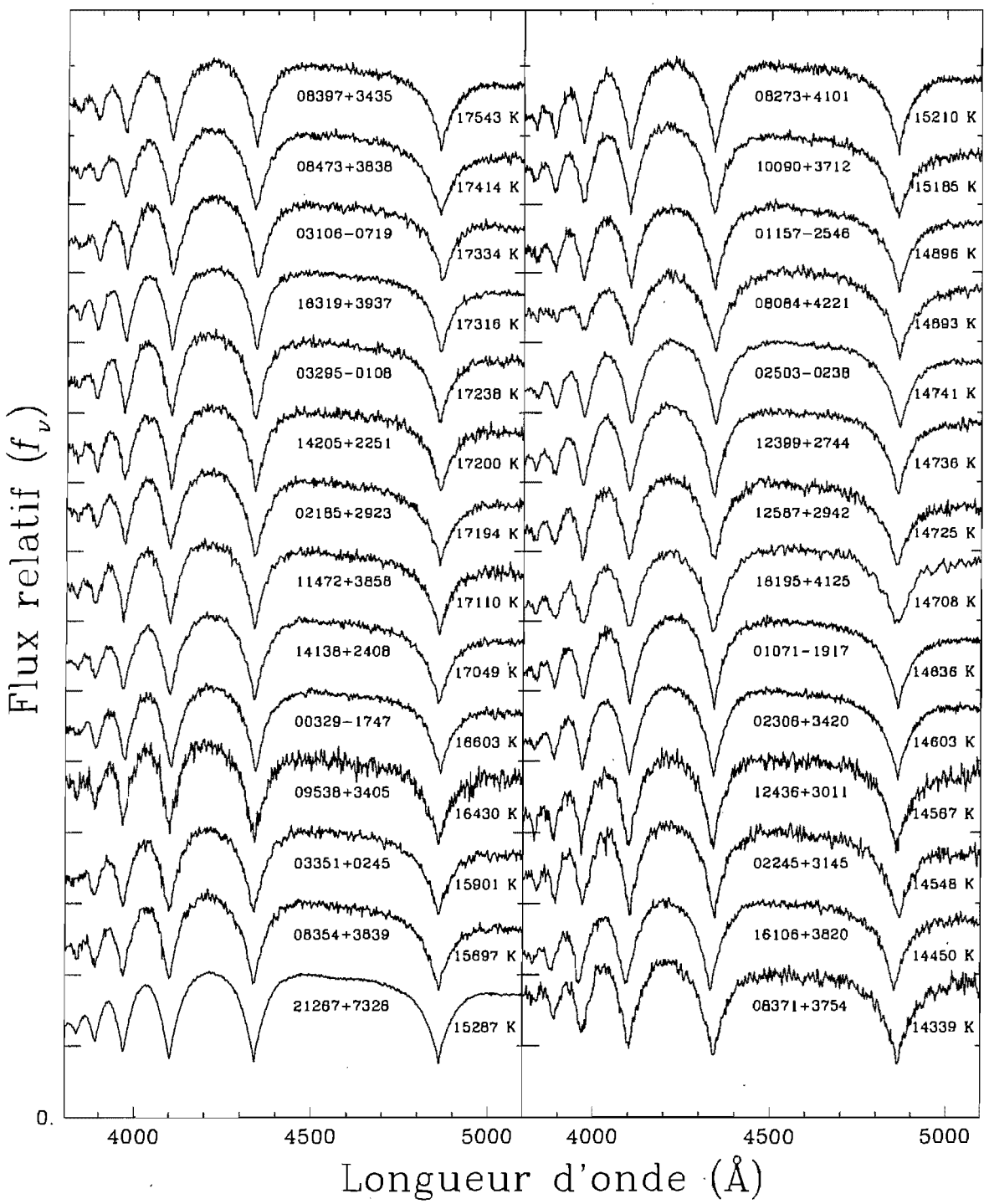

FIG. A.1 – (d) Spectres des naines blanches de type DA - suite. KUV 16195+4125 est un système binaire DA+dM non résolu.

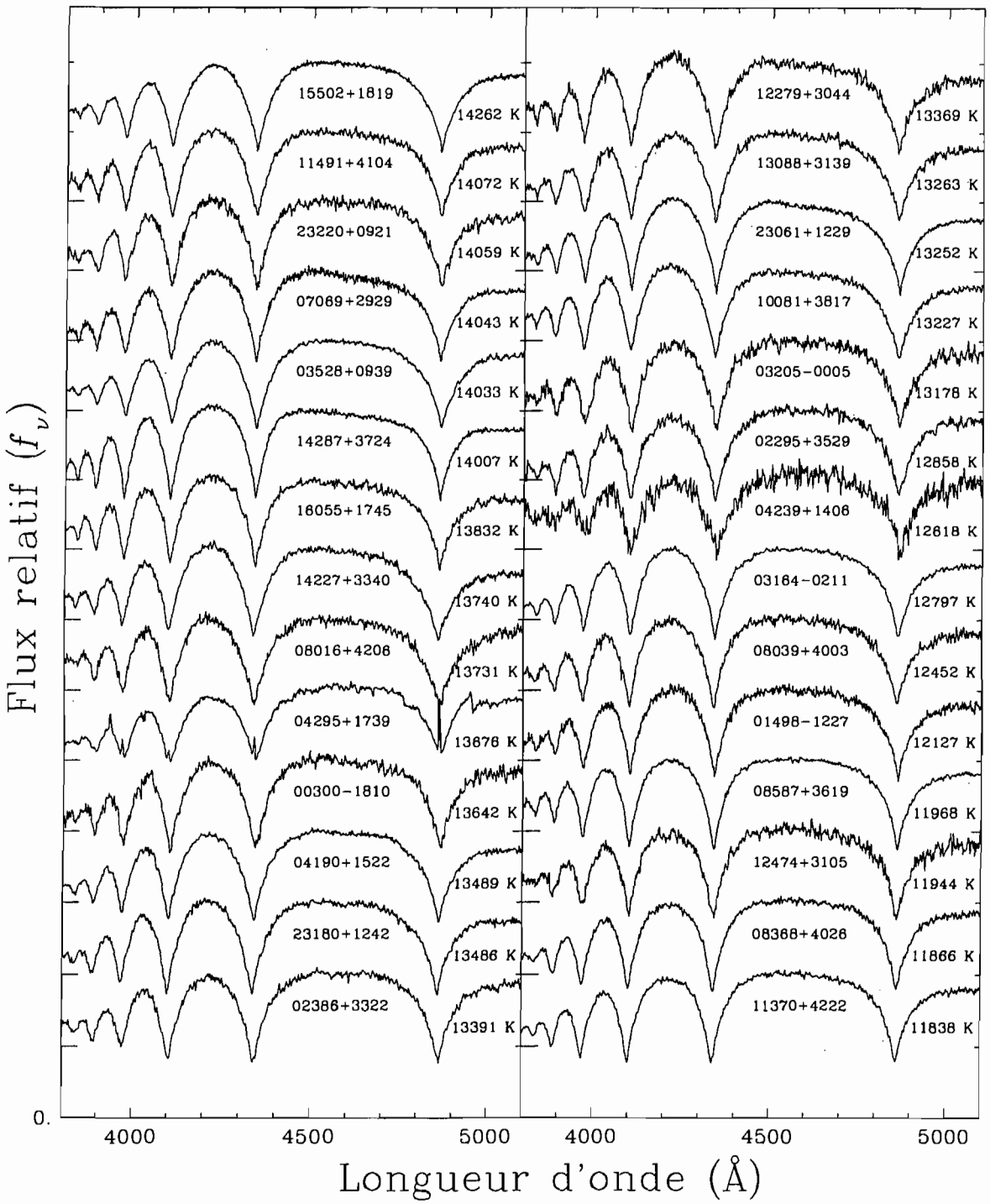

FIG. A.1 – (e) Spectres des naines blanches de type DA - suite. KUV 04295+1739 est un système binaire DA+dM non résolu.

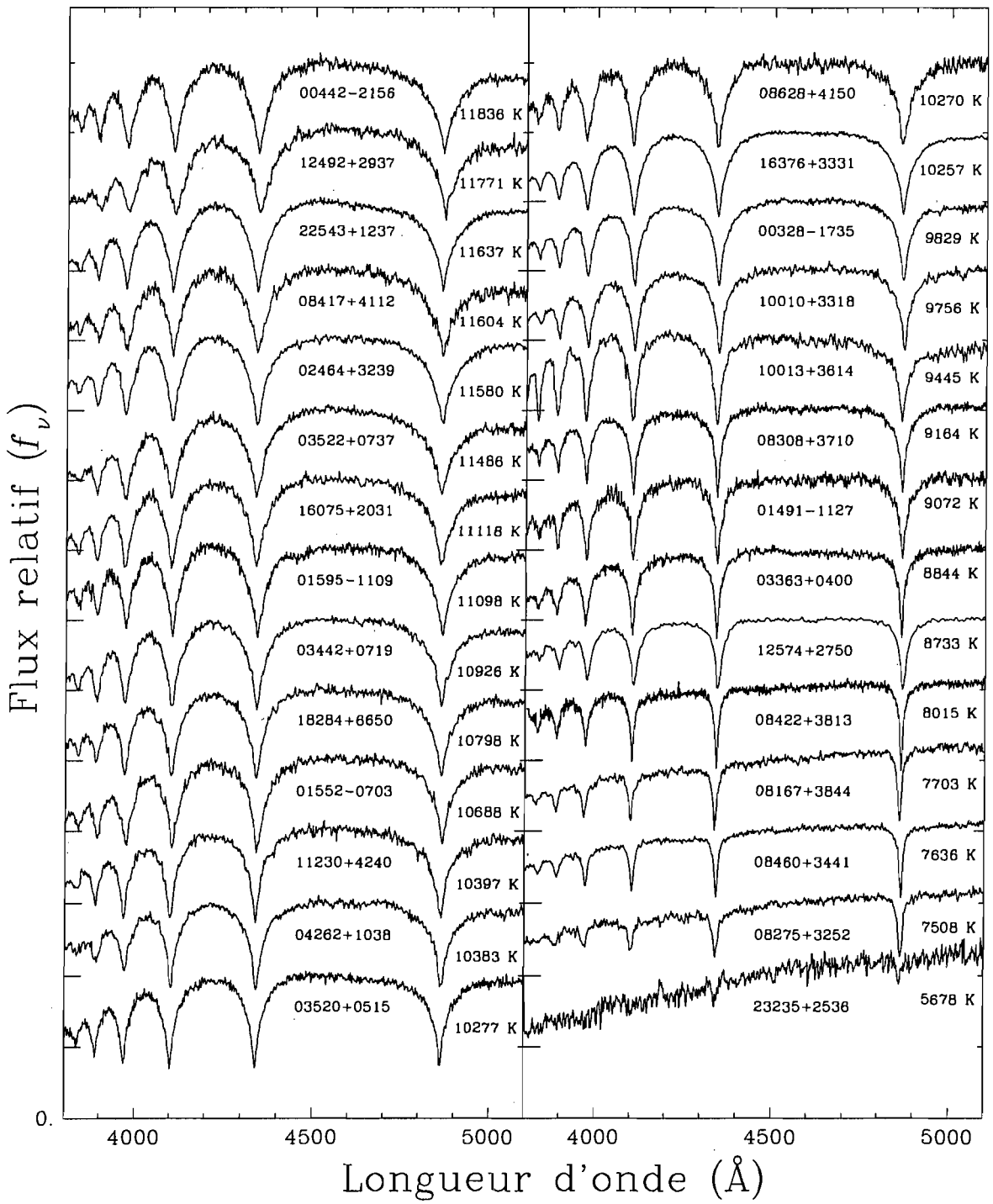

FIG. A.1 – (f) Spectres des naines blanches de type DA - suite.

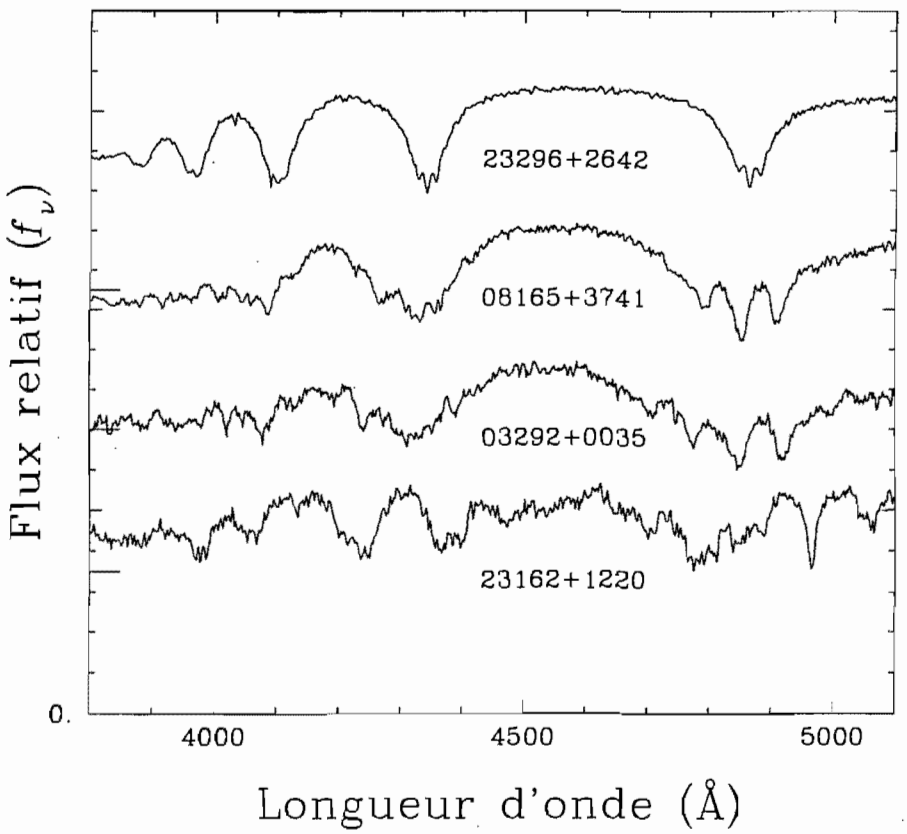

FIG. A.2 – Spectres des naines blanches magnétiques, en ordre croissant de la force du champ magnétique. De haut en bas, la force du champ magnétique passe de 2.3 à 29 MG.

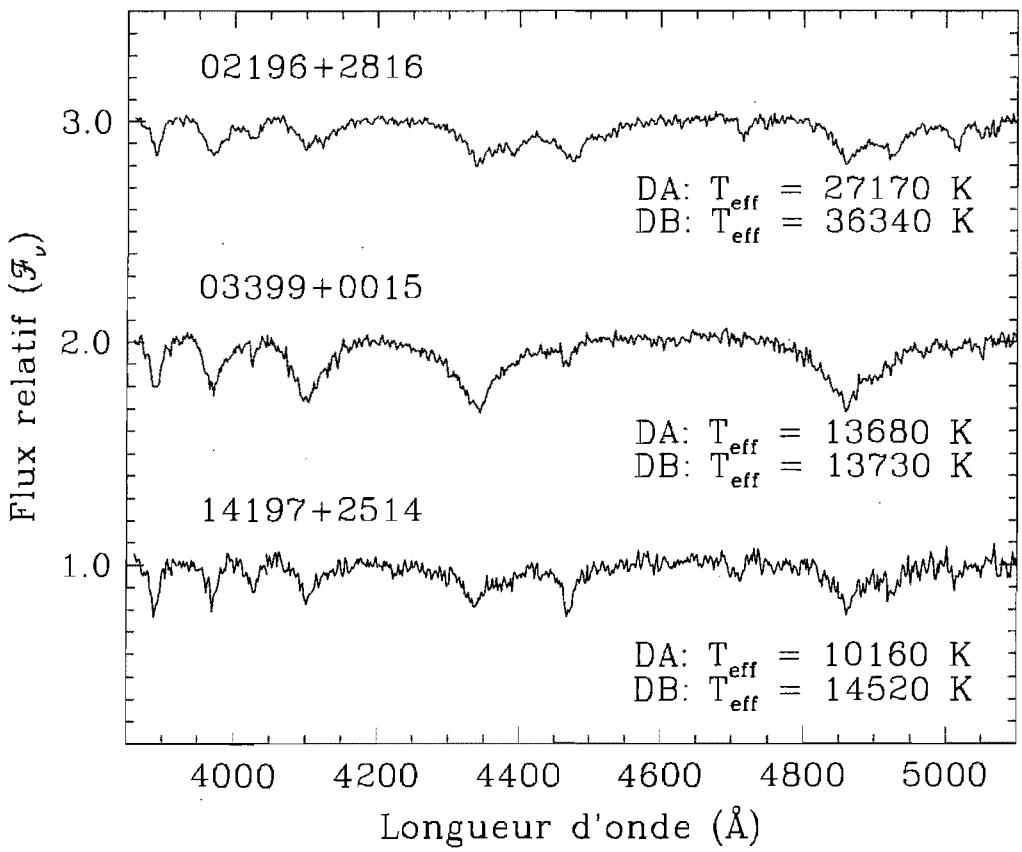

FIG. A.3 – Spectres des systèmes binaires non résolus DA+DB.

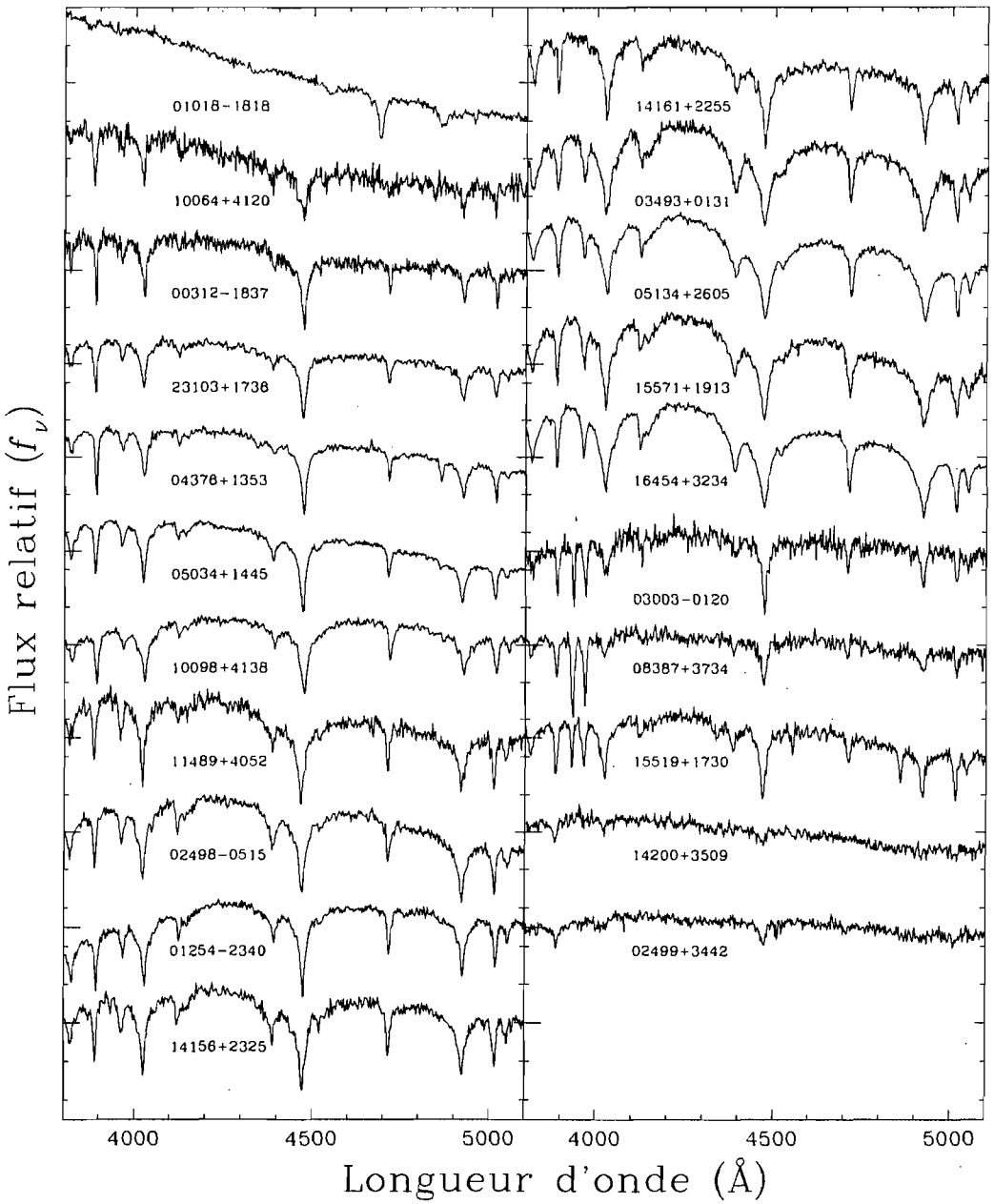

FIG. A.4 – Spectres des naines blanches dont l'atmosphère est dominée par l'hélium. La première étoile en haut à gauche est une DO, puisqu'elle possède des raies He II. KUV 03003−0120, KUV 08387+3734 et KUV 15519+1730 montrent les raies H et K de Ca λ3933 et λ3968, ce qui implique qu'elles sont des DBZ. La raie K λ3968 est mélangée avec la raie He I λ3965. Les autres spectres montrent seulement des raies d'hélium neutre; ce sont donc des DB.

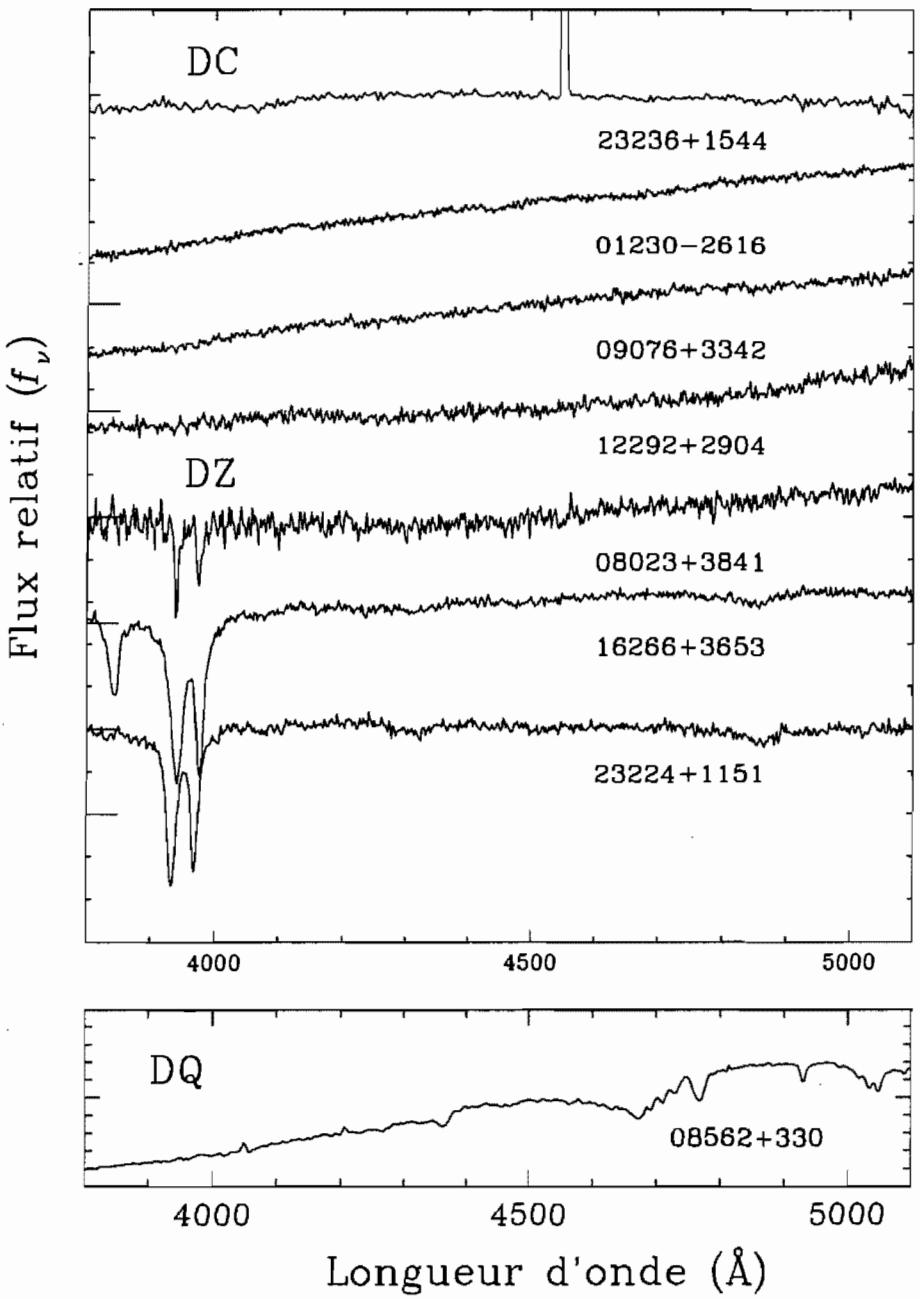

FIG. A.5 – Spectres des DQ, DC et DZ. Les DZA KUV 16266+3653 et KUV 23224+1151 montrent la raie $H\beta$ λ4861.

Annexe B

Les champs du relevé Kiso

Ici sont présentées toutes les informations sur les champs du relevé Kiso pertinentes pour le calcul de la fonction de luminosité. Les données proviennent de Noguchi et al. (1980) et Kondo et al. (1984), ainsi que du Kiso Information Bulletin. L'aire de chacun des champs a été calculée selon les critères de Green (1980), tels que décrits au Chapitre 2. L'aire de départ pour chaque champ est de 36 degrés carrés, et l'aire de recouvrement entre deux champs est attribuée au champ dont la magnitude limite est la plus faible, et soustraite de l'autre.

TAB. B.1 – Description des champs du relevé Kiso

	No du champ	Déclinaison	Longitude galactique	Latitude galactique	$V_{\rm lim}$	Aire ($\circ^2$)
1	1177	−20.	106.98	−82.32	18.0	36.
2	1178	−20.	142.36	−82.18	17.8	36.
3	1251	−25.	195.70	−82.65	17.5	36.
4	1037	−10.	170.26	−65.87	17.5	36.
5	462	30.	145.42	−28.62	17.8	36.
6	391	35.	147.35	−22.31	17.5	36.
7	968	−5.	183.24	−51.62	17.3	35.5
8	896	0.	177.42	−48.30	18.0	33.4
9	897	0.	182.27	−44.59	18.2	32.3
10	826	5.	181.52	−37.54	18.0	33.2
11	898	0.	186.53	−40.69	18.5	36.
12	827	5.	185.39	−33.68	17.0	27.4
13	755	10.	180.81	−30.53	17.5	30.6
14	684	15.	180.02	−23.58	17.2	31.2
15	756	10.	184.34	−26.70	17.8	36.
16	685	15.	183.25	−19.79	17.0	18.4
17	757	10.	187.57	−22.75	17.2	30.3
18	686	15.	186.22	−15.88	17.5	36.
19	543	25.	180.56	−6.33	17.2	36.
20	474	30.	183.09	7.65	18.0	36.
21	476	30.	186.85	15.49	18.0	36.
22	405	35.	183.54	21.22	17.2	35.3
23	343	40.	180.59	30.21	17.8	36.
24	344	40.	181.56	34.73	17.8	28.5
25	409	35.	188.28	37.05	18.5	36.
26	345	40.	182.25	39.29	18.0	36.
27	410	35.	189.10	41.10	16.8	25.9
28	347	40.	182.55	48.48	18.5	36.
29	413	35.	190.32	53.35	18.0	36.
30	348	40.	181.98	53.06	18.2	28.3
31	352	40.	168.48	70.34	17.5	36.
32	493	30.	159.67	86.74	18.2	36.
33	494	30.	80.80	86.45	18.0	36.
34	426	35.	60.03	69.17	17.5	36.
35	570	25.	31.46	69.48	17.3	36.
36	647	20.	34.06	45.92	18.0	36.
37	364	40.	63.38	44.26	17.5	36.
38	433	35.	56.97	40.70	17.2	36.
39	4109	65.	96.59	28.13	17.2	36.
40	49	75.	109.72	18.68	17.0	36.
41	740	15.	87.71	−40.04	18.0	36.
42	8741	15.	90.18	−43.08	17.2	12.5
43	813	10.	89.97	−46.83	17.6	36.
44	597	25.	98.73	−33.38	17.2	36.